Response to reviewers' comments on the paper "Anthropogenic Secondary Organic Aerosols Contribute Substantially to Air Pollution Mortality"

We would like to thank the reviewers for their time and for their useful comments that have helped to improve and clarify our paper. For ease, comments from reviewers are in black, responses in blue, and new text added to paper in **bold blue**.

Reviewer Comments

R1.0 The authors have taken into consideration all comments provided by both reviewers and all issues raised are not addressed. Furthermore now it is clear that authors focus on the anthropogenic SOA from the oxidation of VOCs and why the solid fuel-laden anthropogenic SOA is not considered. Nevertheless I would suggest also to add this clarification in the title of the publication in order to include the fact that SOA is from AVOCs. Other than that the flow of the text is significantly ameliorated and all necessary clarifications that were needed are now added. Therefore I do not see any reason why not to proceed with the publications.

Thank you for the positive re-evaluation and support for publication.

However, it is not correct to say that "solid fuel-laden anthropogenic SOA is not considered." As we had explained in the responses, the impact of solid-fuel precursors and SOA is included in both of the two field studies (that do not show a different trend than the other studies) and the model inventories.

We have updated the title though to reflect that we have focused on SOA from anthropogenic VOCs:

"Secondary Organic Aerosols from Anthropogenic Volatile Organic Compounds Contribute Substantially to Air Pollution Mortality."

Editor Comments

E1.0 Thank you very much for the careful and significant revision of your manuscript, which has improved its readability and clarity. However, there are a few addition corrections to be made as follows.

E1.1 Consider revising the title of the manuscript as suggested by the reviewer and also perform the following corrections:

Please see response to comment R1.0.

E1.2 According to figure's 6 caption, figure 6d, shows the ratio of Figure 6c/Fig6a. I wonder why the values are provided at areas (for instance over the oceans) where Fig 6a shows ASOA equal to zero (white color).

We have added the following for clarification in the caption:

"(d) Ratio between annual average modeled updated SIMPLE (b) and default VBS (a)."

And this:

"Note, for (a) - (b), values less than 0.05 µg m^{-3} are white, and for (c), values less than 0.02 µg m^{-3} are white."

With this, not all values are 0; therefore, a ratio can occur.

E1.3 Line 654: I will not say that the 'new predictions of ASOA are accurate'. I would just say they are 'more accurate than earlier'. Please correct accordingly.

Added "more accurate than earlier".

E1.4 Line 198-202: Replace: 'included ASOA realistically' by 'treated explicitly ASOA'

Added "treated ASOA explicitly"

E1.5 Line 200: replace 'These models' by 'Most models'

Changed

E1.6 Line 202: replace 'over-redirecting POA' by 'over-predicting POA'

Corrected

E1.7 Supplement, lines 47 to 49. This is very confusing. Please explain better how the calculations are done and where the fractions or concentrations come from. What is divided by the amount of total PM measured in the respective size bin ? and also divided by the OA mass in the bin ?

We have added the following text to further clarify this point:

"To estimate the SVOC mass concentration in equilibrium with POA (Table S9), in each bin (e.g., C* = 0, 1, 2), the normalized POA mass concentration is first multiplied by the fraction of POA measured in each bin from literature. For other POA, which includes biomass burning and cooking OA, the fraction of POA found in $\log_{10}C^*$ = 0, 1, and 2 are 0.22, 0.34, and 0.44, respectively (Robinson et al. 2007), and for vehicular POA, the fraction of POA found in $\log_{10}C^*$ = 0, 1, and 2 are 0.42, 0.40, and 0.18, respectively (Worton et al. 2014). So, for example, for NE US, this would correspond to normalized POA mass concentrations (POA/ΔCO) of 5.1, 4.9, and 2.2 μg sm^{-3} $ppmv^{-1}$ for $\log_{10}C^*$ = 0, 1, and 2, respectively. Then the total POA + SVOC normalized mass concentration for that bin is obtained by dividing the amount of material found in the particle-phase for that bin at the average temperature (~298 K) and OA mass concentration (~10 μg sm^{-3}). So, taking NE US as an example, for $\log_{10}C^*$ = 0, 1, and 2, 9%, 50%, and 91% of the material, respectively, will be in the gas-phase versus the aerosol-phase, leading to the normalized mass concentration of SVOC as inputs into the model of 0.39, 3.8, and 17.1 μg sm^{-3} $ppmv^{-1}$. The values of 9%, 50%, and 91% were used for NE US, Los Angeles, London, and Beijing, as the ambient temperatures were ~298 K. For New York City, as the study took place during winter, values of 3%, 22%, and 74% were used as the ambient temperature was ~273 K."

~~Anthropogenic~~ Secondary Organic Aerosols from Anthropogenic Volatile Organic Compounds Contribute Substantially to Air Pollution Mortality

Benjamin A. Nault[1,2,*], Duseong S. Jo[1,2], Brian C. McDonald[2,3], Pedro Campuzano-Jost[1,2], Douglas A. Day[1,2], Weiwei Hu[1,2,**], Jason C. Schroder[1,2,***], James Allan[4,5], Donald R. Blake[6], Manjula R. Canagaratna[7], Hugh Coe[5], Matthew M. Coggon[2,3], Peter F. DeCarlo[8], Glenn S. Diskin[9], Rachel Dunmore[10], Frank Flocke[11], Alan Fried[12], Jessica B. Gilman[3], Georgios Gkatzelis[2,3,****], Jacqui F. Hamilton[10], Thomas F. Hanisco[13], Patrick L. Hayes[14], Daven K. Henze[15], Alma Hodzic[11,16], James Hopkins[10,17], Min Hu[18], L. Greggory Huey[19], B. Thomas Jobson[20], William C. Kuster[3,*****], Alastair Lewis[10,17], Meng Li[2,3], Jin Liao[13,21], M. Omar Nawaz[15], Ilana B. Pollack[22], Jeffrey Peischl[2,3], Bernhard Rappenglück[23], Claire E. Reeves[24], Dirk Richter[12], James M. Roberts[3], Thomas B. Ryerson[3,******], Min Shao[25], Jacob M. Sommers[14,26], James Walega[12], Carsten Warneke[2,3], Petter Weibring[12], Glenn M. Wolfe[13,27], Dominique E. Young[5,*******], Bin Yuan[25], Qiang Zhang[28], Joost A. de Gouw[1,2], and Jose L. Jimenez[1,2,+]

1. Department of Chemistry, University of Colorado, Boulder, Boulder, CO, USA
2. Cooperative Institute for Research in Environmental Sciences, Boulder, Colorado, USA
3. Chemical Sciences Division, NOAA Earth System Research Laboratory, Boulder, CO
4. National Centre for Atmospheric Sciences, School of Earth and Environmental Sciences, University of Manchester, Manchester, UK
5. Centre of Atmospheric Science, School of Earth and Environmental Sciences, University of Manchester, Manchester, UK
6. Department of Chemistry, University of California, Irvine, Irvine, CA, USA
7. Center for Aerosol and Cloud Chemistry, Aerodyne Research Inc., Billerica, MA, USA
8. Department of Environmental Health Engineering, Johns Hopkins University, Baltimore, MD, USA
9. NASA Langley Research Center, Hampton, Virginia, USA
10. Wolfson Atmospheric Chemistry Laboratories, Department of Chemistry, University of York, York, UK
11. Atmospheric Chemistry Observations and Modeling Laboratory, National Center for Atmospheric Research, Boulder, CO, USA
12. Institute of Arctic and Alpine Research, University of Colorado, Boulder, CO, USA
13. Atmospheric Chemistry and Dynamic Laboratory, NASA Goddard Space Flight Center, Greenbelt, MD, USA
14. Department of Chemistry, Université de Montréal, Montréal, QC, Canada
15. Department of Mechanical Engineering, University of Colorado, Boulder, Boulder, CO, USA
16. Laboratoires d'Aréologie, Université de Toulouse, CNRS, UPS, Toulouse, France
17. National Centre for Atmospheric Sciences, Department of Chemistry, University of York, York, UK
18. State Key Joint Laboratory of Environmental Simulation and Pollution Control, College of Environmental Sciences and Engineering, Peking University, Beijing, China
19. School of Earth and Atmospheric Sciences, Georgia Institute of Technology, Atlanta, Georgia, USA
20. Laboratory for Atmospheric Research, Department of Civil and Environmental Engineering, Washington State University, Pullman, WA, USA
21. Universities Space Research Association, GESTAR, Columbia, MD, USA
22. Department of Atmospheric Science, Colorado State University, Fort Collins, CO, USA
23. Department of Earth and Atmospheric Science, University of Houston, Houston, TX, USA
24. Centre for Ocean and Atmospheric Sciences, School of Environmental Sciences, University of East Anglia, Norwich, UK
25. Institute for Environmental and Climate Research, Jinan University, Guangzhou, China
26. Air Quality Research Division, Environment and Climate Change Canada, Toronto, Ontario, Canada
27. Joint Center for Earth Systems Technology, University of Maryland, Baltimore County, Baltimore, MD, USA
28. Ministry of Education Key Laboratory for Earth System Modeling, Department of Earth System Science, Tsinghua University, Beijing, China

*Now at Center for Aerosol and Cloud Chemistry, Aerodyne Research Inc., Billerica, MA, USA
**Now at State Key Laboratory at Organic Geochemistry, Guangzhou Institute of Geochemistry, Chinese Academy of Sciences, Guangzhou, China
***Now at Colorado Department of Public Health and Environment, Denver, CO, USA
****Now at Forschungszentrum Juelich GmbH, Juelich, Germany
*****Has retired and worked on this manuscript as an unaffiliated co-author.
******Now at Scientific Aviation, Boulder, CO, USA

*******Now at Air Quality Research Center, University of California, Davis, CA, USA

+Corresponding author: Jose L. Jimenez (jose.jimenez@colorado.edu)

Abstract

Anthropogenic secondary organic aerosol (ASOA), formed from anthropogenic emissions of organic compounds, constitutes a substantial fraction of the mass of submicron aerosol in populated areas around the world and contributes to poor air quality and premature mortality. However, the precursor sources of ASOA are poorly understood, and there are large uncertainties in the health benefits that might accrue from reducing anthropogenic organic emissions. We show that the production of ASOA in 11 urban areas on three continents is strongly correlated with the reactivity of specific anthropogenic volatile organic compounds. The differences in ASOA production across different cities can be explained by differences in the emissions of aromatics and intermediate- and semi-volatile organic compounds, indicating the importance of controlling these ASOA precursors. With an improved modeling representation of ASOA driven by the observations, we attribute 340,000 $PM_{2.5}$ premature deaths per year to ASOA, which is over an order of magnitude higher than prior studies. A sensitivity case with a more recently proposed model for attributing mortality to $PM_{2.5}$ (the Global Exposure Mortality Model) results in up to 900,000 deaths. A limitation of this study is the extrapolation from cities with detailed studies and regions where detailed emission inventories are available to other regions where uncertainties in emissions are larger. In addition to further development of institutional air quality management infrastructure, comprehensive air quality campaigns in the countries in South and Central America, Africa, South Asia, and the Middle East are needed for further progress in this area.

1. Introduction

Poor air quality is one of the leading causes of premature mortality worldwide (Cohen et al., 2017; Landrigan et al., 2018). Roughly 95% of the world's population live in areas where $PM_{2.5}$ (fine particulate matter with diameter smaller than 2.5 μm) exceeds the World Health Organization's 10 μg m^{-3} annual average guideline (Shaddick et al., 2018). This is especially true for urban areas, where high population density is co-located with increased emissions of $PM_{2.5}$ and its gas-phase precursors from human activities. It is estimated that $PM_{2.5}$ leads to 3 to 4 million premature deaths per year, higher than the deaths associated with other air pollutants (Cohen et al., 2017). More recent analysis using concentration-response relationships derived from studies of populations exposure to high levels of ambient $PM_{2.5}$ suggest the global premature death burden could be up to twice this value (Burnett et al., 2018).

The main method to estimate premature mortality with $PM_{2.5}$ is to use measured $PM_{2.5}$ from ground observations along with derived $PM_{2.5}$ from satellites to fill in missing ground-based observations (van Donkelaar et al., 2015, 2016). To go from total $PM_{2.5}$ to species-dependent and even sector-dependent associated premature mortality from $PM_{2.5}$, chemical transport models (CTMs) are used to predict the fractional contribution of species and/or sector (e.g., Lelieveld et al., 2015; van Donkelaar et al., 2015, 2016; Silva et al., 2016). However, though CTMs may get total $PM_{2.5}$ or even total species, e.g., organic aerosol (OA), correct, the model may be getting the values right for the wrong reason (e.g., de Gouw and Jimenez, 2009; Woody et al., 2016; Murphy et al., 2017; Baker et al., 2018; Hodzic et al., 2020). This is especially important for OA in urban areas, where models have a longstanding issue under predicting secondary OA (SOA) with some instances of over predicting primary OA (POA) (de Gouw and Jimenez, 2009; Dzepina et al.,

2009; Hodzic et al., 2010b; Woody et al., 2016; Zhao et al., 2016a; Janssen et al., 2017; Jathar et al., 2017). Further, this bias has even been observed for highly aged aerosols in remote regions (Hodzic et al., 2020). As has been found in prior studies for urban areas (e.g., Zhang et al., 2007; Kondo et al., 2008; Jimenez et al., 2009; DeCarlo et al., 2010; Hayes et al., 2013; Freney et al., 2014; Hu et al., 2016; Nault et al., 2018; Schroder et al., 2018) and highlighted here (Fig. 1), a substantial fraction of the observed submicron PM is OA, and a substantial fraction of the OA is composed of SOA (approximately a factor of 2 to 3 higher than POA). Thus, to better understand the sources and apportionment of $PM_{2.5}$ that contributes to premature mortality, CTMs must improve their prediction of SOA versus POA, as the sources of SOA precursors and POA can be different.

However, understanding the gas-phase precursors of photochemically-produced anthropogenic SOA (ASOA, defined as the photochemically-produced SOA formed from the photoxidation of anthropogenic volatile organic compounds (AVOC) (de Gouw et al., 2005; DeCarlo et al., 2010)) quantitatively is challenging (Hallquist et al., 2009). Note, for the rest of the paper, unless explicitly stated otherwise, ASOA refers to SOA produced from the photoxidation of AVOCs, as there are potentially other relevant paths for the production of SOA in urban environments (e.g., Petit et al., 2014; Kodros et al., 2018, 2020; Stavroulas et al., 2019). Though the enhancement of ASOA is largest in large cities, these precursors and production of ASOA should be important in any location impacted by anthropogenic emissions (e.g., Fig. 1). ASOA comprises a wide range of condensable products generated by numerous chemical reactions involving AVOC precursors (Hallquist et al., 2009; Hayes et al., 2015; Shrivastava et al., 2017). The number of AVOC precursors, as well as the role of “non-traditional” AVOC

precursors, along with the condensable products and chemical reactions, compound to lead to differences in the observed versus predicted ASOA for various urban environments (e.g., de Gouw and Jimenez, 2009; Dzepina et al., 2009; Hodzic et al., 2010b; Woody et al., 2016; Janssen et al., 2017; Jathar et al., 2017; McDonald et al., 2018). One solution to improve the prediction in CTMs is to use a simplified model, where lumped ASOA precursors react, non-reversibly, at a given rate constant, to produce ASOA (Hodzic and Jimenez, 2011; Hayes et al., 2015; Pai et al., 2020). This simplified model has been found to reproduce the observed ASOA from some urban areas (Hodzic and Jimenez, 2011; Hayes et al., 2015) but issues in other urban areas (Pai et al., 2020). This may stem from the simplified model being parameterized to two urban areas (Hodzic and Jimenez, 2011; Hayes et al., 2015). These inconsistencies impact the model predicted fractional contribution of ASOA to total $PM_{2.5}$ and thus the ability to understand the source attribution to $PM_{2.5}$ and premature deaths.

The main categories of gas-phase precursors that dominate ASOA have been the subject of intensive research. The debate on what dominates can in turn impact the understanding of what precursors to regulate to reduce ASOA, to improve air quality, and to reduce premature mortality associated with ASOA. Transportation-related emissions (e.g., tailpipe, evaporation, refueling) were assumed to be the major precursors of ASOA, which was supported by field studies (Parrish et al., 2009; Gentner et al., 2012; Warneke et al., 2012; Pollack et al., 2013). Yet, budget closure of observed ASOA mass concentrations could not be achieved with transportation-related VOCs (Ensberg et al., 2014). The contribution of urban-emitted biogenic precursors to SOA in urban areas is typically small. Biogenic SOA (BSOA) in urban areas typically results from advection of regional background concentrations rather than processing of

144 locally emitted biogenic VOCs (e.g., Hodzic et al., 2009, 2010a; Hayes et al., 2013; Janssen et
145 al., 2017). BSOA is thought to dominate globally (Hallquist et al., 2009), but as shown in Fig. 1,
146 the contribution of BSOA (1% to 20%) to urban concentrations, while often substantial, is
147 typically smaller than that of ASOA (17% to 39%) (see Sect. S3.1).

148 Many of these prior studies generally investigated AVOC with high volatility, where
149 volatility here is defined as the saturation concentration, C*, in $\mu g\ m^{-3}$ (de Gouw et al., 2005;
150 Volkamer et al., 2006; Dzepina et al., 2009; Freney et al., 2014; Woody et al., 2016). More recent
151 studies have identified lower volatility compounds in transportation-related emissions (e.g., Zhao
152 et al., 2014, 2016b; Lu et al., 2018). These compounds have been broadly identified as
153 intermediate-volatile organic compounds (IVOCs) and semi-volatile organic compounds
154 (SVOCs). IVOCs have a C* generally of 10^3 to 10^6 $\mu g\ m^{-3}$ while SVOCs have a C* generally of
155 1 to 10^2 $\mu g\ m^{-3}$. Due to their lower volatility and functional groups, these classes of compounds
156 generally form ASOA more efficiently than traditional, higher volatile AVOCs; however,
157 S/IVOCs have also been more difficult to measure (e.g., Zhao et al., 2014; Pagonis et al., 2017;
158 Deming et al., 2018). IVOCs generally have been the more difficult of the two classes to measure
159 and identify as these compounds cannot be collected onto filters to be sampled off-line (Lu et al.,
160 2018) and generally show up as unresolved complex mixture for in-situ measurements using
161 gas-chromatography (GC) (Zhao et al., 2014). SVOCs, on the other hand, can be more readily
162 collected onto filters and sampled off-line due to their lower volatility (Lu et al., 2018). Another
163 potential issue has been an under-estimation of the S/IVOC aerosol production, as well as an
164 under-estimation in the contribution of photochemically produced S/IVOC from photooxidized
165 “traditional” VOCs, due to partitioning of these low volatile compounds to chamber walls and

tubing (Krechmer et al., 2016; Ye et al., 2016; Liu et al., 2019). Accounting for this under-estimation increases the predicted ASOA (Ma et al., 2017). The inclusion of these classes of compounds have led to improvement in some urban SOA budget closure; however, many studies still have indicated a general short-fall in ASOA budget even when including these compounds from transportation-related emissions. (Dzepina et al., 2009; Tsimpidi et al., 2010; Hayes et al., 2015; Cappa et al., 2016; Ma et al., 2017; McDonald et al., 2018).

Recent studies have indicated that emissions from volatile chemical products (VCPs), defined as pesticides, coatings, inks, adhesives, personal care products, and cleaning agents (McDonald et al., 2018), as well as cooking emissions (Hayes et al., 2015), asphalt emissions (Khare et al., 2020), and solid fuel emissions from residential wood burning and/or cookstoves (e.g., Hu et al., 2013, 2020; Schroder et al., 2018), are important. While total amounts of ASOA precursors released in cities have dramatically declined (largely due to three-way catalytic converters in cars (Warneke et al., 2012; Pollack et al., 2013; Zhao et al., 2017; Khare and Gentner, 2018)), VCPs have not declined as quickly (Khare and Gentner, 2018; McDonald et al., 2018). Besides a few cities in the US (Coggon et al., 2018; Khare and Gentner, 2018; McDonald et al., 2018), extensive VCP emission quantification has not yet been published.

Due to the uncertainty on the emissions of ASOA precursors and on the amount of ASOA formed from them, the number of premature deaths associated with urban organic emissions is largely unknown. Since numerous studies have shown the importance of VCPs and other non-traditional VOC emission sources, efforts have been made to try to improve the representation and emissions of VCPs (Seltzer et al., 2021), which can reduce the uncertainty in ASOA precursors and the associated premature deaths estimations. Currently, most studies have

not treatedincluded ASOA explicitlyrealistically (e.g., Lelieveld et al., 2015; Silva et al., 2016; Ridley et al., 2018) in source apportionment calculations of the premature deaths associated with long-term exposure of $PM_{2.5}$. MostThese models represented total OA as non-volatile POA and "traditional" ASOA precursors (transportation-based VOCs), which largely under-predict ASOA (Ensberg et al., 2014; Hayes et al., 2015; Nault et al., 2018; Schroder et al., 2018) while over-predicting POA (e.g., Hodzic et al., 2010b; Zhao et al., 2016a; Jathar et al., 2017). This does not reflect the current understanding that POA is volatile and contributes to ASOA mass concentration (e.g., Grieshop et al., 2009; Lu et al., 2018). Though the models are estimating total OA correctly (Ridley et al., 2018; Hodzic et al., 2020; Pai et al., 2020), the attribution of premature deaths to POA instead of SOA formed from "traditional" and "non-traditional" sources, including IVOCs from both sources, could lead to regulations that may not target the emissions that would reduce OA in urban areas. As PM_1 and SOA mass are highest in urban areas (Fig. 1), also shown in Jimenez et al. (2009), it is necessary to quantify the amount and identify the sources of ASOA to target future emission standards that will optimally improve air quality and the associated health impacts. As these emissions are from human activities, they will contribute to SOA mass outside urban regions and to potential health impacts outside urban regions as well. Though there are potentially other important exposure pathways to PM that may increase premature mortality, such as exposure to solid-fuel emissions indoors (e.g., Kodros et al., 2018), the focus of this paper is on exposure to outdoor ASOA and its associated impacts to premature mortality.

Here, we investigate the factors that control ASOA using 11 major urban, including megacities, field studies (Fig. 1 and Table 1). The empirical relationships and numerical models

are then used to quantify the attribution of premature mortality to ASOA around the world, using the observations to improve the modeled representation of ASOA. The results provide insight into the importance of ASOA to global premature mortality due to $PM_{2.5}$ and further understanding of the precursors and sources of ASOA in urban regions.

2. Methods

Here, we introduce the ambient observations from various campaigns used to constrain ASOA production (Sect. 2.1), description of the simplified model used in CTMs to better predict ASOA (Sect. 2.2), and description of how premature mortality was estimated for this study (Sect. 2.3). In the SI, the following can be found: description of the emissions used to calculate the ASOA budget for five different locations (Sect. S1), description of how the ASOA budget was calculated for the five different locations (Sect. S2), description of the CTM (GEOS-Chem) used in this study (Sect. S3 - S4), and error analysis for the observations (Sect. S5).

2.1 Ambient Observations

For values not previously reported in the literature (Table S4), observations taken between 11:00 – 16:00 local time were used to determine the slopes of SOA versus formaldehyde (HCHO) (Fig. S1), peroxy acetyl nitrate (PAN) (Fig. S2), and O_x ($O_x = O_3 + NO_2$) (Fig. S3). For CalNex, there was an approximate 48% difference between the two HCHO measurements (Fig. S4). Therefore, the average between the two measurements were used in this study, similar to what has been done in other studies for other gas-phase species (Bertram et al.,

2007). All linear fits, unless otherwise noted, use the orthogonal distance regression fitting method (ODR).

For values in Table S4 through Table S8 not previously reported in the literature, the following procedure was applied to determine the emissions ratios, similar to the methods of Nault et al. (2018). An OH exposure (OH_{exp} = [OH]×Δt), which is also the photochemical age (PA), was estimated by using the ratio of NO_x/NO_y (Eq. 1) or the ratio of m+p-xylene/ethylbenzene (Eq. 2). For the m+p-xylene/ethylbenzene, the emission ratio (Table S5) was determined by determining the average ratio during minimal photochemistry, similar to prior studies (de Gouw et al., 2017). This was done for only one study, TexAQS 2000. This method could be applied in that case as it was a ground campaign that operated both day and night; therefore, a ratio at night could be determined when there was minimal loss of both VOCs. The average emission ratio for the other VOCs was determined using Eq. 3 after the OH_{exp} was calculated in Eq. 1 or Eq. 2. The rate constants used for determining OH_{exp} and emission ratios are found in Table S12.

$$OH_{exp} = [\mathrm{OH}] \times t = \ln\left(\frac{\left(\frac{[\mathrm{NO_x}]}{[\mathrm{NO_y}]}\right)}{k_{\mathrm{OH+NO_2}}}\right) \quad \text{Eq. 1}$$

$$OH_{exp} = [\mathrm{OH}] \times t = -\frac{1}{k_{m+p-xylene} - k_{ethylbenzene}} \times \ln\left(\frac{[\mathrm{m+p-xylene}]_t}{[ethylbenzene]_t} - \frac{[m+p-xylene]_0}{[ethylbenzene]_0}\right) \quad \text{Eq. 2}$$

$$\frac{[\mathrm{VOC(i)}]}{[\mathrm{CO}]}(0) = -\frac{[\mathrm{VOC(i)}]}{[\mathrm{CO}]}(t) \times \left(1 - \frac{1}{exp\left(-k_i \times [\mathrm{OH}]_{exp} \times t\right)}\right) \times k_i + \frac{[\mathrm{VOC(i)}]}{[\mathrm{CO}]}(t) \times k_i \quad \text{Eq. 3}$$

2.2 Updates to the SIMPLE Model

With the combination of the new dataset, which expands across urban areas on three continents, the SIMPLE parameterization for ASOA (Hodzic and Jimenez, 2011) is updated in the standard GEOS-Chem model to reproduce observed ASOA in Fig. 2a. The parameterization operates as represented by Eq. 4.

$$\text{Emissions} \rightarrow \text{SOAP} \xrightarrow{k \times [OH]} \text{ASOA} \qquad \text{Eq. 4}$$

SOAP represents the lumped precursors of ASOA, k is the reaction rate coefficient with OH (1.25×10^{-11} cm^3 $molecules^{-1}$ s^{-1}), and [OH] is the OH concentration in molecules cm^{-3}. This rate constant is also consistent with observed ASOA formation time scale of ~1 day that has been observed across numerous studies (e.g., de Gouw et al., 2005; DeCarlo et al., 2010; Hayes et al., 2013; Nault et al., 2018; Schroder et al., 2018).

SOAP emissions were calculated based on the relationship between ΔSOA/ΔCO and $R_{aromatics}$/ΔCO in Fig. 2a. First, we calculated $R_{aromatics}$/ΔCO (Eq. 5) for each grid cell and time step as follows:

$$\frac{R_{aromatics}}{\Delta CO} = \frac{E_B \times k_B + E_T \times k_T + E_X \times k_X}{E_{CO}} \qquad \text{Eq. 5}$$

Where E and k stand for the emission rate and reaction rate coefficient with OH, respectively, for benzene (B), toluene (T), and xylenes (X). Ethylbenzene was not included in this calculation because its emission was not available in HTAPv2 emission inventory. However, ethylbenzene contributed a minor fraction of the mixing ratio (~ 7%, Table S5) and reactivity (~6%) of the total BTEX across the campaigns. Reaction rate constants used in this study were 1.22×10^{-12},

5.63×10^{-12}, and 1.72×10^{-11} cm^3 $molec.^{-1}$ s^{-1} for benzene, toluene, and xylene, respectively (Atkinson and Arey, 2003; Atkinson et al., 2006). The $R_{aromatics}/\Delta CO$ allows a dynamic calculation of the E(VOC)/E(CO) = SOA/ΔCO. Hodzic and Jimenez (2011) and Hayes et al. (2015) used a constant value of 0.069 g g^{-1}, which worked well for the two cities investigated, but not for the expanded dataset studied here. Thus, both the aromatic emissions and CO emissions are used in this study to better represent the variable emissions of ASOA precursors (Fig. S5).

Second, E_{SOAP}/E_{CO} can be obtained from the result of Eq. 6, using slope and intercept in Fig. 2a, with a correction factor (F) to consider additional SOA production after 0.5 PA equivalent days, since Fig. 2a shows the comparison at 0.5 PA equivalent days.

$$\frac{E_{SOAP}}{E_{CO}} = \left(Slope \times \frac{R_{Aromatics}}{\Delta CO} + Intercept \right) \times F \qquad \text{Eq. 6}$$

Where slope is 24.8 and intercept is –1.7 from Fig. 2a. F (Eq. 7) can be calculated as follows:

$$F = \frac{ASOA_{t=\infty}}{ASOA_{t=0.5d}} = \frac{SOAP_{t=0}}{SOAP_{t=0} \times (1 - exp(-k \times \Delta t \times [OH]))}, \Delta t = 43200\ s \qquad \text{Eq. 7}$$

F was calculated as 1.8 by using [OH] = 1.5×10^6 molecules cm^{-3}, which was used in the definition of 0.5 PA equivalent days for Fig. 2a.

Finally, E_{SOAP} can be computed by multiplying CO emissions (E_{CO}) for every grid point and time step in GEOS-Chem by the E_{SOAP}/E_{CO} ratio.

2.3 Estimation of Premature Mortality Attribution

Premature deaths were calculated for five disease categories: ischemic heart disease (IHD), stroke, chronic obstructive pulmonary disease (COPD), acute lower respiratory illness

(ALRI), and lung cancer (LC). We calculated premature mortality for the population aged more than 30 years, using Eq. 8.

$$Premature\ Death = Pop \times y_0 \times \frac{RR - 1}{RR} \quad \text{Eq. 8}$$

Mortality rate, y_0, varies according to the particular disease category and geographic region, which is available from Global Burden of Disease (GBD) Study 2015 database (IHME, 2016). Population (Pop) was obtained from Columbia University Center for International Earth Science Information Network (CIESIN) for 2010 (CIESIN, 2017). Relative risk, RR, can be calculated as shown in Eq. 9.

$$RR = 1 + \alpha \times \left(1 - exp\left(\beta \times \left(PM_{2.5} - PM_{2.5,Threshold}\right)^{\rho}\right)\right) \quad \text{Eq. 9}$$

α, β, and ρ values depend on disease category and are calculated from Burnett et al. (2014) (see Table S14 and associated file). If the $PM_{2.5}$ concentrations are below the $PM_{2.5}$ threshold value (Table S14), premature deaths were computed as zero. However, there could be some health impacts at concentrations below the $PM_{2.5}$ threshold values (Krewski et al., 2009); following the methods of the GBD studies, these can be viewed as lower bounds on estimates of premature deaths.

We performed an additional sensitivity analysis using the Global Exposure Mortality Model (GEMM) (Burnett et al., 2018). For the GEMM analysis, we also used age stratified population data from GWPv3. Premature death is calculated the same as shown in Eq. 8; however, the relative risk differs. For the GEMM model, the relative risk can be calculated as shown in Eq. 10.

$$RR = exp(\theta \times \lambda) \text{ with } \lambda = \frac{\log\left(1 + \frac{z}{\alpha}\right)}{\left(1 + \exp\left(\frac{(\hat{\mu} - z)}{\pi}\right)\right)} \quad \text{Eq. 10}$$

Here z = max(0,$PM_{2.5}$-$PM_{2.5,Threshold}$); θ, π, $\hat{\mu}$, α, and $PM_{2.5,Threshold}$ depends on disease category and are from Burnett et al. (2018). Similar to the Eq. 9, if the concentrations are below the threshold (2.4 μg m^{-3}, Burnett et al. (2018)), then premature deaths are computed as zero; however, the GEMM has a lower threshold than the GBD method.

For GBD, we do not consider age-specific mortality rates or risks. For GEMM, we calculate age-specific health impacts with age-specific parameters in the exposure response function (Table S15). We combine the age-specific results of the exposure-response function with age distributed population data from GPW (CIESIN, 2017) and a national mortality rate across all ages to assess age-specific mortality.

We calculated total premature deaths using annual average total $PM_{2.5}$ concentrations derived from satellite-based estimates at the resolution of 0.1°×0.1° from van Donkelaar et al. (2016) . Application of the remote-sensing based $PM_{2.5}$ at the 0.1°×0.1° resolution rather than direct use of the GEOS-Chem model concentrations at the 2°×2.5° resolution helps reduce uncertainties in the quantification of $PM_{2.5}$ exposure inherent in coarser estimates (Punger and West, 2013). We also calculated deaths by subtracting from this amount the total annual average ASOA concentrations derived from GEOS-Chem (Fig. S11). To reduce uncertainties related to spatial gradients and total concentration magnitudes in our GEOS-Chem simulations of $PM_{2.5}$, our modeled ASOA was calculated as the fraction of ASOA to total $PM_{2.5}$ in GEOS-Chem, multiplied by the satellite-based PM2.5 concentrations (Eq. 11).

$$ASOA_{sat} = (ASOA_{mod}/PM_{2.5,mod}) \times PM_{2.5,sat} \quad \text{Eq. 11}$$

Finally, this process for estimating $PM_{2.5}$ health impacts considers only $PM_{2.5}$ mass concentration and does not distinguish toxicity by composition, consistent with the current US EPA position expressed in Sacks et al. (2019).

3. Observations of ASOA Production across Three Continents

3.1 Observational Constraints of ASOA Production across Three Continents

Measurements during intensive field campaigns in large urban areas better constrain concentrations and atmospheric formation of ASOA because the scale of ASOA enhancement is large compared to SOA from a regional background. Generally, ASOA increased with the amount of urban precursor VOCs and with atmospheric PA (de Gouw et al., 2005; de Gouw and Jimenez, 2009; DeCarlo et al., 2010; Hayes et al., 2013; Nault et al., 2018; Schroder et al., 2018; Shah et al., 2018). In addition, ASOA correlates strongly with gas-phase secondary photochemical species, including O_x, HCHO, and PAN (Herndon et al., 2008; Wood et al., 2010; Hayes et al., 2013; Zhang et al., 2015; Nault et al., 2018; Liao et al., 2019) (Table S4; Fig. S1 to Fig. S3), which are indicators of photochemical processing of emissions.

However, as initially discussed by Nault et al. (2018) and shown in Fig. 3, there is large variability in these various metrics across the urban areas evaluated here. To the best of the authors' knowledge, this variability has not been explored and its physical meaning has not been interpreted. As shown in Fig. 3, though, the trends in $\Delta SOA/\Delta CO$ are similar to the trends in the slopes of SOA versus O_x, PAN, or HCHO. For example, Seoul is the highest for nearly all metrics, and is approximately a factor of 6 higher than the urban area, Houston, that generally

showed the lowest photochemical metrics. This suggests that the variability is related to a physical factor, including emissions and chemistry.

The VOC concentration, together with how quickly the emitted VOCs react ($\Sigma k_i \times [VOC]_i$, i.e., the hydroxyl radical, or OH, reactivity of VOCs), where k is the OH rate coefficient for each VOC, are a determining parameter for ASOA formation over urban spatial scales (Eq. 12). ASOA formation is normalized here to the excess CO mixing ratio (ΔCO) to account for the effects of meteorology, dilution, and non-urban background levels, and allow for easier comparison between different studies:

$$\frac{\Delta \mathrm{ASOA}}{\Delta \mathrm{CO}} \propto [\mathrm{OH}] \times \Delta t \times \left(\sum_i k_i \times \left[\frac{\mathrm{VOC}}{\mathrm{CO}} \right]_i \times \mathrm{Y_i} \right) \quad \text{Eq. 12}$$

where Y is the aerosol yield for each compound (mass of SOA formed per unit mass of precursor reacted), and [OH]×Δt is the PA.

BTEX are one group of known ASOA precursors (Gentner et al., 2012; Hayes et al., 2013), and their emission ratio (to CO) was determined for all campaigns (Table S5). BTEX can thus provide insight into ASOA production. Fig. 2a shows that the variation in ASOA (at PA = 0.5 equivalent days) is highly correlated with the emission reactivity ratio of BTEX (R_{BTEX}, $\sum_i [\mathrm{VOC}/\mathrm{CO}]_i$) across all the studies. However, BTEX alone cannot account for much of the ASOA formation (see budget closure discussion below), and instead, BTEX may be better thought of as both partial contributors and also as indicators for the co-emission of other (unmeasured) organic precursors that are also efficient at forming ASOA.

O_x, PAN, and HCHO are produced from the oxidation of a much wider set of VOC precursors (including small alkenes, which do not appreciably produce SOA when oxidized).

These alkenes have similar reaction rate constants with OH as the most reactive BTEX compounds (Table S12); however, their emissions and concentration can be higher than BTEX (Table S7). Thus, alkenes would dominate R_{Total}, leading to O_x, HCHO, and PAN being produced more rapidly than ASOA (Fig. 2b–d). When R_{BTEX} becomes more important for R_{Total}, the emitted VOCs are more efficient in producing ASOA. Thus, the ratio of ASOA to gas-phase photochemical products shows a strong correlation with R_{BTEX}/R_{Total} (Fig. 2b–d).

An important aspect of this study is that most of these observations occurred during spring and summer, when solid fuel emissions are expected to be lower (e.g., Chafe et al., 2015; Lam et al., 2017; Hu et al., 2020). Further, the most important observations used here are during the afternoon, investigating specifically the photochemically produced ASOA. These results here might partially miss any ASOA produced through nighttime aqueous chemistry or oxidation by nitrate radical (Kodros et al., 2020). However, two of the studies included in our analysis, Chinese Outflow (CAPTAIN, 2011) and New York City (WINTER, 2015), occurred in late winter/early spring, when solid fuel emissions were important (Hu et al., 2013; Schroder et al., 2018). We find that these observations lie within the uncertainty in the slope between ASOA and R_{BTEX} (Fig. 2a). Their photochemically produced ASOA observed under strong impact from solid fuel emissions shows similar behavior as the ASOA observed during spring and summer time. Thus, given the limited datasets currently available, photochemically produced ASOA is expected to follow the relationship shown in Fig. 2a and is expected to also follow this relationship for regions impacted by solid fuel burning. Future comprehensive studies in regions strongly impacted by solid fuel burning are needed to further investigate photochemical ASOA production under those conditions.

3.2 Budget Closure of ASOA for 4 Urban Areas on 3 Continents Indicates Reasonable Understanding of ASOA Sources

To investigate the correlation between ASOA and R_{BTEX}, a box model using the emission ratios from BTEX (Table S5), other aromatics (Table S8), IVOCs (Sect. S1), and SVOCs (Sect. S1) was run for five urban areas: New York City, 2002, Los Angeles, Beijing, London, and New York City, 2015 (see Sect. S1 and S3 for more information). The differences in the results shown in Fig. 4 are due to differences in the emissions for each city. We show that BTEX alone cannot explain the observed ASOA budget for urban areas around the world. Fig. 4a shows that approximately 25±6% of the observed ASOA originates from the photooxidation of BTEX. BTEX only explaining 25% of the observed ASOA is similar to prior studies that have done budget analysis of precursor gases and observed SOA (e.g., Dzepina et al., 2009; Ensberg et al., 2014; Hayes et al., 2015; Ma et al., 2017; Nault et al., 2018). Therefore, other precursors must account for most of the ASOA produced.

Because alkanes, alkenes, and oxygenated compounds with carbon numbers less than 6 are not significant ASOA precursors, we focus on emissions and sources of BTEX, other mono-aromatics, IVOCs, and SVOCs. These three classes of VOCs, aromatics, IVOCs, and SVOCs, have been suggested to be significant ASOA precursors in urban atmospheres (Robinson et al., 2007; Hayes et al., 2015; Ma et al., 2017; McDonald et al., 2018; Nault et al., 2018; Schroder et al., 2018; Shah et al., 2018), originating from both fossil fuel and VCP emissions.

Using the best available emission inventories from cities on three continents (EMEP/EEA, 2016; McDonald et al., 2018; Li et al., 2019) and observations, we quantify the emissions of BTEX, other mono-aromatics, IVOCs, and SVOCs for both fossil fuel (e.g., gasoline, diesel, kerosene, etc.), VCPs (e.g., coatings, inks, adhesives, personal care products, and cleaning agents), and cooking sources (Fig. 5). This builds off the work of McDonald et al. (2018) for urban regions on three different continents.

Note, the emissions investigated here ignore any oxygenated VOC emissions not associated with IVOCs and SVOCs due to the challenge in estimating the emission ratios for these compounds (de Gouw et al., 2018). Further, SVOC emission ratios are estimated from the average POA observed by the AMS during the specific campaign and scaled by profiles in literature for a given average temperature and average OA (Robinson et al., 2007; Worton et al., 2014; Lu et al., 2018). As most of the campaigns had an average OA between 1 and 10 μg m^{-3} and temperature of ~298 K, this led to the majority of the estimated emitted SVOC gases in the highest SVOC bin. However, as discussed later, this does not lead to SVOCs dominating the predicted ASOA due to taking into account the fragmentation and overall yield from the photooxidation of SVOC to ASOA.

Combining these inventories and observations for the various locations provide the following insights about the potential ASOA precursors not easily measured or quantified in urban environments (e.g., Zhao et al., 2014; Lu et al., 2018): (1) aromatics from fossil fuel accounts for 14-40% (mean 22%) of the total BTEX and IVOC emissions for the five urban areas investigated in-depth (Fig. 5), agreeing with prior studies that have shown that the observed ASOA cannot be reconciled by the observations or emission inventory of aromatics from fossil

fuels (e.g., Ensberg et al., 2014; Hayes et al., 2015). (2) BTEX from both fossil fuels and VCPs account for 25-95% (mean 43%) of BTEX and IVOC emissions (Fig. 5). China has the lowest contribution of IVOCs, potentially due to differences in chemical make-up of the solvents used daily (Li et al., 2019), but more research is needed to investigate the differences in IVOCs:BTEX from Beijing versus US and UK emission inventories. Nonetheless, this shows the importance of IVOCs for both emissions and ASOA precursors. (3) IVOCs are generally equal to, if not greater than, the emissions of BTEX in 4 of the 5 urban areas investigated here (Fig. 5). (4) Overall, VCPs account for a large fraction of the BTEX and IVOC emissions for all five cities. (5) Finally, SVOCs account for 27-88% (mean 53%) of VOCs generally considered ASOA precursors (VOCs with volatility saturation concentrations $\leq 10^7$ μg m^{-3}) (Fig. S6). Beijing has the highest contribution of SVOCs to ASOA precursors due to the use of solid fuels and cooking emissions (Hu et al., 2016). Also, this indicates the large contribution of a class of VOCs difficult to measure (Robinson et al., 2007) that are an important ASOA precursor (e.g., Hayes et al., 2015), showing further emphasis should be placed in quantifying the emissions of this class of compounds.

These results provide an ability to further investigate the mass balance of predicted and observed ASOA for these urban locations (Fig. 4). The inclusion of IVOCs, other aromatics not including BTEX, and SVOCs leads to the ability to explain, on average, 85±12% of the observed ASOA for these urban locations around the world (Fig. 4a). Further, VCP contribution to ASOA is important for all these urban locations, accounting for, on average, 37±3% of the observed ASOA (Fig. 4b).

This bottom-up mass budget analysis provides important insights to further explain the correlation observed in Fig. 2. First, IVOCs are generally co-emitted from similar sources as BTEX for the urban areas investigated in-depth (Fig. 5). The oxidation of these co-emitted species leads to the ASOA production observed across the urban areas around the world. Second, S/IVOCs generally have similar rate constants as toluene and xylenes ($\geq 1\times10^{-11}$ cm^3 $molec.^{-1}$ s^{-1}) (Zhao et al., 2014, 2017), the compounds that contribute the most to R_{BTEX}, explaining the rapid ASOA production that has been observed in various studies (de Gouw and Jimenez, 2009; DeCarlo et al., 2010; Hayes et al., 2013; Hu et al., 2013, 2016; Nault et al., 2018; Schroder et al., 2018) and correlation (Fig. 2). Finally, the contribution of VCPs and fossil fuel sources to ASOA is similar across the cities, expanding upon and further supporting the conclusion of McDonald et al. (2018) in the importance of identifying and understanding VCP emissions in order to explain ASOA.

This investigation shows that the bottom-up calculated ASOA agrees with observed top-down ASOA within 15%. As highlighted above, this ratio is explained by the co-emissions of IVOCs with BTEX from traditional sources (diesel, gasoline, and other fossil fuel emissions) and VCPs (Fig. 5) along with similar rate constants for these ASOA precursors (Table S12). Thus, the ASOA/R_{BTEX} ratio obtained from Fig. 2 results in accurate predictions of ASOA for the urban areas evaluated here, and this value can be used to better estimate ASOA with chemical transport models (Sect. 4).

4. Improved Urban SIMPLE Model Using Multi-Cities to Constrain

The SIMPLE model was originally designed and tested against the observations collected around Mexico City (Hodzic and Jimenez, 2011). It was then tested against observations collected in Los Angeles (Hayes et al., 2015; Ma et al., 2017). As both data sets have nearly identical ΔSOA/ΔCO and R_{BTEX} (Fig. 2 and Fig. 3), it is not surprising that the SIMPLE model did well in predicting the observed ΔSOA/ΔCO for these two urban regions with consistent parameters. Though the SIMPLE model generally performed better than more explicit models, it generally had lower skill in predicting the observed ASOA in urban regions outside of Mexico City and Los Angeles (Shah et al., 2019; Pai et al., 2020).

This may stem from the original SIMPLE model with constant parameters missing the ability to change the amount and reactivity of the emissions, which are different for the various urban regions, versus the ASOA precursors being emitted proportionally to only CO (Hodzic and Jimenez, 2011; Hayes et al., 2015). For example, in the HTAP emissions inventory, the CO emissions for Seoul, Los Angeles, and Mexico City are all similar (Fig. S8); thus, the original SIMPLE model would suggest similar ΔSOA/ΔCO for all three urban locations. However, as shown in Fig. 2 and Fig. 3, the ΔSOA/ΔCO is different by nearly a factor of 2. The inclusion of the emissions and reactivity, where R_{BTEX} for Seoul is approximately a factor of 2.5 higher than Los Angeles and Seoul, into the improved SIMPLE model better accounts for the variability in SOA production, as shown in Fig. 2. Thus, the inclusion and use of this improved SIMPLE model refines the simplified representation of ASOA in chemical transport models and/or box models.

The “improved” SIMPLE shows higher ASOA compared to the default VBS GEOS-Chem (Fig. 6a,b). In areas strongly impacted by urban emissions (e.g., Europe, East Asia,

India, east and west coast US, and regions impacted by Santiago, Chile, Buenos Aires, Argentina, Sao Paulo, Brazil, Durban and Cape Town, South Africa, and Melbourne and Sydney, Australia), the "improved" SIMPLE model predicts up to 14 μg m^{-3} more ASOA, or ~30 to 60 times more ASOA than the default scheme (Fig. 6c,d). As shown in Fig. 1, during intensive measurements, the ASOA composed 17-39% of PM_1, with an average contribution of ~25%. The default ASOA scheme in GEOS-Chem greatly underestimates the fractional contribution of ASOA to total $PM_{2.5}$ (<2%; Fig. 6e). The "improved" SIMPLE model greatly improves the predicted fractional contribution, showing that ASOA in the urban regions ranges from 15-30%, with an average of ~15% for the grid cells corresponding to the urban areas investigated here (Fig. 6f). Thus, the "improved" SIMPLE predicts the fractional contribution of ASOA to total $PM_{2.5}$ far more realistically, compared to observations. As discussed in Sect. 2.3 and Eq. 11, having the model accurately predict the fractional contribution of ASOA to the total PM is very important, as the total $PM_{2.5}$ is derived from satellite-based estimates (van Donkelaar et al., 2015), and the model fractions are then applied to those total $PM_{2.5}$ estimates. The ability for the "improved" SIMPLE model to better represent the ASOA composition provides confidence attributing the ASOA contribution to premature mortality**.**

5. Preliminary Evaluation of Worldwide Premature Deaths Due to ASOA with Updated SIMPLE Parameterization

The improved SIMPLE parameterization is used along with GEOS-Chem to provide an accurate estimation of ASOA formation in urban areas worldwide and provide an ability to obtain realistic simulations of ASOA based on measurement data. We use this model to quantify

526 the attribution of $PM_{2.5}$ ASOA to premature deaths. Analysis up to this point has been for PM_1;
527 however, both the chemical transport model and epidemiological studies utilize $PM_{2.5}$. For
528 ASOA, this will not impact the discussion and results here because the mass of OA (typically
529 80–90%) is dominated by PM_1 (e.g., Bae et al., 2006; Seinfeld and Pandis, 2006), and ASOA is
530 formed mostly through condensation of oxidized species, which favors partitioning onto smaller
531 particles (Seinfeld and Pandis, 2006).

532 The procedure for this analysis is described in Fig. 7 and Sect. 2.3 and S3. Briefly, we
533 combine high-resolution satellite-based $PM_{2.5}$ estimates (for exposure) and a chemical transport
534 model (GEOS-Chem, for fractional composition) to estimate ASOA concentrations and various
535 sensitivity analysis (van Donkelaar et al., 2015). We calculated ~3.3 million premature deaths
536 (using the Integrated Exposure-Response, IER, function) are due to long-term exposure of
537 ambient $PM_{2.5}$ (Fig. S9, Table S16), consistent with recent literature (Cohen et al., 2017).

538 The attribution of ASOA $PM_{2.5}$ premature deaths can be calculated one of two ways: (a)
539 marginal method (Silva et al., 2016) or (b) attributable fraction method (Anenberg et al., 2019).
540 For method (a), it is assumed that a fraction of the ASOA is removed, keeping the rest of the
541 $PM_{2.5}$ components approximately constant, and the change in deaths is calculated from the deaths
542 associated with the total concentration less the deaths calculated using the reduced total $PM_{2.5}$
543 concentrations. For method (b), the health impact is attributed to each $PM_{2.5}$ component by
544 multiplying the total deaths by the fractional contribution of each component to total $PM_{2.5}$. For
545 method (a), the deaths attributed to ASOA are ~340,000 people per year (Fig. 8); whereas, for
546 method (b), the deaths are ~370,000 people per year. Both of these are based on the IER response
547 function (Cohen et al., 2017).

548 Additional recent work (Burnett et al., 2018) has suggested less reduction in the
549 premature deaths versus $PM_{2.5}$ concentration relationship at higher $PM_{2.5}$ concentrations, and
550 lower concentration limits for the threshold below which this relationship is negligible, both of
551 which lead to much higher estimates of $PM_{2.5}$ associated premature deaths. This is generally
552 termed the Global Exposure Mortality Model (GEMM). Using the two attribution methods
553 described above (a and b), the ASOA $PM_{2.5}$ premature deaths are estimated to be ~640,000
554 (method a) and ~900,000 (method b) (Fig. S9 and Fig. S12 and Table S17).

555 Compared to prior studies using chemical transport models to estimate premature deaths
556 associated with ASOA (e.g., Silva et al., 2016; Ridley et al., 2018), which assumed non-volatile
557 POA and "traditional" ASOA precursors, the attribution of premature mortality due to ASOA is
558 over an order of magnitude higher in this study (Fig. 9). This occurs using either the IER and
559 GEMM approach for estimating premature mortality (Fig. 9). For regions with larger populations
560 and more $PM_{2.5}$ pollution, the attribution is between a factor of 40 to 80 higher. This stems from
561 the non-volatile POA and "traditional" ASOA precursors over-estimating POA and
562 under-estimating ASOA compared to observations (Schroder et al., 2018). These offsetting
563 errors will lead to model predicted total OA similar to observations (Ridley et al., 2018; Schroder
564 et al., 2018), yet different conclusions on whether POA versus SOA is more important for
565 reducing $PM_{2.5}$ associated premature mortality. Using a model constrained to day-time
566 atmospheric observations (Fig. 2 and Fig. 4, see Sect. 4) leads to a more accurate than earlier
567 estimation of the contribution of photochemically-produced ASOA to $PM_{2.5}$ associated
568 premature mortality that has not been possible in prior studies. We note that ozone concentrations
569 change little as we change the ASOA simulation (see Sect. S4 and Fig. S14).

A limitation in this study is the lack of sufficient measurements in South and Southeast Asia, Eastern Europe, Africa, and South America (Fig. 1), though these areas account for 44% of the predicted reduction in premature mortality for the world (Table S16). However, as highlighted in Table S18, these regions likely still consume both transportation fuels and VCPs, although in lower per capita amounts than more industrialized countries. This consumption is expected to lead to the same types of emissions as for the cities studied here, though more field measurements are needed to validate global inventories of VOCs and resulting oxidation products in the developing world. Transportation emissions of VOCs are expected to be more dominant in the developing world due to higher VOC emission factors associated with inefficient combustion engines, such as two-stroke scooters (Platt et al., 2014) and auto-rickshaws (e.g., Goel and Guttikunda, 2015).

Solid fuels are used for residential heating and cooking, which impact the outdoor air quality as well (Hu et al., 2013, 2016; Lacey et al., 2017; Stewart et al., 2020), and which also lead to SOA (Heringa et al., 2011). As discussed in Sect. 3.1, though the majority of the studies evaluated here occurred in spring to summer time, when solid fuel emissions are decreased, two studies occurred during the winter/early spring time, where solid fuel emissions were important (Hu et al., 2013; Schroder et al., 2018). These studies still follow the same relationship between ASOA and R_{BTEX} as the studies that focused on spring/summer time photochemistry. Thus, the limited datasets available indicate that photochemically produced ASOA from solid fuels follow a similar relationship to that from other ASOA sources.

Also, solid fuel sources are included in the inventories used in our modeling. For the HTAP emission inventory used here (Janssens-Maenhout et al., 2015), small-scale combustion,

592 which includes heating and cooking (e.g., solid-fuel use), is included in the residential emission
593 sector. Both CO and BTEX are included in this source, and can account for a large fraction of the
594 total emissions where solid-fuel use may be important (Fig. S15). Thus, as CO and BTEX are
595 used in the updated SIMPLE model, and campaigns that observed solid-fuel emissions fall
596 within the trend for all urban areas, the solid-fuel contribution to photochemically-produced
597 ASOA is accounted for (as accurately as allowed by current datasets) in the estimation of ASOA
598 for the attribution to premature mortality.

599 Note that recent work has observed potential nighttime aqueous chemistry and/or
600 oxidation by nitrate radical from solid fuel emissions to produce ASOA (Kodros et al., 2020).
601 Thus, missing this source of ASOA may lead to an underestimation of total ASOA versus the
602 photochemically-produced ASOA we discuss here, leading to a potential underestimation in the
603 attribution of ASOA to premature mortality. From the studies that investigated "night-time
604 aging" of solid-fuel emissions to form SOA, we predict that the total ASOA may be
605 underestimated by 1 to 3 $\mu g\ m^{-3}$ (Kodros et al., 2020). This potential underestimation, though, is
606 less than the current underestimation in ASOA in GEOS-Chem (default versus "Updated"
607 SIMPLE).

608 Recently, emission factors from Abidjan, Côte d'Ivoire, a developing urban area, showed
609 the dominance of emissions from transportation and solid fuel burning, with BTEX being an
610 important fraction of the total emissions, and that all the emissions were efficient in producing
611 ASOA (Dominutti et al., 2019). Further, investigation of emissions in New Delhi region of India
612 demonstrated the importance of both transportation and solid fuel emissions (Stewart et al.,
613 2020; Wang et al., 2020) while model comparisons with observations show an underestimation

of OA compared to observations due to a combination of emissions and OA representation (Jena et al., 2020). Despite emission source differences, SOA is still an important component of $PM_{2.5}$ (e.g., Singh et al., 2019) and thus will impact air quality and premature mortality in developing regions. Admittedly, though, our estimates will be less accurate for these regions.

6. Conclusions

In summary, ASOA is an important, though inadequately constrained component of air pollution in megacities and urban areas around the world. This stems from the complexity associated with the numerous precursor emission sources, chemical reactions, and oxidation products that lead to observed ASOA concentrations. We have shown here that the variability in observed ASOA across urban areas is correlated with R_{BTEX}, a marker for the co-emissions of IVOC from both transportation and VCP emissions. Global simulations indicate ASOA contributes to a substantial fraction of the premature mortality associated with $PM_{2.5}$. Reductions of the ASOA precursors will reduce the premature deaths associated with $PM_{2.5}$, indicating the importance of identifying and reducing exposure to sources of ASOA. These sources include emissions that are both traditional (transportation) as well as non-traditional emissions of emerging importance (VCPs) to ambient $PM_{2.5}$ concentrations in cities around the world. Further investigation of speciated IVOCs and SVOCs for urban areas around the world along with SOA mass concentration and other photochemical products (e.g., O_x, PAN, and HCHO) for other urban areas, especially in South Asia, throughout Africa, and throughout South America, would provide further constraints to improve the SIMPLE model and our understanding of the emission sources and chemistry that leads to the observed SOA and its impact on premature mortality.

Acknowledgements

This study was partially supported by grants from NASA NNX15AT96G, NNX16AQ26G, Sloan Foundation 2016-7173, NSF AGS-1822664, EPA STAR 83587701-0, NERC NE/H003510/1, NERC NE/H003177/1, NERC NE/H003223/1, NOAA NA17OAR4320101, NCAS R8/H12/83/037, Natural Science and Engineering Research Council of Canada (NSERC, RGPIN/05002-2014), and the Fonds de Recherche du Québec —Nature et technologies (FRQNT, 2016-PR-192364). This manuscript has not been formally reviewed by EPA. The views expressed in this document are solely those of the authors and do not necessarily reflect those of the Agency. EPA does not endorse any products or commercial services mentioned in this publication. We thank Katherine Travis for useful discussions. We acknowledge B J. Bandy, J. Lee, G. P. Mills, d. D. Montzka, J. Stutz, A. J. Weinheimer E. J. Williams, E. C. Wood, and D. R. Worsnop for use of their data.

Data Availability

TexAQS measurements are available at https://esrl.noaa.gov/csl/groups/csl7/measurements/2000TexAQS/LaPorte/DataDownload/ and upon request. NEAQS measurements are available at https://www.esrl.noaa.gov/csl/groups/csl7/measurements/2002NEAQS/. MILAGRO measurements are available at http://doi.org/10.5067/Aircraft/INTEXB/Aerosol-TraceGas. CalNex measurements are available at https://esrl.noaa.gov/csl/groups/csl7/measurements/2010calnex/Ground/DataDownload/. ClearfLo measurements are available at https://catalogue.ceda.ac.uk/uuid/6a5f9eedd68f43348692b3bace3eba45. SEAC^{4}RS measurements are available at http://doi.org/10.5067/Aircraft/SEAC4RS/Aerosol-TraceGas-Cloud. WINTER measurements are available at https://data.eol.ucar.edu/master_lists/generated/winter/. KORUS-AQ measurements are available at http://doi.org/10.5067/Suborbital/KORUSAQ/DATA01. Data from Chinese campaigns are available upon request, and rest of data used were located in papers cited. GEOS-Chem data available upon request. Figures will become accessible at cires1.colorado.edu/jimenez/group_pubs.html.

Competing Interests

The authors declare no competing interests.

Author Contribution

B.A.N., D.S.J., B.C.M., J.A.dG., and J.L.J designed the experiment and wrote the paper. B.A.N., PC.-J., D.A.D., W.H., J.C.S, J.A., D.R.B., M.R.C., H.C., M.M.C., P.F.D, G.S.D., R.D., F.F, A.F., J.B.G., G.G., J.F.H, T.F.H., P.L.H., J.H., M.H., L.G.H., B.T.J., W.C.K., J.L., I.B.P., J.P., B.R.,

C.E.R., D.R., J.M.R., T.B.R, M.S., J.W., C.W., P.W., G.M.W., D.E.Y., B.Y., J.A.dG., and J.L.J. collected and analyzed the data. D.S.J. and A.H. ran the GEOS-Chem model and B.A.N., D.S.J, and J.L.J. analyzed the model output. B.A.N., P.L.H., J.M.S., and J.L.J. ran and analyzed the 0-D model used for ASOA budget analysis of ambient observations. B.C.M., A.L., M.L., and Q.Z. analyzed and provided the emission inventories used for the 0-D box model. D.S.J., D.K.H., and M.O.N. conducted the ASOA attribution to mortality calculation, and B.A.N., D.S.J., D.K.H., M.O.N., J.A.dG, and J.L.J analyzed the results. All authors reviewed the paper.

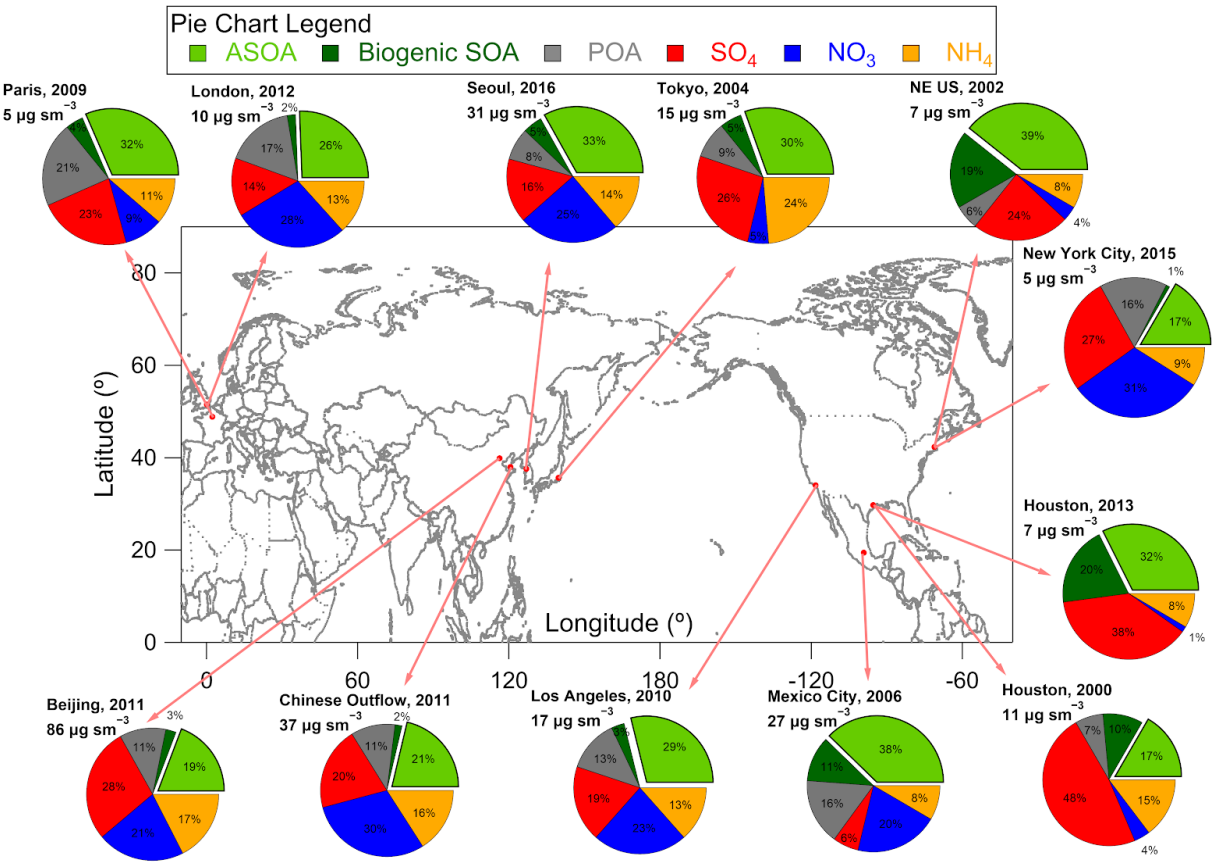

682

683 **Figure 1**. Non-refractory submicron aerosol composition measured in urban and urban outflow
684 regions from field campaigns used in this study, all in units of μg m^{-3}, at standard temperature
685 (273 K) and pressure (1013 hPa) (sm^{-3}). See Sect. S3 and Table 1 for further information on
686 measurements, studies, and apportionment of SOA into ASOA and BSOA.

687

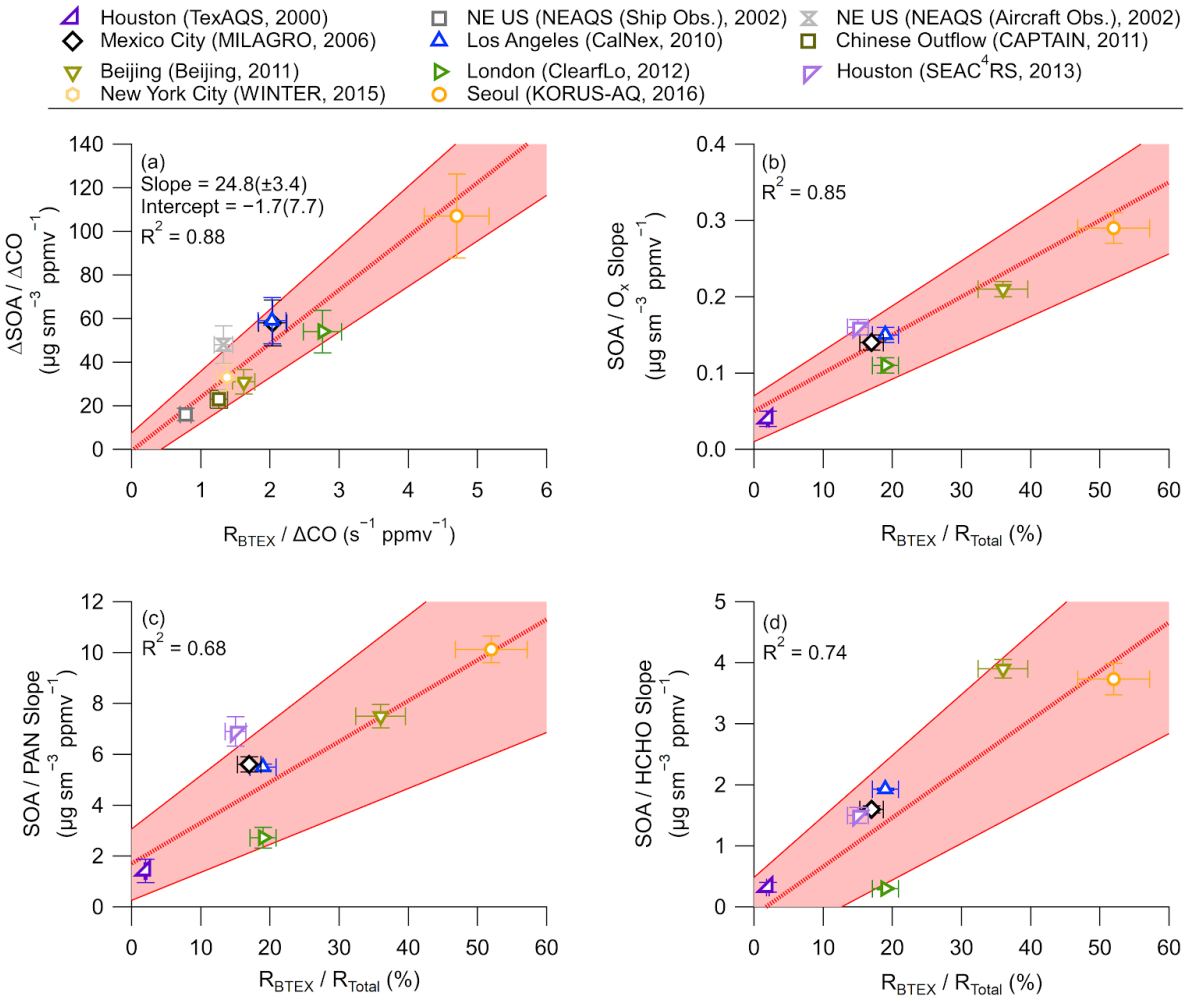

688 **Figure 2**. (a) Scatter plot of background and dilution corrected ASOA concentrations
689 (ΔSOA/ΔCO at PA = 0.5 equivalent days) versus BTEX emission reactivity ratio (R_{BTEX}=
690 $\sum_i [VOC/CO]_i$) for multiple major field campaigns on three continents. Comparison of ASOA
691 versus (b) Ox, (c) PAN, and (d) HCHO slopes versus the ratio of the BTEX/Total emission
692 reactivity, where total is the OH reactivity for the emissions of BTEX + C2-3 alkenes + C2-6
693 alkanes (Table S5 through Table S7), for the campaigns studied here. For all figures, red shading
694 is the ±1σ uncertainty of the slope, and the bars are ±1σ uncertainty of the data (see Sect. S5).

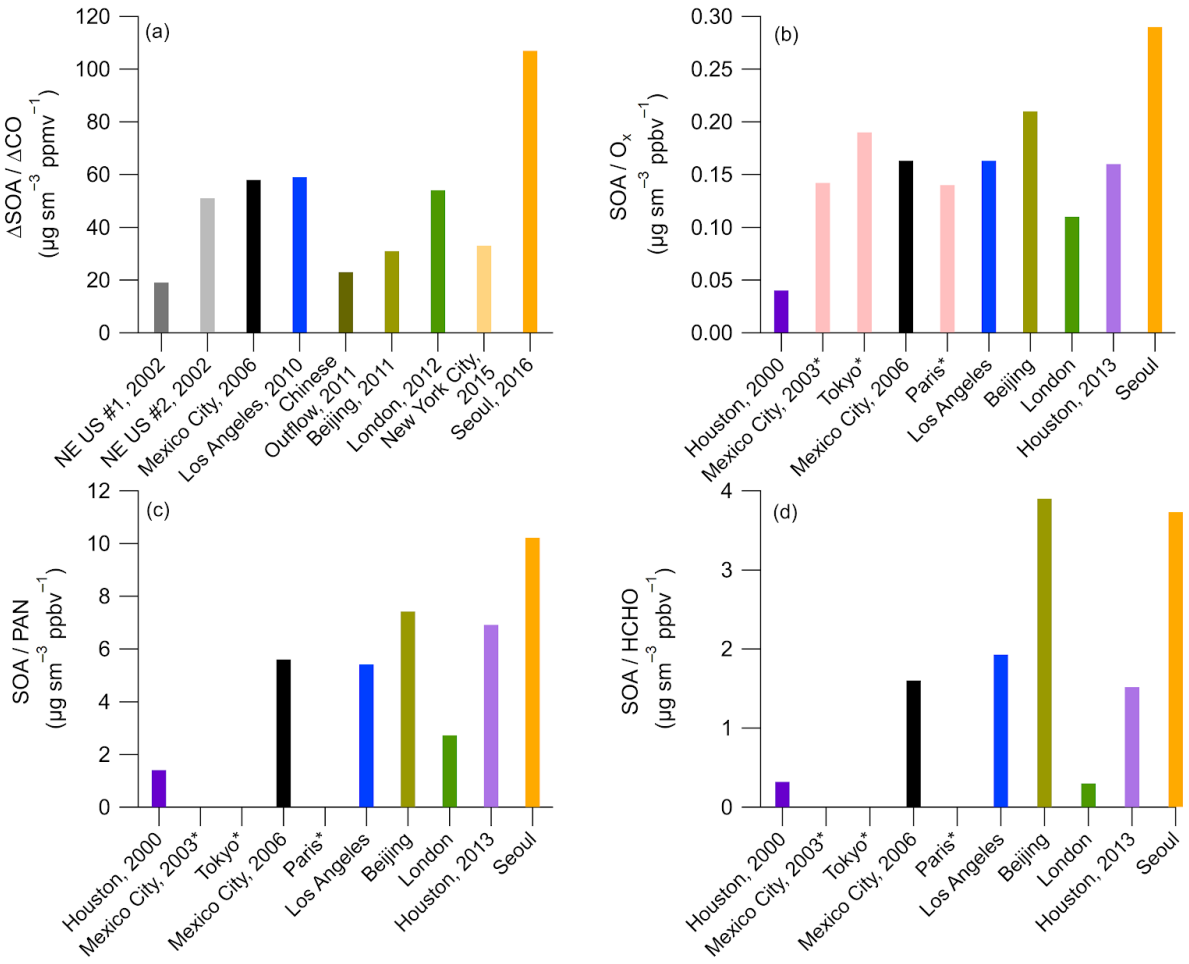

695

696 **Figure 3**. (a) A comparison of the ΔSOA/ΔCO for the urban campaigns on three continents.
697 Comparison of (b) SOA/Ox, (c) SOA/HCHO, and (d) SOA/PAN slopes for the urban areas
698 (Table S4). For (b) through (d), cities marked with * have no HCHO, PAN, or hydrocarbon data.

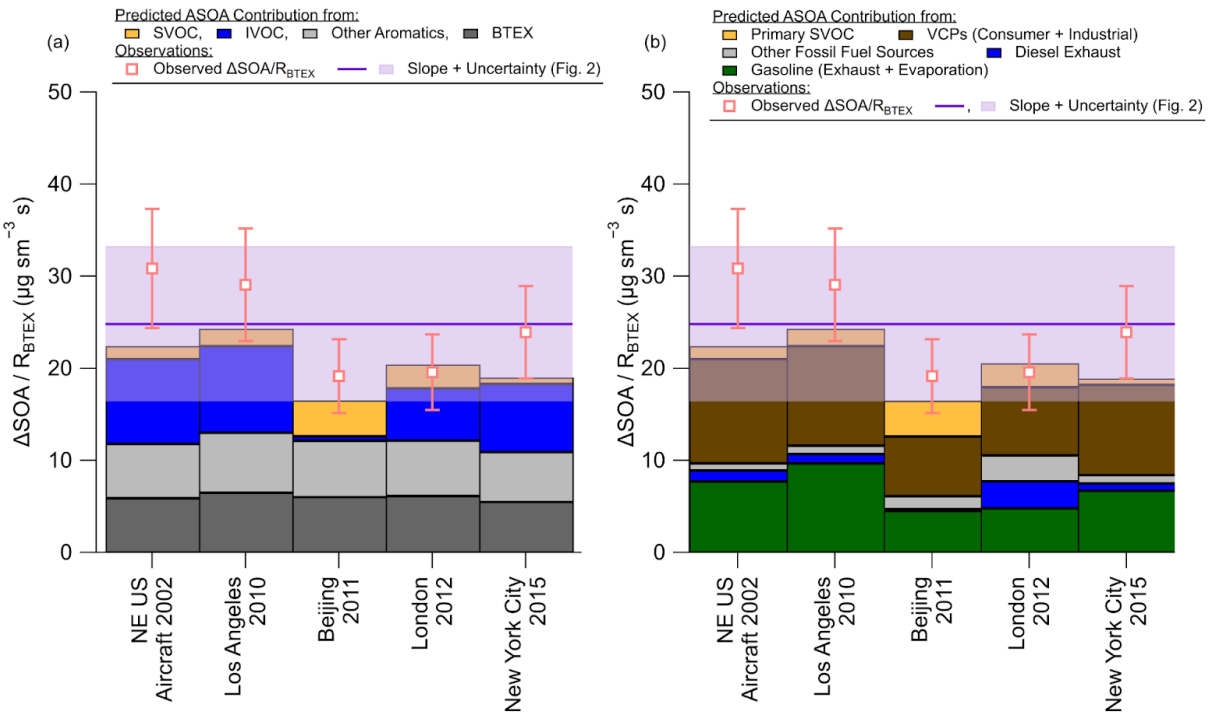

Figure 4. (a) Budget analysis for the contribution of the observed $\Delta SOA/R_{BTEX}$ (Fig. 2) for cities with known emissions inventories for different volatility classes (see SI and Fig. 5 and Fig. S6). (b) Same as (a), but for sources of emissions. For (a) and (b), SVOC is the contribution from both vehicle and other (cooking, etc.) sources. See SI for information about the emissions, ASOA precursor contribution, error analysis, and discussion about sensitivity of emission inventory IVOC/BTEX ratios for different cities and years in the US.

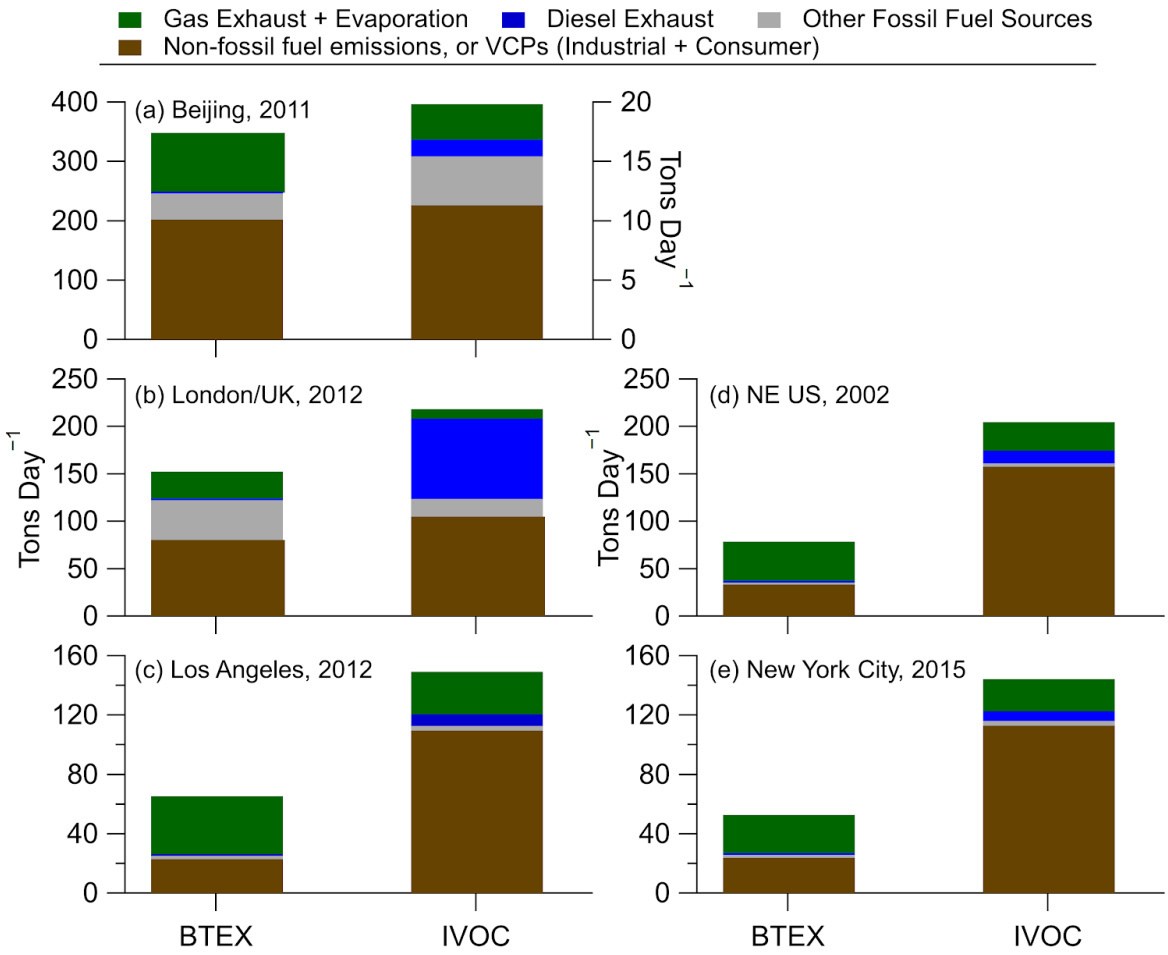

706

707 **Figure 5**. Comparison of BTEX and IVOC sources for (a) Beijing (see SI section about Beijing
708 emission inventory), (b) London (see SI section about London/UK emission inventory), and (c)
709 Los Angeles, (d) Northeast United States, and (e) New York City (see SI section about United
710 States for (c) – (e)). For (a), BTEX is on the left axis and IVOC is on the right axis, due to the
711 small emissions per day for IVOC.

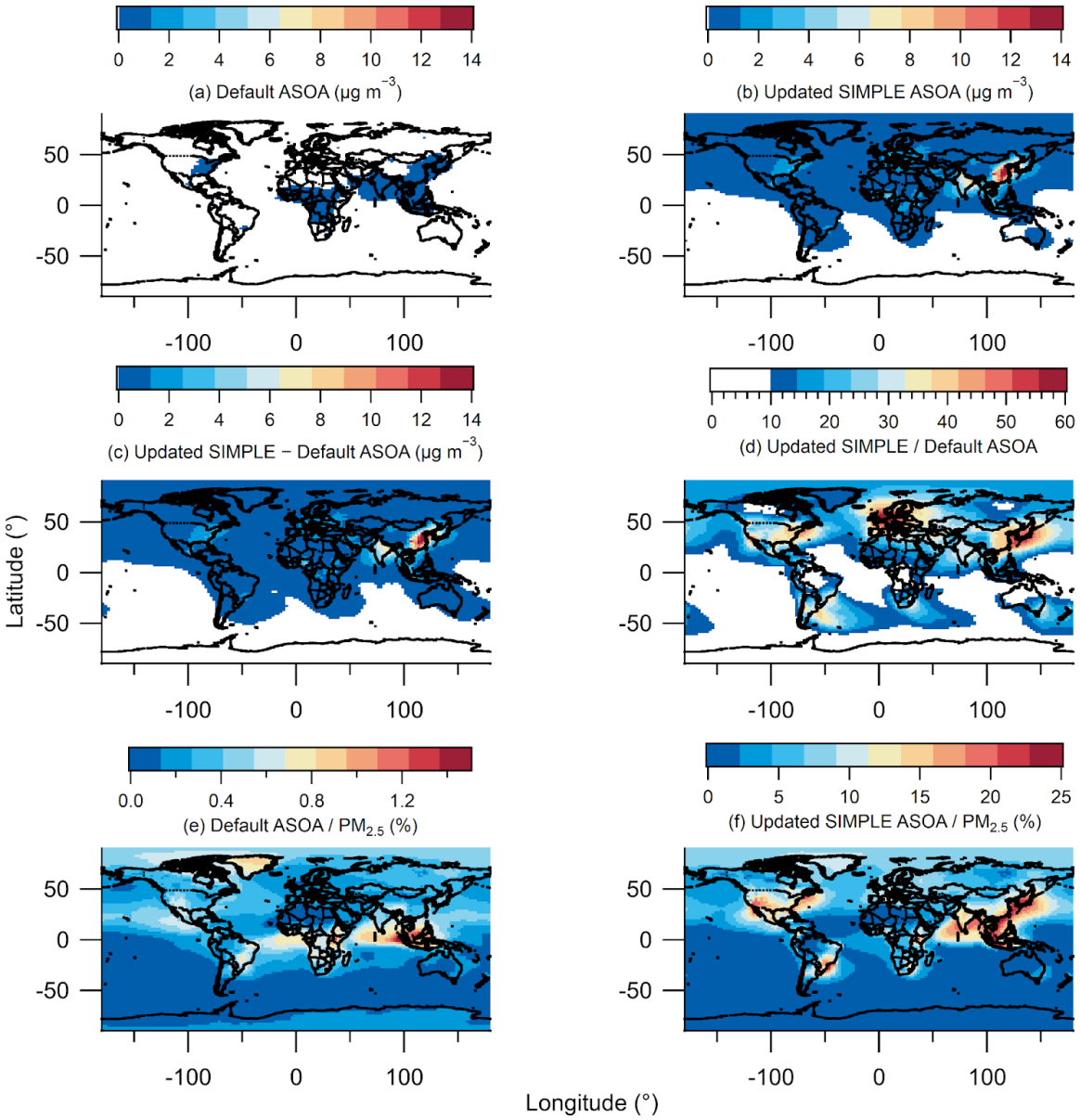

712

713 **Figure 6.** (a) Annual average modeled ASOA using the default VBS. (b) Annual average
714 modeled ASOA using the updated SIMPLE model. (c) Difference between annual average
715 modeled updated SIMPLE and default VBS. Note, for (a) - (b), values less than 0.05 µg m^{-3} are
716 white, and for (c), values less than 0.02 µg m^{-3} are white. (d) Ratio between annual average
717 modeled updated SIMPLE (b) and default VBS (a). (e) Percent contribution of annual average
718 modeled ASOA using default VBS to total modelled $PM_{2.5}$. (f) Percent contribution of annual
719 average modeled ASOA using updated SIMPLE to total modelled $PM_{2.5}$.

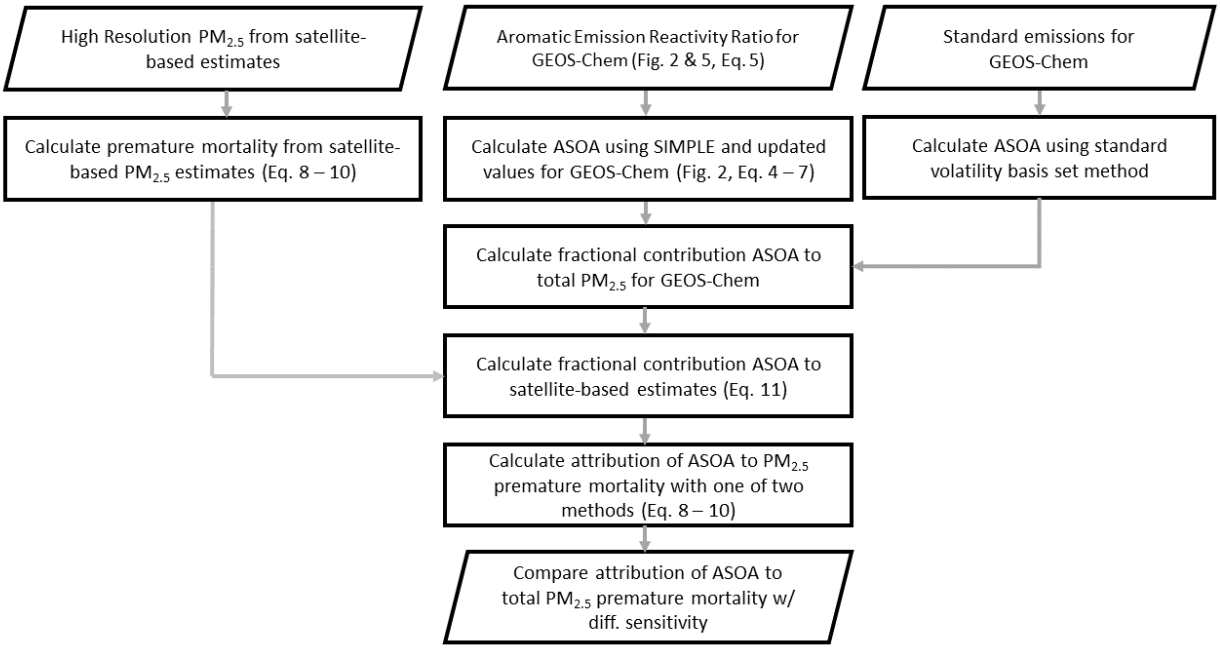

720

721 **Figure 7**. Flowchart describing how observed ASOA production was used to calculate ASOA in
722 GEOS-Chem, and how the satellite-based $PM_{2.5}$ estimates and GEOS-Chem $PM_{2.5}$ speciation was
723 used to estimate the premature mortality and attribution of premature mortality by ASOA. See
724 Sect. 2 and SI for further information about the details in the figure. SIMPLE is described in
725 Eq. 4 and by Hodzic and Jimenez (2011) and Hayes et al. (2015). The one of two methods
726 mentioned include either the Integrated Exposure-Response (IER) (Burnett et al., 2014) with
727 Global Burden of Disease (GBD) dataset (IHME, 2016) or the new Global Exposure Mortality
728 Model (GEMM) (Burnett et al., 2018) methods. For both IER and GEMM, the marginal method
729 (Silva et al., 2016) or attributable fraction method (Anenberg et al., 2019) are used.

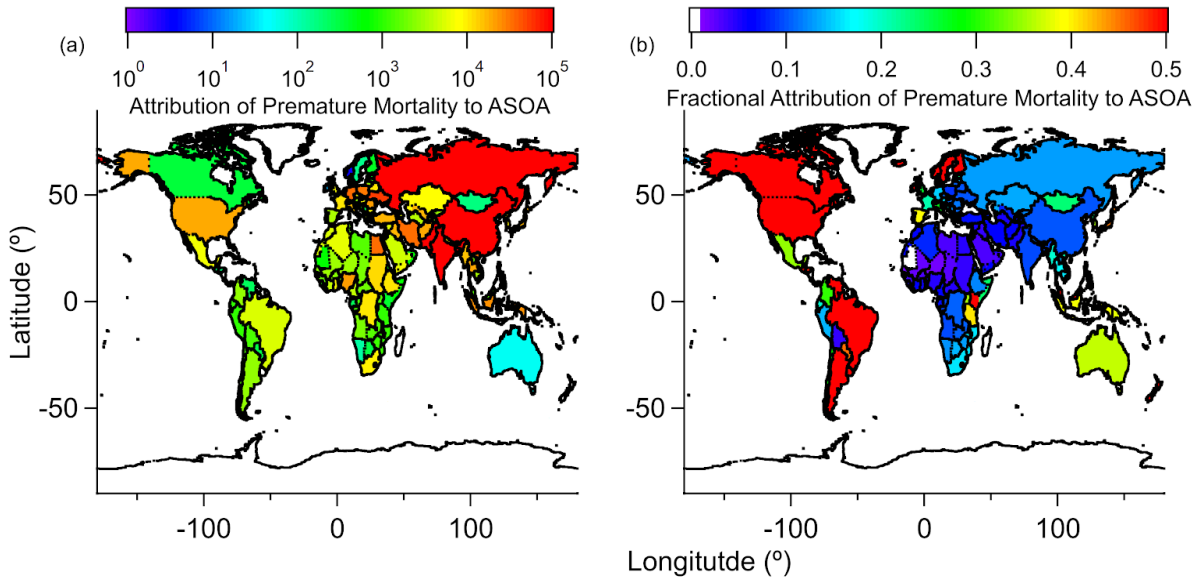

Figure 8. Five-year average (a) estimated reduction in $PM_{2.5}$-associated premature deaths, by country, upon removing ASOA from total $PM_{2.5}$, and (b) fractional reduction (reduction $PM_{2.5}$ premature deaths / total $PM_{2.5}$ premature deaths) in $PM_{2.5}$-associated premature deaths, by country, upon removing ASOA from GEOS-Chem. The IER methods are used here. See Fig. S9 and Fig. S12 for results using GEMM. See Fig. S10 for 10×10 km^2 area results in comparison with country-level results.

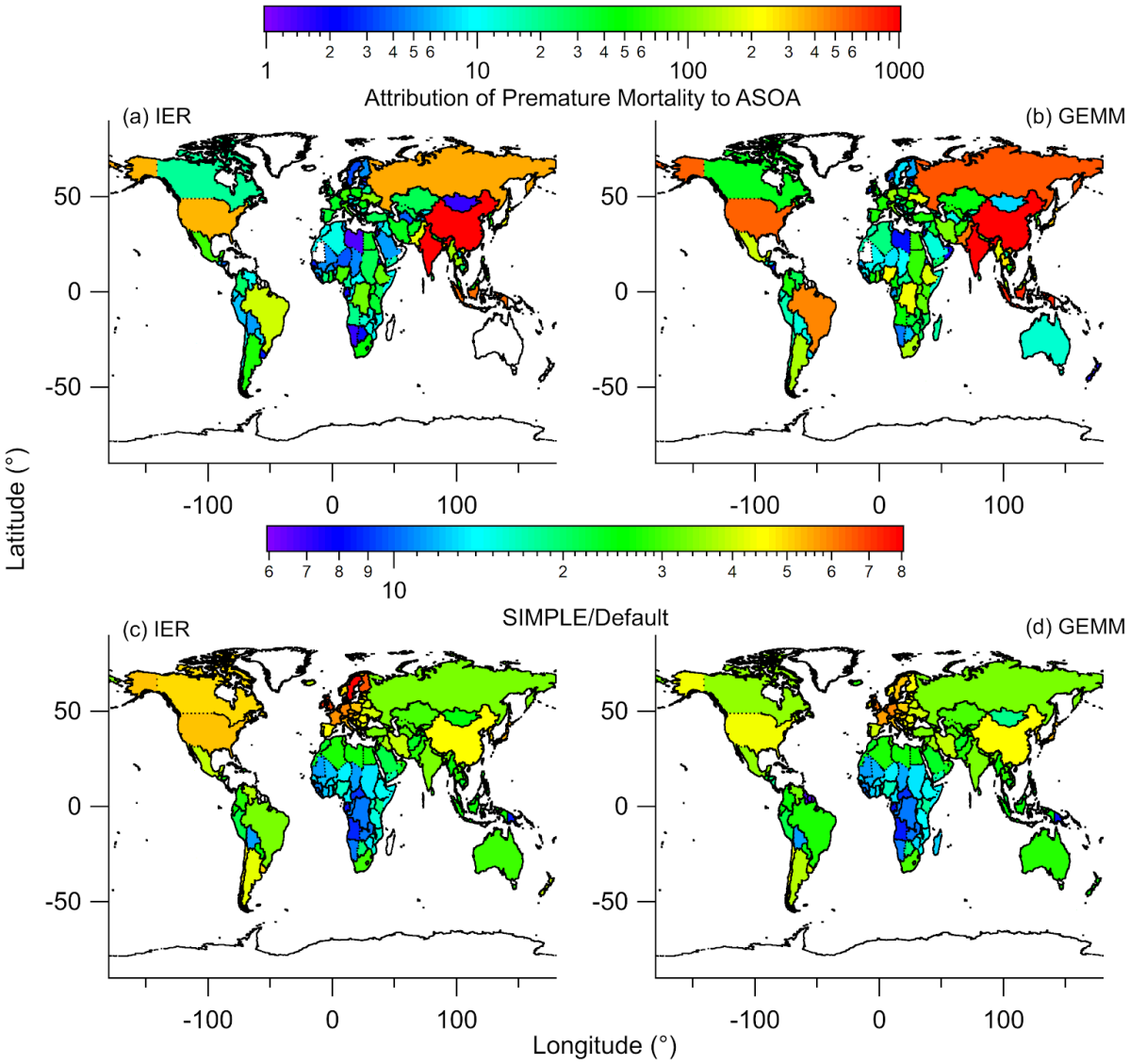

737

738 **Figure 9**. Attribution of premature mortality to ASOA using (a) IER or (b) GEMM, using the
739 non-volatile primary OA and traditional SOA precursors method in prior studies (e.g., Ridley et
740 al., 2018). The increase in attribution of premature mortality to ASOA for the "SIMPLE" model
741 (Fig. 8) versus the non-volatile primary OA and traditional SOA precursor method ("Default"),
742 for (c) IER and (d) GEMM.

Table 1. List of campaigns used here. For values previously reported for those campaigns, they are noted. For Seasons, W = Winter, Sp = Spring, and Su = Summer.

Location	Field Campaign	Coordinates		Time Period	Season	Previous Publication/Campaign Overview
		Long. (°)	Lat. (°)			
Houston, TX, USA (2000)	TexAQS 2000	−95.4	29.8	15/Aug/2000 - 15/Sept/2000	Su	Jimenez et al. (2009)[a], Wood et al. (2010)[b]
Northeast USA (2002)	NEAQS 2002	−78.1 - −70.5	32.8 - 43.1	26/July/2002; 29/July/2002 - 10/Aug/2002	Su	Jimenez et al. (2009)[a], de Gouw and Jimenez (2009)[c], Kleinman et al. (2007)[c]
Mexico City, Mexico (2003)	MCMA-2003	−99.2	19.5	31/Mar/2003 - 04/May/2003	Sp	Molina et al. (2007), Herndon et al. (2008)[b]
Tokyo, Japan (2004)		139.7	35.7	24/July/2004 - 14/Aug/2004	Su	Kondo et al. (2008)[a], Miyakawa et al. (2008)[a], Morino et al. (2014)[b]
Mexico City, Mexico (2006)	MILAGRO	−99.4 - −98.6	19.0 − 19.8	04/Mar/2006 - 29/Mar/2006	Sp	Molina et al. (2010), DeCarlo et al. (2008)[a], Wood et al. (2010)[b], DeCarlo et al. (2010)[c]
Paris, France (2009)	MEGAPOLI	48.9	2.4	13/July/2009 - 29/July/2009	Su	Freney et al. (2014)[a], Zhang et al. (2015)[b]
Pasadena, CA, USA (2010)	CalNex	−118.1	34.1	15/May/2010 - 16/June/2010	Sp	Ryerson et al. (2013), Hayes et al. (2013)[a,b,c]
Changdao Island, China (2011)	CAPTAIN	120.7	38.0	21/Mar/2011 - 24/Apr/2011	Sp	Hu et al. (2013)[a,c]
Beijing, China (2011)	CareBeijing 2011	116.4	39.9	03/Aug/2011 - 15/Sept/2011	Su	Hu et al. (2016)[a,b,c]
London, UK (2012)	ClearfLo	0.1	51.5	22/July/2012 - 18/Aug/2012	Su	Bohnenstengel et al. (2015)
Houston, TX, USA (2013)	SEAC^{4}RS	−96.0 - −94.0	29.2 - 30.3	01/Aug/2013 - 23/Sept/2013	Su	Toon et al. (2016)
New York City, NY, USA (2015)	WINTER	−74.0 - −69.0	39.5 - 42.5	07/Feb/2015	W	Schroder et al. (2018)[a,c]
Seoul, South Korea (2016)	KORUS-AQ	124.6 - 128.0	36.8 - 37.6	01/May/2016 - 10/June/2016	Sp	Nault et al. (2018)[a,b,c,d]

[a]Reference used for PM_1 composition. [b]Reference used for SOA/O_x slope. [c]Reference used for ΔOA/ΔCO value. [d]Reference used for SOA/HCHO and SOA/PAN slopes

References

Anenberg, S., Miller, J., Henze, D. and Minjares, R.: A global snapshot of the air pollution-related health impacts of transportation sector emissions in 2010 and 2015, ICCT, Climate & Clean Air Coalition., 2019.

Atkinson, R. and Arey, J.: Atmospheric Degradation of Volatile Organic Compounds, Chem. Rev., 103, 4605–4638, 2003.

Atkinson, R., Baulch, D. L., Cox, R. A., Crowley, J. N., Hampson, R. F., Hynes, R. G., Jenkin, M. E., Rossi, M. J., Troe, J. and IUPAC Subcommittee: Evaluated kinetic and photochemical data for atmospheric chemistry: Volume II - gas phase reactions of organic species, Atmos. Chem. Phys., 6(11), 3625–4055, 2006.

Bae, M.-S., Demerjian, K. L. and Schwab, J. J.: Seasonal estimation of organic mass to organic carbon in PM2.5 at rural and urban locations in New York state, Atmos. Environ., 40(39), 7467–7479, 2006.

Baker, K. R., Woody, M. C., Valin, L., Szykman, J., Yates, E. L., Iraci, L. T., Choi, H. D., Soja, A. J., Koplitz, S. N., Zhou, L., Campuzano-Jost, P., Jimenez, J. L. and Hair, J. W.: Photochemical model evaluation of 2013 California wild fire air quality impacts using surface, aircraft, and satellite data, Sci. Total Environ., 637-638, 1137–1149, 2018.

Bertram, T. H., Perring, A. E., Wooldridge, P. J., Crounse, J. D., Kwan, A. J., Wennberg, P. O., Scheuer, E., Dibb, J., Avery, M., Sachse, G., Vay, S. A., Crawford, J. H., McNaughton, C. S., Clarke, A., Pickering, K. E., Fuelberg, H., Huey, G., Blake, D. R., Singh, H. B., Hall, S. R., Shetter, R. E., Fried, A., Heikes, B. G. and Cohen, R. C.: Direct Measurements of the Convective Recycling of the Upper Troposphere, Science, 315(5813), 816–820, 2007.

Bohnenstengel, S. I., Belcher, S. E., Aiken, A., Allan, J. D., Allen, G., Bacak, A., Bannan, T. J., Barlow, J. F., Beddows, D. C. S., Bloss, W. J., Booth, A. M., Chemel, C., Coceal, O., Di Marco, C. F., Dubey, M. K., Faloon, K. H., Fleming, Z. L., Furger, M., Gietl, J. K., Graves, R. R., Green, D. C., Grimmond, C. S. B., Halios, C. H., Hamilton, J. F., Harrison, R. M., Heal, M. R., Heard, D. E., Helfter, C., Herndon, S. C., Holmes, R. E., Hopkins, J. R., Jones, A. M., Kelly, F. J., Kotthaus, S., Langford, B., Lee, J. D., Leigh, R. J., Lewis, A. C., Lidster, R. T., Lopez-Hilfiker, F. D., McQuaid, J. B., Mohr, C., Monks, P. S., Nemitz, E., Ng, N. L., Percival, C. J., Prévôt, A. S. H., Ricketts, H. M. A., Sokhi, R., Stone, D., Thornton, J. A., Tremper, A. H., Valach, A. C., Visser, S., Whalley, L. K., Williams, L. R., Xu, L., Young, D. E., Zotter, P., Bohnenstengel, S. I., Belcher, S. E., Aiken, A., Allan, J. D., Allen, G., Bacak, A., Bannan, T. J., Barlow, J. F., Beddows, D. C. S., Bloss, W. J., Booth, A. M., Chemel, C., Coceal, O., Marco, C. F. D., Dubey, M. K., Faloon, K. H., Fleming, Z. L., Furger, M., Gietl, J. K., Graves, R. R., Green, D. C., Grimmond, C. S. B., Halios, C. H., Hamilton, J. F., Harrison, R. M., Heal, M. R., Heard, D. E., Helfter, C., Herndon, S. C., Holmes, R. E., Hopkins, J. R., Jones, A. M., Kelly, F. J., Kotthaus, S., Langford, B., Lee, J. D., Leigh, R. J., Lewis, A. C., Lidster, R. T., Lopez-Hilfiker, F. D., et al.: Meteorology, Air Quality, and Health in London: The ClearfLo Project, Bull. Am. Meteorol.

Soc., 96(5), 779–804, 2015.

Burnett, R., Chen, H., Szyszkowicz, M., Fann, N., Hubbell, B., Pope, C. A., Apte, J. S., Brauer, M., Cohen, A., Weichenthal, S., Coggins, J., Di, Q., Brunekreef, B., Frostad, J., Lim, S. S., Kan, H., Walker, K. D., Thurston, G. D., Hayes, R. B., Lim, C. C., Turner, M. C., Jerrett, M., Krewski, D., Gapstur, S. M., Diver, W. R., Ostro, B., Goldberg, D., Crouse, D. L., Martin, R. V., Peters, P., Pinault, L., Tjepkema, M., van Donkelaar, A., Villeneuve, P. J., Miller, A. B., Yin, P., Zhou, M., Wang, L., Janssen, N. A. H., Marra, M., Atkinson, R. W., Tsang, H., Quoc Thach, T., Cannon, J. B., Allen, R. T., Hart, J. E., Laden, F., Cesaroni, G., Forastiere, F., Weinmayr, G., Jaensch, A., Nagel, G., Concin, H. and Spadaro, J. V.: Global estimates of mortality associated with long-term exposure to outdoor fine particulate matter, Proc. Natl. Acad. Sci. U. S. A., 115(38), 9592–9597, 2018.

Burnett, R. T., Pope, C. A., Ezzati, M., Olives, C., Lim, S. S., Mehta, S., Shin, H. H., Singh, G., Hubbell, B., Brauer, M., Anderson, H. R., Smith, K. R., Balmes, J. R., Bruce, N. G., Kan, H., Laden, F., Prüss-Ustün, A., Turner, M. C., Gapstur, S. M., Diver, W. R. and Cohen, A.: An integrated risk function for estimating the global burden of disease attributable to ambient fine particulate matter exposure, Environ. Health Perspect., 122(4), 397–403, 2014.

Cappa, C. D., Jathar, S. H., Kleeman, M. J., Docherty, K. S., Jimenez, J. L., Seinfeld, J. H. and Wexler, A. S.: Simulating secondary organic aerosol in a regional air quality model using the statistical oxidation model - Part 2: Assessing the influence of vapor wall losses, Atmos. Chem. Phys., 16(5), 3041–3059, 2016.

Chafe, Z., Brauer, M., Heroux, M.-E., Klimont, Z., Lanki, T., Salonen, R. O. and Smith, K. R.: Residential heating with wood and coal: Health impacts and policy options in Europe and North America, WHO/UNECE LRTAP., 2015.

CIESIN: Gridded Population of the World (GPW), v4, SEDAC [online] Available from: https://sedac.ciesin.columbia.edu/data/collection/gpw-v4 (Accessed 12 May 2020), 2017.

Coggon, M. M., McDonald, B. C., Vlasenko, A., Veres, P. R., Bernard, F., Koss, A. R., Yuan, B., Gilman, J. B., Peischl, J., Aikin, K. C., DuRant, J., Warneke, C., Li, S.-M. and de Gouw, J. A.: Diurnal Variability and Emission Pattern of Decamethylcyclopentasiloxane (D_5) from the Application of Personal Care Products in Two North American Cities, Environ. Sci. Technol., 52(10), 5610–5618, 2018.

Cohen, A. J., Brauer, M., Burnett, R., Anderson, H. R., Frostad, J., Estep, K., Balakrishnan, K., Brunekreef, B., Dandona, L., Dandona, R., Feigin, V., Freedman, G., Hubbell, B., Jobling, A., Kan, H., Knibbs, L., Liu, Y., Martin, R., Morawska, L., Pope, C. A., Shin, H., Straif, K., Shaddick, G., Thomas, M., van Dingenen, R., van Donkelaar, A., Vos, T., Murray, C. J. L. and Forouzanfar, M. H.: Estimates and 25-year trends of the global burden of disease attributable to ambient air pollution: an analysis of data from the Global Burden of Diseases Study 2015, Lancet, 389(10082), 1907–1918, 2017.

DeCarlo, P. F., Dunlea, E. J., Kimmel, J. R., Aiken, A. C., Sueper, D., Crounse, J., Wennberg, P.

O., Emmons, L., Shinozuka, Y., Clarke, A., Zhou, J., Tomlinson, J., Collins, D. R., Knapp, D., Weinheimer, A. J., Montzka, D. D., Campos, T. and Jimenez, J. L.: Fast airborne aerosol size and chemistry measurements above Mexico City and Central Mexico during the MILAGRO campaign, Atmos. Chem. Phys., 8(14), 4027–4048, 2008.

DeCarlo, P. F., Ulbrich, I. M., Crounse, J., de Foy, B., Dunlea, E. J., Aiken, A. C., Knapp, D., Weinheimer, A. J., Campos, T., Wennberg, P. O. and Jimenez, J. L.: Investigation of the sources and processing of organic aerosol over the Central Mexican Plateau from aircraft measurements during MILAGRO, Atmos. Chem. Phys., 10(12), 5257–5280, 2010.

Deming, B., Pagonis, D., Liu, X., Talukdar, R. K., Roberts, J. M., Veres, P. R., Krechmer, J. E., de Gouw, J. A., Jimenez, J. L. and Zieman, P. J.: Measurements of Delays of Gas-Phase Compounds in a Wide Variety of Tubing Materials due to Gas-Wall Partitioning, Atmos. Meas. Tech., In Prep., 2018.

Dominutti, P., Keita, S., Bahino, J., Colomb, A., Liousse, C., Yoboué, V., Galy-Lacaux, C., Morris, E., Bouvier, L., Sauvage, S. and Borbon, A.: Anthropogenic VOCs in Abidjan, southern West Africa: from source quantification to atmospheric impacts, Atmos. Chem. Phys., 19(18), 11721–11741, 2019.

van Donkelaar, A., Martin, R. V., Brauer, M. and Boys, B. L.: Use of Satellite Observations for Long-Term Exposure Assessment of Global Concentrations of Fine Particulate Matter, Environ. Health Perspect., 123(2), 135–143, 2015.

van Donkelaar, A., Martin, R. V., Brauer, M., Hsu, N. C., Kahn, R. A., Levy, R. C., Lyapustin, A., Sayer, A. M. and Winker, D. M.: Global Estimates of Fine Particulate Matter using a Combined Geophysical-Statistical Method with Information from Satellites, Models, and Monitors, Environ. Sci. Technol., 50(7), 3762–3772, 2016.

Dzepina, K., Volkamer, R. M., Madronich, S., Tulet, P., Ulbrich, I. M., Zhang, Q., Cappa, C. D., Ziemann, P. J. and Jimenez, J. L.: Evaluation of recently-proposed secondary organic aerosol models for a case study in Mexico City, Atmos. Chem. Phys., 9(15), 5681–5709, 2009.

EMEP/EEA: EMEP/EEA Air Pollutant Emission Inventory Guidebook 2016, EEA, Luxembourg., 2016.

Ensberg, J. J., Hayes, P. L., Jimenez, J. L., Gilman, J. B., Kuster, W. C., de Gouw, J. A., Holloway, J. S., Gordon, T. D., Jathar, S., Robinson, A. L. and Seinfeld, J. H.: Emission factor ratios, SOA mass yields, and the impact of vehicular emissions on SOA formation, Atmos. Chem. Phys., 14(5), 2383–2397, 2014.

Freney, E. J., Sellegri, K., Canonaco, F., Colomb, A., Borbon, A., Michoud, V., Crumeyrolle, S., Amarouche, N., Bourianne, T., Gomes, L., Prevot, A. S. H., Beekmann, M. and Schwarzenböeck, A.: Characterizing the impact of urban emissions on regional aerosol particles: Airborne measurements during the MEGAPOLI experiment, Atmos. Chem. Phys., 14(3), 1397–1412, 2014.

Gentner, D. R., Isaacman, G., Worton, D. R., Chan, A. W. H., Dallmann, T. R., Davis, L., Liu, S., Day, D. A., Russell, L. M., Wilson, K. R., Weber, R., Guha, A., Harley, R. A. and Goldstein, A. H.: Elucidating secondary organic aerosol from diesel and gasoline vehicles through detailed characterization of organic carbon emissions, Proc. Natl. Acad. Sci. U. S. A., 109(45), 18318–18323, 2012.

Goel, R. and Guttikunda, S. K.: Evolution of on-road vehicle exhaust emissions in Delhi, Atmos. Environ., 105, 78–90, 2015.

de Gouw, J. A. and Jimenez, J. L.: Organic Aerosols in the Earth's Atmosphere, Environ. Sci. Technol., 43(20), 7614–7618, 2009.

de Gouw, J. A., Middlebrook, A. M., Warneke, C., Goldan, P. D., Kuster, W. C., Roberts, J. M., Fehsenfeld, F. C., Worsnop, D. R., Canagaratna, M. R., Pszenny, A. A. P., Keene, W. C., Marchewka, M., Bertman, S. B. and Bates, T. S.: Budget of organic carbon in a polluted atmosphere: Results from the New England Air Quality Study in 2002, J. Geophys. Res. D: Atmos., 110(16), 1–22, 2005.

de Gouw, J. A., Gilman, J. B., Kim, S.-W., Lerner, B. M., Isaacman-VanWertz, G., McDonald, B. C., Warneke, C., Kuster, W. C., Lefer, B. L., Griffith, S. M., Dusanter, S., Stevens, P. S. and Stutz, J.: Chemistry of Volatile Organic Compounds in the Los Angeles basin: Nighttime Removal of Alkenes and Determination of Emission Ratios, J. Geophys. Res.: Atmos., 122(21), 11,843–11,861, 2017.

de Gouw, J. A., Gilman, J. B., Kim, S.-W., Alvarez, S. L., Dusanter, S., Graus, M., Griffith, S. M., Isaacman-VanWertz, G., Kuster, W. C., Lefer, B. L., Lerner, B. M., McDonald, B. C., Rappenglück, B., Roberts, J. M., Stevens, P. S., Stutz, J., Thalman, R., Veres, P. R., Volkamer, R., Warneke, C., Washenfelder, R. A. and Young, C. J.: Chemistry of volatile organic compounds in the Los Angeles basin: Formation of oxygenated compounds and determination of emission ratios, J. Geophys. Res., 123(4), 2298–2319, 2018.

Grieshop, A. P., Logue, J. M., Donahue, N. M. and Robinson, A. L.: Laboratory investigation of photochemical oxidation of organic aerosol from wood fires 1: measurement and simulation of organic aerosol evolution, Atmos. Chem. Phys., 9(4), 1263–1277, 2009.

Hallquist, M., Wenger, J. C., Baltensperger, U., Rudich, Y., Simpson, D., Claeys, M., Dommen, J., Donahue, N. M., George, C., Goldstein, A. H., Hamilton, J. F., Herrmann, H., Hoffmann, T., Iinuma, Y., Jang, M., Jenkin, M. E., Jimenez, J. L., Kiendler-Scharr, A., Maenhaut, W., McFiggans, G., Mentel, T. F., Monod, A., Prévôt, A. S. H., Seinfeld, J. H., Surratt, J. D., Szmigielski, R. and Wildt, J.: The formation, properties and impact of secondary organic aerosol: current and emerging issues, Atmos. Chem. Phys., 9(14), 5155–5236, 2009.

Hayes, P. L., Ortega, A. M., Cubison, M. J., Froyd, K. D., Zhao, Y., Cliff, S. S., Hu, W. W., Toohey, D. W., Flynn, J. H., Lefer, B. L., Grossberg, N., Alvarez, S., Rappenglück, B., Taylor, J. W., Allan, J. D., Holloway, J. S., Gilman, J. B., Kuster, W. C., de Gouw, J. A., Massoli, P., Zhang, X., Liu, J., Weber, R. J., Corrigan, A. L., Russell, L. M., Isaacman, G., Worton, D. R.,

Kreisberg, N. M., Goldstein, A. H., Thalman, R., Waxman, E. M., Volkamer, R., Lin, Y. H., Surratt, J. D., Kleindienst, T. E., Offenberg, J. H., Dusanter, S., Griffith, S., Stevens, P. S., Brioude, J., Angevine, W. M. and Jimenez, J. L.: Organic aerosol composition and sources in Pasadena, California, during the 2010 CalNex campaign, J. Geophys. Res. D: Atmos., 118(16), 9233–9257, 2013.

Hayes, P. L., Carlton, A. G., Baker, K. R., Ahmadov, R., Washenfelder, R. A., Alvarez, S., Rappenglück, B., Gilman, J. B., Kuster, W. C., de Gouw, J. A., Zotter, P., Prévôt, A. S. H., Szidat, S., Kleindienst, T. E., Ma, P. K. and Jimenez, J. L.: Modeling the formation and aging of secondary organic aerosols in Los Angeles during CalNex 2010, Atmos. Chem. Phys., 15(10), 5773–5801, 2015.

Heringa, M. F., DeCarlo, P. F., Chirico, R., Tritscher, T., Dommen, J., Weingartner, E., Richter, R., Wehrle, G., Prévôt, A. S. H. and Baltensperger, U.: Investigations of primary and secondary particulate matter of different wood combustion appliances with a high-resolution time-of-flight aerosol mass spectrometer, Atmos. Chem. Phys., 11(12), 5945–5957, 2011.

Herndon, S. C., Onasch, T. B., Wood, E. C., Kroll, J. H., Canagaratna, M. R., Jayne, J. T., Zavala, M. A., Knighton, W. B., Mazzoleni, C., Dubey, M. K., Ulbrich, I. M., Jimenez, J. L., Seila, R., de Gouw, J. A., de Foy, B., Fast, J., Molina, L. T., Kolb, C. E. and Worsnop, D. R.: Correlation of secondary organic aerosol with odd oxygen in Mexico City, Geophys. Res. Lett., 35(15), L15804, 2008.

Hodzic, A. and Jimenez, J. L.: Modeling anthropogenically controlled secondary organic aerosols in a megacity: A simplified framework for global and climate models, Geosci. Model Dev., 4(4), 901–917, 2011.

Hodzic, A., Jimenez, J. L., Madronich, S., Aiken, A. C., Bessagnet, B., Curci, G., Fast, J., Lamarque, J.-F., Onasch, T. B., Roux, G., Schauer, J. J., Stone, E. A. and Ulbrich, I. M.: Modeling organic aerosols during MILAGRO: importance of biogenic secondary organic aerosols, Atmos. Chem. Phys., 9(18), 6949–6981, 2009.

Hodzic, A., Jimenez, J. L., Prévôt, A. S. H., Szidat, S., Fast, J. D. and Madronich, S.: Can 3-D models explain the observed fractions of fossil and non-fossil carbon in and near Mexico City?, Atmos. Chem. Phys., 10(22), 10997–11016, 2010a.

Hodzic, A., Jimenez, J. L., Madronich, S., Canagaratna, M. R., DeCarlo, P. F., Kleinman, L. and Fast, J.: Modeling organic aerosols in a megacity: potential contribution of semi-volatile and intermediate volatility primary organic compounds to secondary organic aerosol formation, Atmos. Chem. Phys., 10(12), 5491–5514, 2010b.

Hodzic, A., Campuzano-Jost, P., Bian, H., Chin, M., Colarco, P. R., Day, D. A., Froyd, K. D., Heinold, B., Jo, D. S., Katich, J. M., Kodros, J. K., Nault, B. A., Pierce, J. R., Ray, E., Schacht, J., Schill, G. P., Schroder, J. C., Schwarz, J. P., Sueper, D. T., Tegen, I., Tilmes, S., Tsigaridis, K., Yu, P. and Jimenez, J. L.: Characterization of Organic Aerosol across the Global Remote Troposphere: A comparison of ATom measurements and global chemistry models, Atmos.

Chem. Phys., 20(8), 4607–4635, 2020.

Hu, W., Hu, M., Hu, W., Jimenez, J. L., Yuan, B., Chen, W., Wang, M., Wu, Y., Chen, C., Wang, Z., Peng, J., Zeng, L. and Shao, M.: Chemical composition, sources, and aging process of submicron aerosols in Beijing: Contrast between summer and winter, J. Geophys. Res. D: Atmos., 121(4), 1955–1977, 2016.

Hu, W., Downward, G., Wong, J. Y. Y., Reiss, B., Rothman, N., Portengen, L., Li, J., Jones, R. R., Huang, Y., Yang, K., Chen, Y., Xu, J., He, J., Bassig, B., Seow, W. J., Hosgood, H. D., Zhang, L., Wu, G., Wei, F., Vermeulen, R. and Lan, Q.: Characterization of outdoor air pollution from solid fuel combustion in Xuanwei and Fuyuan, a rural region of China, Sci. Rep., 10(1), 11335, 2020.

Hu, W. W., Hu, M., Yuan, B., Jimenez, J. L., Tang, Q., Peng, J. F., Hu, W., Shao, M., Wang, M., Zeng, L. M., Wu, Y. S., Gong, Z. H., Huang, X. F. and He, L. Y.: Insights on organic aerosol aging and the influence of coal combustion at a regional receptor site of central eastern China, Atmos. Chem. Phys., 13(19), 10095–10112, 2013.

IHME: Global Burden of Disease Study 2015 (GBD 2015) Data Resources, GHDx [online] Available from: http://ghdx.healthdata.org/gbd-2015 (Accessed 2019), 2016.

Janssen, R. H. H., Tsimpidi, A. P., Karydis, V. A., Pozzer, A., Lelieveld, J., Crippa, M., Prévôt, A. S. H., Ait-Helal, W., Borbon, A., Sauvage, S. and Locoge, N.: Influence of local production and vertical transport on the organic aerosol budget over Paris, J. Geophys. Res. D: Atmos., 122(15), 8276–8296, 2017.

Janssens-Maenhout, G., Crippa, M., Guizzardi, D., Dentener, F., Muntean, M., Pouliot, G., Keating, T., Zhang, Q., Kurokawa, J., Wankmüller, R., Denier van der Gon, H., Kuenen, J. J. P., Klimont, Z., Frost, G., Darras, S., Koffi, B. and Li, M.: HTAP_v2.2: a mosaic of regional and global emission grid maps for 2008 and 2010 to study hemispheric transport of air pollution, Atmos. Chem. Phys., 15(19), 11411–11432, 2015.

Jathar, S. H., Woody, M., Pye, H. O. T., Baker, K. R. and Robinson, A. L.: Chemical transport model simulations of organic aerosol in southern California: model evaluation and gasoline and diesel source contributions, Atmos. Chem. Phys., 17(6), 4305–4318, 2017.

Jena, C., Ghude, S. D., Kulkarni, R., Debnath, S., Kumar, R., Soni, V. K., Acharja, P., Kulkarni, S. H., Khare, M., Kaginalkar, A. J., Chate, D. M., Ali, K., Nanjundiah, R. S. and Rajeevan, M. N.: Evaluating the sensitivity of fine particulate matter ($PM_{2.5}$) simulations to chemical mechanism in Delhi, Atmos. Chem. Phys. Discuss., doi:10.5194/acp-2020-673, 2020.

Jimenez, J. L., Canagaratna, M. R., Donahue, N. M., Prevot, A. S. H., Zhang, Q., Kroll, J. H., DeCarlo, P. F., Allan, J. D., Coe, H., Ng, N. L., Aiken, A. C., Docherty, K. S., Ulbrich, I. M., Grieshop, A. P., Robinson, A. L., Duplissy, J., Smith, J. D., Wilson, K. R., Lanz, V. A., Hueglin, C., Sun, Y. L., Tian, J., Laaksonen, A., Raatikainen, T., Rautiainen, J., Vaattovaara, P., Ehn, M., Kulmala, M., Tomlinson, J. M., Collins, D. R., Cubison, M. J., Dunlea, E. J., Huffman, J. A.,

Onasch, T. B., Alfarra, M. R., Williams, P. I., Bower, K., Kondo, Y., Schneider, J., Drewnick, F., Borrmann, S., Weimer, S., Demerjian, K., Salcedo, D., Cottrell, L., Griffin, R., Takami, A., Miyoshi, T., Hatakeyama, S., Shimono, A., Sun, J. Y., Zhang, Y. M., Dzepina, K., Kimmel, J. R., Sueper, D., Jayne, J. T., Herndon, S. C., Trimborn, A. M., Williams, L. R., Wood, E. C., Middlebrook, A. M., Kolb, C. E., Baltensperger, U. and Worsnop, D. R.: Evolution of organic aerosols in the atmosphere, Science, 326(5959), 1525–1529, 2009.

Khare, P. and Gentner, D. R.: Considering the future of anthropogenic gas-phase organic compound emissions and the increasing influence of non-combustion sources on urban air quality, Atmos. Chem. Phys., 18(8), 5391–5413, 2018.

Khare, P., Machesky, J., Soto, R., He, M., Presto, A. A. and Gentner, D. R.: Asphalt-related emissions are a major missing nontraditional source of secondary organic aerosol precursors, Sci Adv, 6(36), doi:10.1126/sciadv.abb9785, 2020.

Kleinman, L. I., Daum, P. H., Lee, Y.-N., Senum, G. I., Springston, S. R., Wang, J., Berkowitz, C., Hubbe, J., Zaveri, R. A., Brechtel, F. J., Jayne, J., Onasch, T. B. and Worsnop, D.: Aircraft observations of aerosol composition and ageing in New England and Mid-Atlantic States during the summer 2002 New England Air Quality Study field campaign, J. Geophys. Res. D: Atmos., 112(D9), D09310, 2007.

Kodros, J. K., Carter, E., Brauer, M., Volckens, J., Bilsback, K. R., L'Orange, C., Johnson, M. and Pierce, J. R.: Quantifying the Contribution to Uncertainty in Mortality Attributed to Household, Ambient, and Joint Exposure to PM2.5 From Residential Solid Fuel Use, Geohealth, 2(1), 25–39, 2018.

Kodros, J. K., Papanastasiou, D. K., Paglione, M., Masiol, M., Squizzato, S., Florou, K., Skyllakou, K., Kaltsonoudis, C., Nenes, A. and Pandis, S. N.: Rapid dark aging of biomass burning as an overlooked source of oxidized organic aerosol, Proc. Natl. Acad. Sci. U. S. A., 117(52), 33028–33033, 2020.

Kondo, Y., Morino, Y., Fukuda, M., Kanaya, Y., Miyazaki, Y., Takegawa, N., Tanimoto, H., McKenzie, R., Johnston, P., Blake, D. R., Murayama, T. and Koike, M.: Formation and transport of oxidized reactive nitrogen, ozone, and secondary organic aerosol in Tokyo, J. Geophys. Res. D: Atmos., 113(D21), D21310, 2008.

Krechmer, J. E., Pagonis, D., Ziemann, P. J. and Jimenez, J. L.: Quantification of Gas-Wall Partitioning in Teflon Environmental Chambers Using Rapid Bursts of Low-Volatility Oxidized Species Generated in Situ, Environ. Sci. Technol., 50(11), 5757–5765, 2016.

Krewski, D., Jerrett, M., Burnett, R. T., Ma, R., Hughes, E., Shi, Y., Turner, M. C., Arden, C., Thurston, G., Calle, E. E., Thun, M. J., Beckerman, B., Deluca, P., Finkelstein, N., Ito, K., Moore, D. K., Newbold, K. B., Ramsay, T., Ross, Z., Shin, H. and Tempalski, B.: Extended Follow-Up and Spatial Analysis of the American Cancer Society Study Linking Particulate Air Pollution and Mortality Number 140 May 2009 PRESS VERSION., 2009.

Lacey, F. G., Henze, D. K., Lee, C. J., van Donkelaar, A. and Martin, R. V.: Transient climate and ambient health impacts due to national solid fuel cookstove emissions, Proc. Natl. Acad. Sci. U. S. A., 114(6), 1269–1274, 2017.

Lam, N. L., Upadhyay, B., Maharjan, S., Jagoe, K., Weyant, C. L., Thompson, R., Uprety, S., Johnson, M. A. and Bond, T. C.: Seasonal fuel consumption, stoves, and end-uses in rural households of the far-western development region of Nepal, Environ. Res. Lett., 12(12), 125011, 2017.

Landrigan, P. J., Fuller, R., Acosta, N. J. R., Adeyi, O., Arnold, R., Basu, N., Baldé, A. B., Bertollini, R., Bose-O'Reilly, S., Boufford, J. I., Breysse, P. N., Chiles, T., Mahidol, C., Coll-Seck, A. M., Cropper, M. L., Fobil, J., Fuster, V., Greenstone, M., Haines, A., Hanrahan, D., Hunter, D., Khare, M., Krupnick, A., Lanphear, B., Lohani, B., Martin, K., Mathiasen, K. V., McTeer, M. A., Murray, C. J. L., Ndahimananjara, J. D., Perera, F., Potočnik, J., Preker, A. S., Ramesh, J., Rockström, J., Salinas, C., Samson, L. D., Sandilya, K., Sly, P. D., Smith, K. R., Steiner, A., Stewart, R. B., Suk, W. A., van Schayck, O. C. P., Yadama, G. N., Yumkella, K. and Zhong, M.: The Lancet Commission on pollution and health, Lancet, 391(10119), 462–512, 2018.

Lelieveld, J., Evans, J. S., Fnais, M., Giannadaki, D. and Pozzer, A.: The contribution of outdoor air pollution sources to premature mortality on a global scale, Nature, 525(7569), 367–371, 2015.

Liao, J., Hanisco, T. F., Wolfe, G. M., St. Clair, J., Jimenez, J. L., Campuzano-Jost, P., Nault, B. A., Fried, A., Marais, E. A., Gonzalez Abad, G., Chance, K., Jethva, H. T., Ryerson, T. B., Warneke, C. and Wisthaler, A.: Towards a satellite formaldehyde – in situ hybrid estimate for organic aerosol abundance, Atmos. Chem. Phys., 19(5), 2765–2785, 2019.

Li, M., Zhang, Q., Zheng, B., Tong, D., Lei, Y., Liu, F., Chaopeng, H., Kang, S., Yan, L., Zhang, Y., Bo, Y., Su, H., Cheng, Y. and He, K.: Persistent growth of anthropogenic non-methane volatile organic compound (NMVOC) emissions in China during 1990-2017: drivers, speciation and ozone formation potential, Atmos. Chem. Phys., 19, 8897–8913, 2019.

Liu, X., Deming, B., Pagonis, D., Day, D. A., Palm, B. B., Talukdar, R., Roberts, J. M., Veres, P. R., Krechmer, J. E., Thornton, J. A., de Gouw, J. A., Ziemann, P. J. and Jimenez, J. L.: Effects of gas–wall interactions on measurements of semivolatile compounds and small polar molecules, , doi:10.5194/amt-12-3137-2019, 2019.

Lu, Q., Zhao, Y. and Robinson, A. L.: Comprehensive organic emission profiles for gasoline, diesel, and gas-turbine engines including intermediate and semi-volatile organic compound emissions, Atmos. Chem. Phys., 18, 17637–17654, 2018.

Ma, P. K., Zhao, Y., Robinson, A. L., Worton, D. R., Goldstein, A. H., Ortega, A. M., Jimenez, J. L., Zotter, P., Prévôt, A. S. H., Szidat, S. and Hayes, P. L.: Evaluating the impact of new observational constraints on P-S/IVOC emissions, multi-generation oxidation, and chamber wall losses on SOA modeling for Los Angeles, CA, Atmos. Chem. Phys., 17(15), 9237–9259, 2017.

McDonald, B. C., de Gouw, J. A., Gilman, J. B., Jathar, S. H., Akherati, A., Cappa, C. D., Jimenez, J. L., Lee-Taylor, J., Hayes, P. L., McKeen, S. A., Cui, Y. Y., Kim, S.-W., Gentner, D. R., Isaacman-VanWertz, G., Goldstein, A. H., Harley, R. A., Frost, G. J., Roberts, J. M., Ryerson, T. B. and Trainer, M.: Volatile chemical products emerging as largest petrochemical source of urban organic emissions, Science, 359(6377), 760–764, 2018.

Miyakawa, T., Takegawa, N. and Kondo, Y.: Photochemical evolution of submicron aerosol chemical composition in the Tokyo megacity region in summer, J. Geophys. Res. D: Atmos., 113(D14), D14304, 2008.

Molina, L. T., Kolb, C. E., de Foy, B., Lamb, B. K., Brune, W. H., Jimenez, J. L., Ramos-Villegas, R., Sarmiento, J., Paramo-Figueroa, V. H., Cardenas, B., Gutierrez-Avedoy, V. and Molina, M. J.: Air quality in North America's most populous city – overview of the MCMA-2003 campaign, Atmos. Chem. Phys., 7(10), 2447–2473, 2007.

Molina, L. T., Madronich, S., Gaffney, J. S., Apel, E., de Foy, B., Fast, J., Ferrare, R., Herndon, S., Jimenez, J. L., Lamb, B., Osornio-Vargas, A. R., Russell, P., Schauer, J. J., Stevens, P. S., Volkamer, R. and Zavala, M.: An overview of the MILAGRO 2006 Campaign: Mexico City emissions and their transport and transformation, Atmos. Chem. Phys., 10(18), 8697–8760, 2010.

Morino, Y., Tanabe, K., Sato, K. and Ohara, T.: Secondary organic aerosol model intercomparison based on secondary organic aerosol to odd oxygen ratio in Tokyo, J. Geophys. Res.: Atmos., 119(23), 13,489–13,505, 2014.

Murphy, B. N., Woody, M. C., Jimenez, J. L., Carlton, A. M. G., Hayes, P. L., Liu, S., Ng, N. L., Russell, L. M., Setyan, A., Xu, L., Young, J., Zaveri, R. A., Zhang, Q. and Pye, H. O. T.: Semivolatile POA and parameterized total combustion SOA in CMAQv5.2: impacts on source strength and partitioning, Atmos. Chem. Phys., 17(18), 11107–11133, 2017.

Nault, B. A., Campuzano-Jost, P., Day, D. A., Schroder, J. C., Anderson, B., Beyersdorf, A. J., Blake, D. R., Brune, W. H., Choi, Y., Corr, C. A., de Gouw, J. A., Dibb, J., DiGangi, J. P., Diskin, G. S., Fried, A., Huey, L. G., Kim, M. J., Knote, C. J., Lamb, K. D., Lee, T., Park, T., Pusede, S. E., Scheuer, E., Thornhill, K. L., Woo, J.-H. and Jimenez, J. L.: Secondary Organic Aerosol Production from Local Emissions Dominates the Organic Aerosol Budget over Seoul, South Korea, during KORUS-AQ, Atmos. Chem. Phys., 18, 17769–17800, 2018.

Pagonis, D., Krechmer, J. E., de Gouw, J., Jimenez, J. L. and Ziemann, P. J.: Effects of Gas-Wall Partitioning in Teflon Tubing and Instrumentation on Time-Resolved Measurements of Gas-Phase Organic Compounds, Atmospheric Measurement Techniques Discussions, 1–19, 2017.

Pai, S. J., Heald, C. L., Pierce, J. R., Farina, S. C., Marais, E. A., Jimenez, J. L., Campuzano-Jost, P., Nault, B. A., Middlebrook, A. M., Coe, H., Shilling, J. E., Bahreini, R., Dingle, J. H. and Vu, K.: An evaluation of global organic aerosol schemes using airborne

observations, Atmos. Chem. Phys., 20(5), 2637–2665, 2020.

Parrish, D. D., Kuster, W. C., Shao, M., Yokouchi, Y., Kondo, Y., Goldan, P. D., de Gouw, J. A., Koike, M. and Shirai, T.: Comparison of air pollutant emissions among mega-cities, Atmos. Environ., 43(40), 6435–6441, 2009.

Petit, J.-E., Favez, O., Sciare, J., Canonaco, F., Croteau, P., Močnik, G., Jayne, J., Worsnop, D. and Leoz-Garziandia, E.: Submicron aerosol source apportionment of wintertime pollution in Paris, France by double positive matrix factorization (PMF^2) using an aerosol chemical speciation monitor (ACSM) and a multi-wavelength Aethalometer, Atmos. Chem. Phys., 14(24), 13773–13787, 2014.

Platt, S. M., Haddad, I. E., Pieber, S. M., Huang, R.-J., Zardini, A. A., Clairotte, M., Suarez-Bertoa, R., Barmet, P., Pfaffenberger, L., Wolf, R., Slowik, J. G., Fuller, S. J., Kalberer, M., Chirico, R., Dommen, J., Astorga, C., Zimmermann, R., Marchand, N., Hellebust, S., Temime-Roussel, B., Baltensperger, U. and Prévôt, A. S. H.: Two-stroke scooters are a dominant source of air pollution in many cities, Nat. Commun., 5(1), 3749, 2014.

Pollack, I. B., Ryerson, T. B., Trainer, M., Neuman, J. A., Roberts, J. M. and Parrish, D. D.: Trends in ozone, its precursors, and related secondary oxidation products in Los Angeles, California: A synthesis of measurements from 1960 to 2010, J. Geophys. Res. D: Atmos., 118(11), 5893–5911, 2013.

Punger, E. M. and West, J. J.: The effect of grid resolution on estimates of the burden of ozone and fine particulate matter on premature mortality in the USA, Air Qual. Atmos. Health, 6(3), 563–573, 2013.

Ridley, D. A., Heald, C. L., Ridley, K. J. and Kroll, J. H.: Causes and consequences of decreasing atmospheric organic aerosol in the United States, Proc. Natl. Acad. Sci. U. S. A., 115(2), 290–295, 2018.

Robinson, A. L., Donahue, N. M., Shrivastava, M. K., Weitkamp, E. A., Sage, A. M., Grieshop, A. P., Lane, T. E., Pierce, J. R. and Pandis, S. N.: Rethinking Organic Aerosols: Semivolatile Emissions and Photochemical Aging, Science, 315(5816), 1259–1262, 2007.

Ryerson, T. B., Andrews, A. E., Angevine, W. M., Bates, T. S., Brock, C. A., Cairns, B., Cohen, R. C., Cooper, O. R., de Gouw, J. A., Fehsenfeld, F. C., Ferrare, R. A., Fischer, M. L., Flagan, R. C., Goldstein, A. H., Hair, J. W., Hardesty, R. M., Hostetler, C. A., Jimenez, J. L., Langford, A. O., McCauley, E., McKeen, S. A., Molina, L. T., Nenes, A., Oltmans, S. J., Parrish, D. D., Pederson, J. R., Pierce, R. B., Prather, K., Quinn, P. K., Seinfeld, J. H., Senff, C. J., Sorooshian, A., Stutz, J., Surratt, J. D., Trainer, M., Volkamer, R., Williams, E. J. and Wofsy, S. C.: The 2010 California Research at the Nexus of Air Quality and Climate Change (CalNex) field study, J. Geophys. Res. D: Atmos., 118(11), 5830–5866, 2013.

Sacks, J., Buckley, B., Alexis, N., Angrish, M., Beardslee, R., Benson, A., Brown, J., Buckley, B., Campen, M., Chan, E., Coffman, E., Davis, A., Dutton, S. J., Eftim, S., Gandy, J., Hemming,

B. L., Hines, E., Holliday, K., Kerminen, V.-M., Kiomourtzoglou, M.-A., Kirrane, E., Kotchmar, D., Koturbash, I., Kulmala, M., Lassiter, M., Limaye, V., Ljungman, P., Long, T., Luben, T., Malm, W., McDonald, J. F., McDow, S., Mickley, L., Mikati, I., Mulholland, J., Nichols, J., Patel, M. M., Pinder, R., Pinto, J. P., Rappazzo, K., Richomond-Bryant, J., Rosa, M., Russell, A., Schichtel, B., Stewart, M., Stanek, L. W., Turner, M., Van Winkle, L., Wagner, J., Weaver, Christopher, Wellenius, G., Whitsel, E., Yeckel, C., Zanobetti, A. and Zhang, M.: Integrated Science Assessment (ISA) for Particulate Matter (Final Report, Dec 2019), Environmental Protection Agency. [online] Available from: https://cfpub.epa.gov/ncea/isa/recordisplay.cfm?deid=347534 (Accessed 20 October 2020), 2019.

Schroder, J. C., Campuzano-Jost, P., Day, D. A., Shah, V., Larson, K., Sommers, J. M., Sullivan, A. P., Campos, T., Reeves, J. M., Hills, A., Hornbrook, R. S., Blake, N. J., Scheuer, E., Guo, H., Fibiger, D. L., McDuffie, E. E., Hayes, P. L., Weber, R. J., Dibb, J. E., Apel, E. C., Jaeglé, L., Brown, S. S., Thronton, J. A. and Jimenez, J. L.: Sources and Secondary Production of Organic Aerosols in the Northeastern US during WINTER, J. Geophys. Res. D: Atmos., doi:10.1029/2018JD028475, 2018.

Seinfeld, J. H. and Pandis, S. N.: Atmospheric Chemistry and Physics: From Air Pollution to Climate Change, Second., John Wiley & Sons, Inc., Hoboken, NJ USA., 2006.

Seltzer, K. M., Pennington, E., Rao, V., Murphy, B. N., Strum, M., Isaacs, K. K. and Pye, H. O. T.: Reactive organic carbon emissions from volatile chemical products, Atmos. Chem. Phys., 21, 5079–5100, 2021.

Shaddick, G., Thomas, M. L., Amini, H., Broday, D., Cohen, A., Frostad, J., Green, A., Gumy, S., Liu, Y., Martin, R. V., Pruss-Ustun, A., Simpson, D., van Donkelaar, A. and Brauer, M.: Data Integration for the Assessment of Population Exposure to Ambient Air Pollution for Global Burden of Disease Assessment, Environ. Sci. Technol., 52(16), 9069–9078, 2018.

Shah, V., Jaeglé, L., Thornton, J. A., Lopez-Hilfiker, F. D., Lee, B. H., Schroder, J. C., Campuzano-Jost, P., Jimenez, J. L., Guo, H., Sullivan, A. P., Weber, R. J., Green, J. R., Fiddler, M. N., Bililign, S., Campos, T. L., Stell, M., Weinheimer, A. J., Montzka, D. D. and Brown, S. S.: Chemical feedbacks weaken the wintertime response of particulate sulfate and nitrate to emissions reductions over the eastern United States, Proc. Natl. Acad. Sci. U. S. A., 115(32), 8110–8115, 2018.

Shah, V., Jaeglé, L., Jimenez, J. L., Schroder, J. C., Campuzano-Jost, P., Campos, T. L., Reeves, J. M., Stell, M., Brown, S. S., Lee, B. H., Lopez-Hilfiker, F. D. and Thornton, J. A.: Widespread Pollution from Secondary Sources of Organic Aerosols during Winter in the Northeastern United States, Geophys. Res. Lett., doi:10.1029/2018GL081530, 2019.

Shrivastava, M., Cappa, C. D., Fan, J., Goldstein, A. H., Guenther, A. B., Jimenez, J. L., Kuang, C., Laskin, A., Martin, S. T., Ng, N. L., Petaja, T., Pierce, J. R., Rasch, P. J., Roldin, P., Seinfeld, J. H., Shilling, J., Smith, J. N., Thornton, J. A., Volkamer, R., Wang, J., Worsnop, D. R., Zaveri, R. A., Zelenyuk, A. and Zhang, Q.: Recent advances in understanding secondary organic aerosol:

Implications for global climate forcing, Rev. Geophys., 55(2), 509–559, 2017.

Silva, R. A., Adelman, Z., Fry, M. M. and West, J. J.: The Impact of Individual Anthropogenic Emissions Sectors on the Global Burden of Human Mortality due to Ambient Air Pollution, Environ. Health Perspect., 124(11), 1776–1784, 2016.

Singh, A., Satish, R. V. and Rastogi, N.: Characteristics and sources of fine organic aerosol over a big semi-arid urban city of western India using HR-ToF-AMS, Atmos. Environ., 208, 103–112, 2019.

Stavroulas, I., Bougiatioti, A., Grivas, G., Paraskevopoulou, D., Tsagkaraki, M., Zarmpas, P., Liakakou, E., Gerasopoulos, E. and Mihalopoulos, N.: Sources and processes that control the submicron organic aerosol composition in an urban Mediterranean environment (Athens): a high temporal-resolution chemical composition measurement study, Atmos. Chem. Phys., 19(2), 901–919, 2019.

Stewart, G. J., Nelson, B. S., Acton, W. J. F., Vaughan, A. R., Farren, N. J., Hopkins, J. R., Ward, M. W., Swift, S. J., Arya, R., Mondal, A., Jangirh, R., Ahlawat, S., Yadav, L., Sharma, S. K., Yunus, S. S. M., Hewitt, C. N., Nemitz, E., Mullinger, N., Gadi, R., Sahu, L. K., Tripathi, N., Rickard, A. R., Lee, J. D., Mandal, T. K. and Hamilton, J. F.: Emissions of intermediate-volatility and semi-volatile organic compounds from domestic fuels used in Delhi, India, Atmos. Chem. Phys. Discuss., doi:10.5194/acp-2020-860, 2020.

Toon, O. B., Maring, H., Dibb, J., Ferrare, R., Jacob, D. J., Jensen, E. J., Luo, Z. J., Mace, G. G., Pan, L. L., Pfister, L., Rosenlof, K. H., Redemann, J., Reid, J. S., Singh, H. B., Thompson, A. M., Yokelson, R., Minnis, P., Chen, G., Jucks, K. W. and Pszenny, A.: Planning, implementation, and scientific goals of the Studies of Emissions and Atmospheric Composition, Clouds and Climate Coupling by Regional Surveys (SEAC^{4}RS) field mission, J. Geophys. Res. D: Atmos., 121(9), 4967–5009, 2016.

Tsimpidi, A. P., Karydis, V. A., Zavala, M., Lei, W., Molina, L., Ulbrich, I. M., Jimenez, J. L. and Pandis, S. N.: Evaluation of the volatility basis-set approach for the simulation of organic aerosol formation in the Mexico City metropolitan area, Atmos. Chem. Phys., 10(2), 525–546, 2010.

Volkamer, R., Jimenez, J. L., San Martini, F., Dzepina, K., Zhang, Q., Salcedo, D., Molina, L. T., Worsnop, D. R. and Molina, M. J.: Secondary organic aerosol formation from anthropogenic air pollution: Rapid and higher than expected, Geophys. Res. Lett., 33(17), L17811, 2006.

Wang, L., Slowik, J. G., Tripathi, N., Bhattu, D., Rai, P., Kumar, V., Vats, P., Satish, R., Baltensperger, U., Ganguly, D., Rastogi, N., Sahu, L. K., Tripathi, S. N. and Prévôt, A. S. H.: Source characterization of volatile organic compounds measured by proton-transfer-reaction time-of-flight mass spectrometers in Delhi, India, Atmos. Chem. Phys., 20(16), 9753–9770, 2020.

Warneke, C., de Gouw, J. A., Holloway, J. S., Peischl, J., Ryerson, T. B., Atlas, E., Blake, D., Trainer, M. and Parrish, D. D.: Multiyear trends in volatile organic compounds in Los Angeles,

California: Five decades of decreasing emissions, J. Geophys. Res. D: Atmos., 117(D21), D00V17, 2012.

Wood, E. C., Canagaratna, M. R., Herndon, S. C., Onasch, T. B., Kolb, C. E., Worsnop, D. R., Kroll, J. H., Knighton, W. B., Seila, R., Zavala, M., Molina, L. T., Decarlo, P. F., Jimenez, J. L., Weinheimer, A. J., Knapp, D. J., Jobson, B. T., Stutz, J., Kuster, W. C. and Williams, E. J.: Investigation of the correlation between odd oxygen and secondary organic aerosol in Mexico City and Houston, Atmos. Chem. Phys., 10(18), 8947–8968, 2010.

Woody, M. C., Baker, K. R., Hayes, P. L., Jimenez, J. L., Koo, B. and Pye, H. O. T.: Understanding sources of organic aerosol during CalNex-2010 using the CMAQ-VBS, Atmos. Chem. Phys., 16(6), 4081–4100, 2016.

Worton, D. R., Isaacman, G., Gentner, D. R., Dallmann, T. R., Chan, A. W. H., Ruehl, C., Kirchstetter, T. W., Wilson, K. R., Harley, R. A. and Goldstein, A. H.: Lubricating Oil Dominates Primary Organic Aerosol Emissions from Motor Vehicles, Environ. Sci. Technol., 48(7), 3698–3706, 2014.

Ye, P., Ding, X., Hakala, J., Hofbauer, V., Robinson, E. S. and Donahue, N. M.: Vapor wall loss of semi-volatile organic compounds in a Teflon chamber, Aerosol Sci. Technol., 50(8), 822–834, 2016.

Zhang, Q., Jimenez, J. L., Canagaratna, M. R., Allan, J. D., Coe, H., Ulbrich, I., Alfarra, M. R., Takami, A., Middlebrook, A. M., Sun, Y. L., Dzepina, K., Dunlea, E., Docherty, K., DeCarlo, P. F., Salcedo, D., Onasch, T., Jayne, J. T., Miyoshi, T., Shimono, A., Hatakeyama, S., Takegawa, N., Kondo, Y., Schneider, J., Drewnick, F., Borrmann, S., Weimer, S., Demerjian, K., Williams, P., Bower, K., Bahreini, R., Cottrell, L., Griffin, R. J., Rautiainen, J., Sun, J. Y., Zhang, Y. M. and Worsnop, D. R.: Ubiquity and dominance of oxygenated species in organic aerosols in anthropogenically-influenced Northern Hemisphere midlatitudes, Geophys. Res. Lett., 34(13), L13801, 2007.

Zhang, Q. J., Beekmann, M., Freney, E., Sellegri, K., Pichon, J. M., Schwarzenboeck, A., Colomb, A., Bourrianne, T., Michoud, V. and Borbon, A.: Formation of secondary organic aerosol in the Paris pollution plume and its impact on surrounding regions, Atmos. Chem. Phys., 15(24), 13973–13992, 2015.

Zhao, B., Wang, S., Donahue, N. M., Jathar, S. H., Huang, X., Wu, W., Hao, J. and Robinson, A. L.: Quantifying the effect of organic aerosol aging and intermediate-volatility emissions on regional-scale aerosol pollution in China, Sci. Rep., 6, 28815, 2016a.

Zhao, Y., Hennigan, C. J., May, A. A., Daniel, S., Gouw, J. A. D., Gilman, J. B., Kuster, W. C. and Robinson, A. L.: Intermediate-Volatility Organic Compounds: A Large Source of Secondary Organic Aerosol, Environ. Sci. Technol, 48(23), 13743–13750, 2014.

Zhao, Y., Nguyen, N. T., Presto, A. A., Hennigan, C. J., May, A. A. and Robinson, A. L.: Intermediate Volatility Organic Compound Emissions from On-Road Gasoline Vehicles and

Small Off-Road Gasoline Engines, Environ. Sci. Technol., 50(8), 4554–4563, 2016b.

Zhao, Y., Saleh, R., Saliba, G., Presto, A. A., Gordon, T. D., Drozd, G. T., Goldstein, A. H., Donahue, N. M. and Robinson, A. L.: Reducing secondary organic aerosol formation from gasoline vehicle exhaust, Proc. Natl. Acad. Sci. U. S. A., 114(27), 6984–6989, 2017.

Supplemental Information for:

~~Anthropogenic~~ Secondary Organic Aerosols from Anthropogenic Volatile Organic Compounds Contribute Substantially to Air Pollution Mortality

Benjamin A. Nault et al.

Correspondence: Jose L. Jimenez (jose.jimenez@colorado.edu)

S1 Emission Inventories for Various Urban Areas around the World

All BTEX (benzene, toluene, ethylbenzene, and xylenes) and non-BTEX aromatic emissions are shown in Table S5 (BTEX) or Table S8 (non-BTEX aromatics). The emission ratios are derived from ambient measurements utilizing photochemical aging techniques (Nault et al., 2018).

Details of the emission inventories for cities in the US, for Beijing, and for London/UK used here to estimate the IVOC:BTEX emission ratio (Fig. 5) and thus the IVOC emissions can be found below. Briefly, emissions for the US are based on McDonald et al. (2018), for China on the Multi-resolution Emission Inventory for China (MEIC) (Zhang et al., 2009; Zheng et al., 2014, 2018; Liu et al., 2015; Li et al., 2017, 2019), and for the UK on the National Atmospheric Emissions Inventory (NAEI) (EMEP/EEA, 2016). The IVOC:BTEX emission ratio from inventories are multiplied with the observed BTEX, either reported value from studies (NE US aircraft (Warneke et al., 2007), Los Angeles (de Gouw et al., 2017), Beijing (Wang et al., 2014), and New York City (Warneke et al., 2007)) or estimated from Eq. 3 (London), to estimate IVOCs emitted in each region (Table S5). This ensures IVOC emissions used in our calculations properly reflect differences in mixtures of emission sources (e.g., mobile sources versus VCPs) that vary by continent for each field campaign. Additionally, we rely on inventories for estimating atmospheric abundances of IVOCs because it has been challenging to measure the full range of IVOC precursors that are emitted into urban air due to many of the IVOCs from VCPs being oxygenated VOCs. These compounds are challenging to measure using traditional instrumentation (e.g., gas chromatography-mass spectrometry), leading to potential underestimation of the IVOC emission ratios (Zhao et al., 2014, 2017; Lu et al., 2018). The

bottom-up IVOC:BTEX ratios for the US, Beijing, and UK are described in greater detail below. IVOC emissions are classified based on their vapor pressure (effective saturation concentration: $10^3 < C^* < 10^6$ μg m^{-3}), with the vapor pressure estimated by the SIMPOL.1 model (Pankow and Asher, 2008). The ASOA yields and rate constants for IVOC oxidation were parameterized with data from n-tridecane and n-pentadecane for gasoline and diesel emissions, respectively (Jathar et al., 2014), and for VCPs, the yields and rate constants for IVOC oxidation were parameterized with data from n-tetradecane (McDonald et al., 2018).

Similar to IVOCs, the ability to measure the full range of SVOCs emitted into urban air is challenging. Therefore, we estimate SVOC emission ratios relative to POA mass concentrations (Table S9), as described by Ma et al. (2017). For the hydrocarbon-like portion, we used the volatility distribution from Worton et al. (2014) to estimate SVOC, as this is associated with fossil fuel emissions from transportation (Zhang et al., 2005). For the other POA, we used the volatility distribution from Robinson et al. (2007), as this POA is typically cooking primary aerosol. These profiles were selected to be consistent with Ma et al. (2017).

To estimate the SVOC mass concentration in equilibrium with POA (Table S9), in each bin (e.g., C* = 0, 1, 2), the normalized POA mass concentration is first multiplied by the fraction of POA measured in each bin from literature. For other POA, which includes biomass burning and cooking OA, the fraction of POA found in $\log_{10}C^*$ = 0, 1, and 2 are 0.22, 0.34, and 0.44, respectively (Robinson et al. 2007), and for vehicular POA, the fraction of POA found in $\log_{10}C^*$ = 0, 1, and 2 are 0.42, 0.40, and 0.18, respectively (Worton et al. 2014). So, for example, for NE US, this would correspond to normalized POA mass concentrations (POA/ΔCO) of 5.1, 4.9, and 2.2 μg sm^{-3} $ppmv^{-1}$ for $\log_{10}C^*$ = 0, 1, and 2, respectively. Then the total POA + SVOC

normalized mass concentration for that bin is obtained by dividing the amount of material found in the particle-phase for that bin at the average temperature (~298 K) and OA mass concentration (~10 μg sm^{-3}). So, taking NE US as an example, for $\log_{10}C^* = 0$, 1, and 2, 9%, 50%, and 91% of the material, respectively, will be in the gas-phase versus the aerosol-phase, leading to the normalized mass concentration of SVOC as inputs into the model of 0.39, 3.8, and 17.1 μg sm^{-3} $ppmv^{-1}$. The values of 9%, 50%, and 91% were used for NE US, Los Angeles, London, and Beijing, as the ambient temperatures were ~298 K. For New York City, as the study took place during winter, values of 3%, 22%, and 74% were used as the ambient temperature was ~273 K.~~To estimate the SVOC mass concentration in equilibrium with the POA (Table S9) in each bin, the POA mass concentration is first multiplied by the fraction of POA measured in each bin from literature. This yields the concentration of POA for that specific volatility bin. Then the total POA + SVOC concentration for that bin is obtained divided by the amount of material found in the particle phase for that bin for the average temperature (~298 K) and OA mass concentration (~10 μg m-3). Then, the gas-phase SVOC concentration is calculated by multiplying the total concentration by the gas-phase fraction. Thus, e.g., SVOC in the C* = 100 μg m-3 bin, ~91% of the SVOC mass will be found in the gas-phase.~~

Fig. S6 shows the calculated emission ratio versus saturation concentration (c*) for the cities with emission inventories. The saturation concentration for SVOC was determined as part of the estimation procedure discussed above. For IVOC, the emission ratios for the different sources (gasoline, diesel, other fossil fuel sources, and VCP emissions) were split into the volatility bins, as in McDonald et al. (2018). Finally, for BTEX and non-BTEX aromatics, and other VOC emission ratios (see Fig. S6 for references for the other VOC emission ratios), CRC

(Rumble, 2019) or SIMPOL.1 (Pankow and Asher, 2008) (for estimating vapor pressures not in CRC) was used to estimate the saturation concentrations.

S1.1 US Emission Inventories

Anthropogenic VOC emissions

The US emissions of VOCs is based on a mass balance estimate of the petrochemical industry reported by McDonald et al. (2018). Briefly, fuel sales and chemical product use are estimated from publicly available reports on energy use, chemical production, economic surveys, and freight shipments. Mobile source emission factors are from prior work quantifying both on-road and off-road engines (McDonald et al., 2013, 2015). Evaporative sources of transportation fuels are considered in addition to tailpipe exhaust (Pierson et al., 1999). VCP emission factors are based on literature values, including from the indoor environment, and reported in McDonald et al. (2018). Other fossil energy sources of VOCs, such as from oil refineries and industry, are taken from official inventories reported by the California Air Resources Board (CARB, 2013) or US Environmental Protection Agency (NEI, 2015). McDonald et al. (2018) reported fossil-VOC emissions for the Los Angeles basin in the year 2010.

Speciation of VOC emissions

The total VOC emissions are speciated to estimate BTEX and IVOC emissions from petrochemical VOC sources. Briefly, gasoline and diesel exhaust, gasoline fuel, and headspace vapors are based on profiles reported in the literature from the Caldecott Tunnel (Gentner et al.,

2012, 2013). Speciation profiles of VCPs are based on California Air Resources Board surveys of architectural coatings (Davis, 2007) and consumer products (CCPR, 2015). Other industrial solvent uses and point/area source emissions are from the EPA SPECIATE (v4.4) database (EPA, 2014).

Extrapolating IVOC/BTEX ratios from 2010 Los Angeles to other field campaigns

In the ASOA mass closure estimation, three separate field campaigns are utilized from the US: NEAQS 2002 (Boston/New York City), CalNex 2010 (Los Angeles), and WINTER 2015 (New York City outflow). These field campaigns span two megacities (Los Angeles and New York City), ~one decade, and two seasons (summer versus winter). Here, we discuss how each of these variables could affect the IVOC/BTEX emissions ratio. We focus the discussion on mobile sources and VCPs because these are the dominant contributors to BTEX and IVOCs.

The IVOC/BTEX emissions ratio could be affected by the population density of a city. It is well-established that per capita transportation fuel use decreases with increasing population density (Gately et al., 2015), whereas VCP usage is expected to scale with population. Relative to Los Angeles, the per capita fuel use in New York City is ~2 times lower (Gately et al., 2015), resulting in lower on-road transportation VOC emissions relative to VCPs. Because aromatics are mainly found in gasoline, whereas the IVOCs have a higher contribution from VCPs, the IVOC/BTEX ratio is expected to be higher in New York City than Los Angeles.

To assess impacts of annual trends on the IVOC/BTEX ratio, we utilize long-term trend analyses of mobile source VOC emissions in Los Angeles (McDonald et al., 2013, 2015; Hassler et al., 2016). The main effect is that on-road gasoline emissions have decreased with time, both

from the tailpipe of vehicles (McDonald et al., 2013) and of gasoline-related VOCs in ambient air measurements (Warneke et al., 2012). We utilize the EPA Trends Report to scale VOC emissions for other anthropogenic sectors, including VCPs and industrial sources (https://www.epa.gov/air-emissions-inventories/air-pollutant-emissions-trends-data). The EPA Trends Report suggests that VCP (or solvent) emissions decreased by ~30% between 2002 and 2010, including efforts to reduce the VOC content of architectural coatings (Matheson, 2002). After 2010, the emissions have been slightly increasing, likely due to population growth. Because both mobile sources and VCP emissions are decreasing with time, the IVOC/BTEX emissions ratio is not significantly altered.

Lastly, the effects of seasonality influence on-road transportation emissions through: (i) increased VOC emissions in winter relative to summer from cold-starting engines, and (ii) lower evaporative emissions due to colder ambient temperatures. We estimate that exhaust emissions from passenger vehicles increases by ~50% due to higher cold-start emissions in winter relative to summer based on the EPA MOVES model (MOVES, 2015). Evaporated gasoline and headspace vapors are known to exhibit a temperature-dependence (Rubin et al., 2006), and estimated to be ~20% and ~80% lower, respectively, based on typical wintertime temperatures of New York City relative to summertime Los Angeles. Due to compensating factors between cold-start engines and evaporated fuels, the IVOC/BTEX emissions are not significantly affected by seasonality.

Overall, when taking into account differences in population density between Los Angeles and New York City, trends of mobile source and VCP emissions over time, and seasonality, the IVOC/BTEX emission ratios range between ~2.3 to 2.7, which is a relatively small range. This

sensitivity analysis helps explain why the enhancement observed in SOA scales with BTEX levels in the urban atmosphere.

S1.2 Beijing Emission Inventory

Anthropogenic VOC emissions

The total VOC emissions of Beijing were developed following the bottom-up framework of the Multi-resolution Emission Inventory for China (MEIC) model (available at http://www.meicmodel.org), based on a technology-based methodology. The details of activity rates, emission factors, technology distribution, and control measures configured in the MEIC model are summarized in a series of papers (Zhang et al., 2009; Zheng et al., 2014, 2018; Liu et al., 2015; Li et al., 2017, 2019).

In the MEIC model, a detailed four-level source classification system, representing sector, fuel/product, technology/solvent type, and end-of-pipe pollutant abatement facilities, was established by including over 700 emitting sources for each province. All anthropogenic sources, including power plants, industrial sources, volatile chemical products, fossil fuel burning in residential stoves, transportation were all considered.

Power plants are treated as point sources in the MEIC model. The VOC emissions were derived from the China coal-fired Power Plant Emissions Database (CPED, (Liu et al., 2015)), which is developed based on information of each unit on fuel type, fuel quality, combustion technology, etc.

Volatile chemical products are comprised of solvent use applied for architecture, vehicles, wood, and other industrial purposes, glue use, printing, pesticide use, and domestic solvent use.

The market share of waterborne and solvent-based paint is further taken into account for each source category. For the on-road transportation sector, the improved emissions developed by Zheng et al. (2014) were integrated into the framework of MEIC, which estimated the vehicle population and emission factors at a county level. Both the VOC emissions in running mode and evaporation were considered. Emission standards covering pre-Euro I and Euro I to Euro V in Beijing were applied for each vehicle type (Zheng et al., 2018; Li et al., 2019). Regarding oxygenated volatile organic compounds (OVOCs), the emission factors for on-road vehicles were corrected, as current emission factors are only for non-methane hydrocarbons (NMHC). Correction ratios of 1.32, 1.08, 1.10, and 1.06 were applied for heavy-duty and light-duty diesel vehicles, and heavy-duty and light-duty gasoline vehicles, respectively, to the original values to comply with the follow-up speciation for the total VOC, following the method of Li et al. (2014, 2019).

Speciation of VOC emissions

Emissions by individual chemical species were developed based on the profile-assignment approach (Li et al., 2014, 2019). First, a "composite" profile database for China was established by integrating the local profiles and supplementing it with the SPECIATE v4.5 database for absent sources ((Simon et al., 2010), available at: https://www.epa.gov/air-emissions-modeling/speciate-version-45-through-40). The detailed procedure for developing the composite profile database is illustrated in Li et al. (2014). In brief, for sources where there are significant differences in technology or legislation between China and western countries, only local profiles are used; otherwise, all candidate profiles are included

for further compilation in the composite profile database. Local profiles covering most of the important sources were gathered and reviewed, including biofuel combustion, coal combustion, asphalt production, oil production, refinery, paint use, gasoline evaporation, gasoline vehicle exhaust, diesel vehicles, and so on, as detailed illustrated in Li et al. (2019).

Then, profiles for all combustion-related sources, including fossil fuel combustion in power plants, industry, residential, and transportation sectors were reviewed, and incomplete profiles that were absent from the OVOC fractions were corrected by appending the component of "OVOC" with fractions derived from the "complete" profiles for the same source. After OVOC correction, all "candidate" profiles were averaged by species to establish the composite profile database. Finally, the composite profile to each source was assigned by setting up the source linkage between the profile database and the inventory. Emissions by individual chemical species for each source were then further developed.

S1.3 London/United Kingdom Emission Inventory

Anthropogenic VOC emissions

The National Atmospheric Emissions Inventory (NAEI) estimates UK emissions of VOCs from anthropogenic sources following methods in the EMEP/EEA Emissions Inventory Guidebook (EMEP/EEA, 2016) for submission under the revised EU Directive 2016/2284/EU on National Emissions Ceilings (NECD), available at: https://eur-lex.europa.eu/legal-content/EN/TXT/PDF/?uri=CELEX:32016L2284&from=EN, and the United Nations Economic Commission for Europe (UNECE) Convention on Long-Range Transboundary Air Pollution (CLRTAP), available at:

http://www.ceip.at/ms/ceip_home1/ceip_home/reporting_instructions/reporting_programme/. The NECD and CLRTAP define those VOC sources to be included and excluded from the national inventory (for example, emissions of NMVOCs from biogenic sources are not included). The Guidebook provides estimation methodologies and default emission factors for each source category, although countries can use country-specific emission factors where these are deemed relevant. The NAEI currently covers organic emissions from around 400 individual source categories, with a large contribution from a diverse range of industrial processes and solvents, but with very few individually dominant sources. The inventory then speciates emissions into ~650 individual compounds, or groups of compounds. Groupings of organics, for example, expressed as 'sum of all C14 compounds,' make up a substantial fraction of IVOC emissions, rather than being reported as individual compounds.

Emissions from the use of solvents and other volatile chemicals in industry and in consumer products, fuel production and distribution, food and drink manufacture and other non-combustion industrial processes accounted for 72% of all UK NMVOC emissions in 2017, according to the NAEI. Both the solvent and industrial process sectors cover a diverse range of emission source categories: the NAEI identifies 136 separate categories across the two sectors

For the road transport sector, the NAEI reports exhaust emissions of NMVOCs and its emissions from evaporative losses of fuel vapor from petrol vehicles. Emissions from re-fueling at filling stations are reported separately under the fugitive emissions from the fuel distribution sector. The method used for road transport in the NAEI follows the method in the European COPERT 5 model and described in the EMEP/EEA Emissions Inventory Guidebook. The method uses average speed-related emission factors for hot exhaust emissions of total

hydrocarbons for detailed vehicle categories (vehicle type, weight and/or engine size) and Euro standards for petrol cars, diesel cars, petrol and diesel light goods vehicles, rigid and articulated HGVs, buses and coaches, and mopeds and motorcycles, and combines these with detailed traffic and fleet activity data derived from information provided by DfT. Separate estimates are made of methane emissions for each vehicle type and subtracted from the THC emissions to derive the NMVOC emissions.

Evaporative emissions from vehicles are estimated in the NAEI, using the Guidebook method for three different processes: diurnal losses, hot soak, and running losses. Emissions are dependent on ambient temperature and fuel vapor pressure and different factors are provided for vehicles with and without carbon canisters for evaporative emission controls. All vehicles from Euro 1 onwards are fitted with these devices; so, evaporative emission have been decreasing from the early 1990s with the penetration of these vehicles in the fleet. The method also takes into account the reduction in Reid Vapour Petrol of petrol sold in the UK since 2000, as required for compliance with the EU Fuel Quality Directive 98/70/EC, amended by Directive 2009/30/EC.

Speciation of VOC emissions

The NAEI is considered to adequately reflect annual real world emissions of BTEX (see, for example, eddy covariance flux comparisons in London by Langford et al. (2010) and Vaughn et al. (2017)); so, those values are taken directly from the NAEI and used here. IVOCs, and particularly long chain hydrocarbons, are included in many cases in the inventory as groups, but their emissions are known to be significantly underestimated when compared against field

observations. We use the observations of Dunmore et al. (2015), made in wintertime central London in 2012, as guide to uprate NAEI emissions for IVOC species based on the estimated discrepancies between inventory and field observation reported for each carbon number above C10. This leads to some significant multipliers being applied to the inventory values, sometimes of the order 60 to 70. We assume that the same multipliers apply to all sources, since field data does not provide any means to attribute different factors to road transport IVOCs compared with IVOCs from VCP sources.

Since the NAEI represents a reporting of emissions for the purposes of compliance with international treaties, some fraction of those emissions are not released on the mainland UK. For this paper, offshore BTEX and IVOC emissions, arising for example from offshore oil and gas activity, aircraft in cruise, or shipping and emissions associated with overseas Crown Dependencies are removed from the UK total, since they play no part in determining the chemical environment of London. The annual NAEI totals are then divided equally to give a daily national emission.

S2 ASOA Budget Analysis of Ambient Observations

To calculate the ASOA budget, we used the observed BTEX (Table S5) and non-BTEX aromatic (Table S8) emission ratios, the emission inventories for IVOC (see above), and estimated SVOCs from the primary OA emissions (see above). The methods to calculate ASOA from emissions have been described in detail elsewhere (Hayes et al., 2015; Ma et al., 2017; Schroder et al., 2018), and are briefly described here. All calculations described were conducted with the KinSim v4.02 chemical kinetics simulator (Peng and Jimenez, 2019) within Igor Pro 7

(Lake Oswego, Oregon), and are summarized in Fig. S7. A typical average particle diameter for urban environments of ~200 nm (Seinfeld and Pandis, 2006) is used to estimate the condensational sink term for the partitioning of gas-to-particle, although condensation is always fast compared to the experiment timescales. Further, we assume an average 250 g mol^{-1} molar mass for OA and an average SOA density of 1.4 g cm^{-3} (Vaden et al., 2011; Kuwata et al., 2012). Finally, all models are initialized with the campaign specific OA background (typically ~2 μg sm^{-3}) and POA (Table S9) for partitioning of gases to the particle phase, and ran at the average temperature for the campaign.

For the modeled VOCs (BTEX and non-BTEX aromatics), each species undergoes temperature-dependent OH oxidation (Table S12), forming four SVOCs that partition between gas- and particle-phase, using updated SOA yields that account for wall loss (Ma et al., 2017). For IVOCs, the emission weighted SOA yields and rate constants from the "Zhao" option (Zhao et al., 2014) of Ma et al. (2017) are used, and the products are apportioned into three SVOC bins and one low-volatility organic compound (LVOC) bin (Fig. S7). Finally, SVOCs undergo photooxidation at a rate of 4×10^{-11} cm^3 $molecules^{-1}$ s^{-1} (Dzepina et al., 2009; Hodzic et al., 2010; Tsimpidi et al., 2010; Hodzic and Jimenez, 2011; Hayes et al., 2015; Ma et al., 2017; Schroder et al., 2018), producing one product per oxidation step, with yields from Robinson et al. (2007) for cooking and other SVOCs and yields from Worton et al. (2014) for fossil fuel related SVOCs, as recommended by Ma et al. (2017). The products from SVOC and IVOC oxidation are allowed to further oxidize, as highlighted in Fig. S7 and described in prior studies (Hayes et al., 2015; Ma et al., 2017; Schroder et al., 2018). Generally, each product reacts at a rate of 4×10^{-11} cm^3 $molecules^{-1}$ s^{-1} to produce some product at one volatility bin lower, adding one oxygen to the

compound for each oxidation (Dzepina et al., 2009; Tsimpidi et al., 2010; Hodzic and Jimenez, 2011; Hayes et al., 2015; Ma et al., 2017; Schroder et al., 2018). An update includes fragmentation for a fraction of the molecules that are oxidized, as described in Schroder et al. (2018) and Koo et al. (2014). As shown in Fig. S7, fragmentation of the compound occurs as it is oxidized and goes down one volatility bin. For further oxidation of SVOCs from the oxidation of primary IVOCs, one oxygen is added and 0.25 carbon is removed per step, leading to an increase in mass of 1.03 (instead of 1.07) per oxidation step (Koo et al., 2014; Schroder et al., 2018). For further oxidation of products from primary SVOC emissions, one oxygen is added and 0.5 carbon is removed per step, leading to a decrease in mass of 1% (instead of 1.07) per oxidation step (Koo et al., 2014; Schroder et al., 2018).

S3 GEOS-Chem Modeling

The model used in this study is GEOS-Chem v12.0.0 (Bey et al., 2001; The International GEOS-Chem User Community, 2018). This model is used for the following calculations: (1) ASOA apportionment (Fig. 1), (2) apportionment of ASOA to total PM2.5 for premature mortality calculations (Sect. 5), and (3) sensitivity analysis for ASOA production and emissions on premature mortality calculations. GEOS-Chem is operated at 2°×2.5° horizontal resolution. Goddard Earth Observing System – Forward Processing (GEOS-FP) assimilated data from the NASA Global Modeling and Assimilation Office (GMAO) were used for input meteorological fields. The model was run for 2013 to 2018 to take into account interannual variability of meteorological impacts onto $PM_{2.5}$ (therefore, averaging $PM_{2.5}$ over variations in meteorology). However, the HTAPv2 emission inventory, which was used for anthropogenic emissions

316 (Janssens-Maenhout et al., 2015), was kept constant for the 5 years. Analysis of the HTAP
317 emissions, compared to other emission inventories, generally showed the highest correlation with
318 observations (R^2 = 0.54), versus the other inventories (CEDS R^2 = 0.26, MACCity R^2 = 0.00, and
319 RETROv2 R^2 = 0.04), leading to the selection of this emission inventory. GEOS-Chem simulates
320 gas and aerosol chemistry with ~700 chemical reactions. GEOS-Chem calculates the following
321 $PM_{2.5}$ species: sulfate, ammonium, nitrate (Park et al., 2006); black carbon and POA (Park et al.,
322 2005); SOA (Pye and Seinfeld, 2010; Marais et al., 2016); sea salt (accumulation mode only
323 (Jaeglé et al., 2011)); and, dust (Duncan Fairlie et al., 2007).
324
325 **S3.1 Biogenic SOA**
326 For monoterpene and sesquiterpene SOAs, we used the default complex SOA scheme
327 (without semi-volatile POA) using the two-product model framework (Pye and Seinfeld, 2010).
328 This scheme calculates initial oxidation of VOCs with OH, O_3, and NO_3, and resulting products
329 are assigned to four different gas-phase semi-volatile species (TSOA0–3) based on volatilities
330 (c* = 0.1, 1, 10, 100 μg m^{-3}). Aerosol and gas species fractions are calculated online using the
331 partitioning theory, and all are removed by dry and wet deposition processes.
332 For isoprene SOA, we used the explicit isoprene chemistry developed by Marais et al.
333 (2016). All the isoprene-derived gas-phase products, including isoprene peroxy radical,
334 ISOPOOH, IEPOX, glyoxal, and methylglyoxal, are explicitly simulated. Irreversible
335 heterogeneous uptake of precursors to aqueous aerosols are further calculated using online
336 aerosol pH and surface area.

GEOS-Chem was used to estimate the relative fractions of the measured SOA in our studies between anthropogenic and biogenic (isoprene and monoterpene) sources (Fig. 1). Extensive research has been conducted to evaluate and improve the models performance in predicting BSOA, as summarized in Table S3. Though these evaluations mainly occurred in the southeast US, a recent study has also included more global observations to compare with GEOS-Chem (Pai et al., 2020). Generally, GEOS-Chem appears to overestimate biogenically derived SOA; however, the model predicted SOA is typically within the uncertainty of the AMS (Table S3). The overestimation, though, would suggest that the fraction of urban SOA may be under-predicted by this method, whereas the BSOA may be over-predicted. Therefore, in urban regions, the amount of SOA from biogenic sources may be lower, especially after the rapid SOA enhancements (within 12 to 24 equivalent photochemical hours that have been observed around the world (Nault et al., 2018)). Typically the BSOA is present as a regional background and subtracted for the analyses used in this work, which focus on strong urban plumes on top of that background (Hayes et al., 2013, 2015).

S3.2 Default GEOS-Chem Sensitivity to ASOA Simulations

For the sensitivity calculation using the "traditional" ASOA precursors, we used the two-product model framework (Pye and Seinfeld, 2010). Benzene, toluene, and xylene are oxidized with OH and converted to peroxy radicals. These peroxy radicals react with HO_2 or NO, resulting in non-volatile ASOA (HO_2 pathway, ASOAN species in GEOS-Chem) or semi-volatile ASOA tracers (NO pathway, ASOA1-3 in GEOS-Chem). As is the case for monoterpene and sesquiterpene SOA above, GEOS-Chem calculates online partitioning and

dry/wet deposition processes for semi-volatile ASOA tracers. Other conditions including mortality calculation are kept the same as the base simulation above.

S4 Ozone Sensitivity to ASOA Simulations

A potential issue in the attribution of premature mortality to AOSA is that reducing emissions that lead to ASOA is that this may impact ozone concentrations. A sensitivity analysis was conducted, where the ASOA emissions were reduced by 20% (Fig. S14). In general, there is a less than 1% reduction in total ozone concentration in the boundary layer. This is due to the fact that the most important AVOCs that contribute to ozone formation are light alkenes (e.g., ethylene and propylene, Fig. 2), which are not ASOA precursors. Though the reaction rate constant of the ASOA precursors is generally high (Table S12), the concentration of the precursors is low and they thus account for a low percentage of the total ozone production potential (Table S5 through Table S9). For example, the measured OH reactivity (Sect. 3) for two different urban regions was between 15 to 25 s^{-1} (Griffith et al., 2016; Whalley et al., 2016) while the OH reactivity for the ASOA precursors for the same region was between 2 to 4 s^{-1}. The small contribution to the OH reactivity is in line to the minimal impact to the ozone concentration observed in Fig. S14.

S5 Error Analysis of Observations

The errors that will be discussed here are in reference to Fig. 2 and Fig. 4 and Table S4 either come from the 1σ uncertainty in the slopes (the SOA versus O_x, HCHO, or PAN values) or propagation of uncertainty in observations. For SOA, we estimate the 1σ uncertainty of ~15%,

which is lower than the typical 1σ uncertainty of the AMS (Bahreini et al., 2009) due to the careful calibrations and excellent intercomparisons in the various campaigns (see Table 1 for references for the AMS comparisons). For ΔCO, the largest uncertainty is associated with the CO background (Hayes et al., 2013; Nault et al., 2018), and is estimated to be ~10% at 0.5 photochemical equivalent days (Hayes et al., 2013). The uncertainty in the emission ratios is ~10% (Wang et al., 2014; de Gouw et al., 2017); though, it may be higher for the values calculated here due to the uncertainty in CO background, rate constants, and photochemical age. Therefore, for Fig. 2a, the uncertainty in the y-values is 18% and the uncertainty in the x-values is 10%. For Fig. 4, the uncertainty in the measurement is 21%.

Another potential source of uncertainty may stem from the fit of the data in Fig. 2a, as the data point from Seoul (KORUS-AQ) could be impacting the fit due to the difference in its value compared to the other locations. Statistical analysis for the influence of the data from Seoul on the figure was conducted, including a T-test, Cook's Distance test, and Difference in Fits test (Table S11). All three statistical tests show that the data from Seoul (and all the data in general) is not overly influencing the reported slope.

A further potential source of uncertainty in this analysis is the calculated VOC emission ratios for the studies that did not have ratios published previously (Houston 2000, London, Houston 2013, and Seoul). To investigate how well Eq. 3 does in estimating the VOC emission ratios, a comparison of the estimated VOC emission ratios versus previously published ratios for two different cities, Mexico City (Apel et al., 2010; Bon et al., 2011) and Los Angeles (de Gouw et al., 2017) was made (Table S10). Also, for Mexico City, two locations, an urban and a

suburban site, were compared both against each other (Apel et al., 2010; Bon et al., 2011) and the calculated values from Eq. 3.

First, as shown in Table S10, even for the same location (suburban Mexico City), different values in the emission ratio, especially for the alkanes, can be observed, by as much as a factor of 7. This can be partially explained by differences in how the emission ratios were determined. For both Apel et al. (2010) and Bon et al. (2011), the authors took the slope of VOCs versus CO and used different regression techniques and different time periods. Comparing their technique with ours, we generally estimate VOC emission ratios within 50% of the reported values, and the estimation improves for shorter lived compounds (e.g., aromatics). However, de Gouw et al. (2017) more carefully took chemistry into consideration for any potential losses of the VOCs prior to observation to determine emission ratios, similar to this study. We believe the comparison with de Gouw et al. (2017) provides a more useful comparison in the method presented here. We find, at most, a 30% difference in the emission ratios, with an average difference of 4±15% for all compounds. Thus, from this analysis, we conclude that (1) there is large variability in VOC emission ratios across urban areas around the world, which has been highlighted in other studies (Warneke et al., 2007), and (2) the method that considers losses of VOCs is the more accurate procedure to estimate VOC emissions and leads to the best reproducibility across studies and lowest uncertainty (< 30%, ~4% on average).

Supporting Information Tables

Table S1. List of instruments whose observations are used in this study. In some cases ΔSOA/ΔCO (Table S4), SOA versus O_x slope (Table S4), or VOC emission ratios (Table S5 through Table S8) had already been reported, and, in those cases, we use the previous literature reports in our analyses.

Location	SOA	O_x	HCHO	PAN	VOCs	CO
Houston, TX, USA (2000)	Q-AMS[a]	CL & UV Absortpion[b]	DOAS[c]	GC-ECD[d]	GC-FID, GC-MS[e]	Infrared Absortion[f]
Mexico City, Mexico (2006)	HR-ToF-AMS[g]	CL[h]	TDLAS[i]	CIMS[j]	WAS[k]	UV RF[l]
Los Angeles, CA, USA (2010)	HR-ToF-AMS[g]	CL & UV Absorption[m]	Average of DOAS[c] & Hantzsch Reaction[n]	GC-ECD[d]	GC-MS[o]	UV RF[l]
Beijing, China (2011)	HR-ToF-AMS[g]	CL & UV Absorption[p]	PTR-MS[q]	GC-ECD[r]	GC-FID[s]	IR Absorption[p]
London, UK (2012)	C-ToF-AMS[t]	CL & UV Absorption[u]	Hantzsch Reaction[n]	GC-ECD[v]	GC-FID & GC×GC-FID[w]	UV RF[l]
Houston, TX, USA (2013)	HR-ToF-AMS[g]	CL[x]	Average of LIF[y] & CAMS[z]	CIMS[j]	WAS[k]	DACOM[aa]
Seoul, South Korea (2016)	HR-ToF-AMS[g]	CL[h]	CAMS[z]	CIMS[j]	WAS[k]	DACOM[aa]

[a]Quadrupole Aerosol Mass Spectrometer (Q-AMS) (Jayne et al., 2000)
[b]Chemiluminescence (CL) and UV Absorption (Williams et al., 1997)
[c]Differential Optical Absorption Spectrometry (DOAS) (Stutz and Platt, 1996, 1997)
[d]Gas chromatography-electron capture detector (GC-ECD) (Williams et al., 2000; Roberts et al., 2002)
[e]Gas chromatography-flame ionization detector (GC-FID) and gas chromatography mass spectrometer (Roberts et al., 2001)
[f]TECO Model 48s IR gas-filter
[g]High Resolution Time-of-Flight Aerosol Mass Spectrometer (HR-ToF-AMS) (DeCarlo et al., 2006)
[h]Chemiluminescence (CL) and UV Absorption (Weinheimer et al., 1994)
[i]Tunable diode laser absorption spectroscopic (TDLAS) measurements (Fried et al., 2003)
[j]Chemical ionization mass spectrometer (CIMS) (Huey L Tanner D Slusher D Dibb J Arimoto R Chen G Davis D Buhr M Nowak J Mauldin R Eisele F, 2004; Slusher et al., 2004; Kim et al., 2007)
[k]Whole air sample, followed by analysis with GC-FID and/or GC-MS (Blake et al., 2003)
[l]UV Resonance Fluorescence (RF) (Gerbig et al., 1999)

[m]Chemiluminescence (CL) and UV Absorption (Hayes et al., 2013)
[n]Hantzsch reaction (Cárdenas et al., 2000)
[o]Gas chromatograph mass spectrometer (Gilman et al., 2010)
[p]Chemiluminescence (CL), UV Absorption, and IR Absorption (Hu et al., 2016)
[q]Proton transfer reaction mass spectrometer (PTR-MS) (Warneke et al., 2011)
[r]Gas chromatography electron capture detector (GC-ECD) (Zhang et al., 2017)
[s]Gas chromatography flame ionization detector (GC-FID) (Wang et al., 2014)
[t]Compact Time-of-Flight Aerosol Mass Spectrometer (C-ToF-AMS) (Drewnick et al., 2005)
[u]Chemiluminescence (CL) and UV Absorption (Whalley et al., 2016)
[v]Gas chromatography electron capture detector (GC-ECD) (Whalley et al., 2016)
[w]Gas chromatography flame ionization detector (GC-FID) (Dunmore et al., 2015)
[x]Chemiluminescence (CL) (Ryerson et al., 1999; Pollack et al., 2010)
[y]Laser induced fluorescence (LIF) (Cazorla et al., 2015)
[z]Compact Atmospheric Multi-species Spectrometer (CAMS) difference frequency absorption spectrometer (Weibring et al., 2010)
[aa]Tunable diode laser absorption spectroscopy (Sachse et al., 1987)

Table S2. Concentrations of PM_1 components shown in Fig. 1. References for the measurements can be found in Table 1.

Dataset Location	Average Concentration (μg sm^{-3}) of submicron aerosol under standard temperature and pressure				
	SOA	**HOA**	**SO_4**	**NO_3**	**NH_4**
Houston, TX, USA (2000)	2.7	0.7	4.9	0.4	1.5
Northeast USA (2002)	4.9	0.5	2.0	0.3	0.7
Tokyo, Japan (2004)	6.0	1.5	4.4	0.9	4.0
Mexico City, Mexico (2006)	11.2	4.8	1.9	6.0	2.5
Paris, France (2009)	1.9	1.1	1.2	0.5	0.6
Los Angeles, CA, USA (2010)	5.0	2.0	2.9	3.6	2.1
Changdao Island, China (2011)	9.4	4.4	8.3	12.2	6.5
Beijing, China (2011)	17.1	8.9	22.0	16.8	13.7
London, UK (2012)	2.7	1.6	1.4	2.7	1.3
Houston, TX, USA (2013)	3.7	0.0	2.7	0.1	0.6
New York City, NY, USA (2015)	0.8	0.7	1.2	1.4	0.4
Seoul, South Korea (2016)	11.9	1.3	5.0	7.9	4.4

Table S3. Table summarizing the results of recent GEOS-Chem performance evaluations for modeling BSOA.

Study	Observed Data	Species	Details
Fisher et al. (2016)[a]	SEAC^{4}RS, below 1 km (spatial pattern), below 500 m (bias)	Isoprene	Spatial patterns well captured, and biases are +34% for isoprene and +3% for monoterpenes
		Monoterpene	
		Organic Nitrates from Isoprene	Spatial patterns well captured, and biases are -0.6% for first- and -35% for second-generation isoprene nitrates
	SEAC^{4}RS, 0 - 4 km vertical profiles	Isoprene	Agreed well but GEOS-Chem somewhat overestimated observed concentrations near 1km
		Monoterpene	
		HCHO	
		Organic Nitrates from Isoprene	Agreed within measurement uncertainties
	SOAS, at the surface	Isoprene	Underestimated isoprene and monoterpenes (-28% and -54%), but overestimated first- and second- generation isoprene nitrates (+85% and +43%)
		Monoterpene	
		HCHO	
		Organic Nitrates from Isoprene	
Travis et al. (2016)	SEAC^{4}RS, 0 - 12 km	First Generation from Isoprene Nitrates	Good agreement for ISOPOOH and ISOPN, underestimation of HPALDs by a factor of two
		ISOPOOH	
		HPALDS	
Marais et al. (2016)	SOAS, at the surface	IEPOX-SOA	Good agreement for isoprene derived aerosols, mean concentrations were almost the same
		ISOPOOH-SOA	
	SEAC^{4}RS, below 2 km (spatial pattern)	IEPOX-SOA	Spatial patterns well captured

[a]This study decreased isoprene emissions by 15% and doubled monoterpene emissions of MEGANv2.1.

Table S3 cont.

Study	Observed Data	Species	Details
Kaiser et al. (2018)[a]	SEAC^{4}RS	Isoprene	All were overestimated, except for first generation isoprene nitrates
		HCHO	
		ISOPOOH	
		MVK + MACR	
		First Generation Isoprene Nitrates	
Pai et al. (2020)	15 airborne campaigns (SEAC^{4}RS, GoAmazon, SENEX, OP3, etc.)	OA under biognic dominant conditions	Slight overestimation, but generally very similar in magnitude

[a]NEI NO_x emissions other than power plants decreased by 60%, soil NO_x emissions were reduced by 50% across the Midwestern US. With the decrease of NO_x emissions, ISOPOOH concentrations were increased in GEOS-Chem.

Table S4. Dilution-corrected SOA concentrations at 0.5 equivalent days and slopes of SOA versus O_x, HCHO, and PAN used in Fig. 2 and Fig. 3. References for the values can be found either in Table 1 or found in Fig. S2 through Fig. S4. Uncertainty is 1σ, and either represents propagation in uncertainty in measurements (see Sect. S5) for ΔSOA/ΔCO or uncertainty in slopes for SOA versus the three photochemical species.

Dataset Location	ΔSOA/ΔCO at 0.5 eq. days	SOA vs. O_x Slopes	SOA vs. HCHO Slopes	SOA vs. PAN Slopes
Houston, TX, USA (2000)		0.04±0.01[a]	0.32±0.08	1.41±0.46
Northeast USA (2002)	16±3[b] 48±9[c]			
Mexico City, Mexico (2003)		0.14±0.01[a]		
Tokyo, Japan (2004)		0.19±0.01[a]		
Mexico City, Mexico (2006)	58±10	0.16±0.01	1.60±0.06	5.60±0.30
Paris, France (2009)		0.14±0.01[a]		
Pasadena, CA, USA (2010)	59±11	0.16±0.01	1.93±0.02	5.41±0.12
Changdao Island, China (2011)	23±4			
Beijing, China (2011)	31±6	0.21±0.01	3.90±0.15	7.42±0.46
London, UK (2012)	54±10	0.13±0.01	0.36±0.02	3.37±0.41
Houston, TX, USA (2013)		0.16±0.01	1.52±0.13	6.92±0.58
New York City, NY, USA (2015)	33±6			
Seoul, South Korea (2016)	107±19	0.29±0.02	3.73±0.26	10.13±0.52

[a]Missing reported uncertainty; therefore, assuming ±0.01, as that is typical for other campaigns [b]From de Gouw et al. (2005). [c]From Kleinman et al. (2007).

Table S5. Emission ratios of BTEX aromatics used in this study. If no reference is listed, then the emission ratio was calculated using Eq. 3.

Dataset Location	Emission Ratios (ppbv aromatic/ppmv CO)					References
	Benzene	Toluene	Ethylbenzene	m+p-xylene	o-xylene	
Houston, TX, USA (2000)	2.6	3.5	0.6	2.8	0.8	
NE USA, Ship (2002)	0.9	2.0	0.2	0.6	0.3	Baker et al. (2008)
NE USA, Aircraft (2002)	0.8	2.9	0.4	1.2	0.5	Warneke et al. (2007)
Mexico City, Mexico (2006)	0.9	7.5	0.9	1.1	0.4	Apel et al. (2010)
Los Angeles, CA, USA (2010)	1.3	3.4	0.6	2.1	0.8	de Gouw et al. (2017)
Changdao Island, China (2011)	2.3	1.9	0.5	1.3	0.4	Yuan et al. (2013)
Beijing, China (2011)	1.2	2.4	1.0	1.6	0.6	Wang et al. (2014)
London, UK (2012)	1.8	6.3	1.2	2.2	1.1	
Houston, TX, USA (2013)	2.3	3.0	0.6	3.9	1.2	
New York City, NY, USA (2015)	0.8	2.9	0.4	1.2	0.5	Warneke et al. (2007)[a]
Seoul, South Korea (2016)	1.1	13.1	2.4	3.3	2.3	

[a]Using the emissions from Warneke et al. (2007) instead of Schroder et al. (2018) as Schroder et al. found significant uncertainty in the emissions calculated from observations.

Table S6. Emission ratios of alkanes used in this study. If no reference is listed, then the emission ratio was calculated using Eq. 3.

Dataset Location	Emission Ratios (ppbv alkane/ppmv CO)							References
	Ethane	Propane	n-Butane	i-Butane	n-Pentane	i-Pentane	n-Hexane	
Houston, TX, USA (2000)	40.9	24.3	9.0	14.7	3.1	10.0	3.1	
NE USA, Ship (2002)	8.3	2.3	1.8	1.3	1.0	2.8	0.9	Baker et al. (2008)
NE USA, Aircraft (2002)	9.9	9.0	2.4	1.3	2.0	5.4	0.6	Warneke et al. (2007)
Mexico City, Mexico (2006)	7.4	41.5	15.1	4.8	2.1	2.7	1.5	Apel et al. (2010)
Los Angeles, CA, USA (2010)	16.5	13.4	5.0	3.2	3.4	8.7	1.4	de Gouw et al. (2017)
Changdao Island, China (2011)	7.7	4.5	2.5	1.2	1.0	1.5	0.5	Yuan et al. (2013)
Beijing, China (2011)	4.3	3.9	2.5	2.5	1.2	2.0	0.6	Wang et al. (2014)
London, UK (2012)	33.0	17.8	17.3	8.4	4.6	11.3	1.3	
Houston, TX, USA (2013)	86.5	37.3	14.6	10.6	7.0	10.5	3.0	
Seoul, South Korea (2016)	16.1	0.4	6.0	3.4	3.1	3.7	1.7	

Table S7. Emission ratios of alkenes used in this study. If no reference is listed, then the emission ratio was calculated using Eq. 3.

Dataset Location	Emission Ratios (ppbv alkene/ppmv CO)		References
	Ethene	Propene	
Houston, TX, USA (2000)	24.4	28.4	
NE USA, Ship (2002)	4.4	1.1	Baker et al. (2008)
NE USA, Aircraft (2002)	4.9	1.4	Warneke et al. (2007)
Mexico City, Mexico (2006)	8.4	2.6	Apel et al. (2010)
Los Angeles, CA, USA (2010)	11.2	4.1	de Gouw et al. (2017)
Changdao Island, China (2011)	5.3	1.4	Yuan et al. (2013)
Beijing, China (2011)	4.4	1.4	Wang et al. (2014)
London, UK ()2012)	10.3	6.2	
Houston, TX, USA (2013)	12.0	15.8	
Seoul, South Korea (2016)	5.4	2.1	

Table S8. Emission ratios of non-BTEX aromatics used in this study. If no reference is listed, then the emission ratio was calculated using Eq. 3.

Dataset Location	Emission Ratios (ppbv aromatic/ppmv CO)			References
	Trimethylbenzenes	Ethyltoluenes	Propylbenzene	
NE USA, Aircraft (2002)	0.71	0.58	0.14	Warneke et al. (2007)
Los Angeles, CA, USA (2010)	1.47	0.56	0.13	de Gouw et al.(2017)
Beijing, China (2011)	0.57	0.41	0.09	Wang et al. (2014)
London, UK (2012)	0.49	0.23	0.58	
New York City, NY, USA (2015)	0.71	0.58	0.14	Warneke et al. (2007)

Table S9. Normalized mass concentration of primary organic aerosol (POA/CO) measured in various campaigns, used to determine SVOC emission ratios.

Dataset Location	Normalized Mass Concentration (μg sm^{-3} $ppmv^{-1}$)		References
	HOA/CO	Other POA/CO	
NE USA (2002)	12.2	-	de Gouw et al. (2005)
Los Angeles, CA, USA (2010)	5.3	7.7	Hayes et al. (2013)
Beijing, China (2011)	6.1	9.9	Hu et al. (2016)
London, UK (2012)	17.9	14.1	Young et al. (2015)
New York City, NY, USA (2015)	5.6	14.4	Schroder et al. (2018)

Table S10. Comparison of estimated VOC emission ratios from two studies from Mexico City (Apel et al., 2010; Bon et al., 2011), one study from Los Angeles (de Gouw et al., 2017), and this study.

VOC Ratio	Apel et al. (2010) Downtown MC	This Study	Apel et al. (2010) Suburbs MC	Bon et al. (2011) Outskirt MC	This Study	de Gouw et al. (2017) LA	This Study
Ethane	7.4	8.2	3.0	21.5	8.2	16.5	18.9
Propane	41.5	36.9	49.3	61.7	38.4	13.4	14.0
n-Butane	15.1	14.9	15.3	21.7	14.1	5.0	5.7
i-Butane	4.8	4.8	5.3	7.2	4.9	3.2	3.5
n-Pentane	2.1	2.9	2.1	2.5	2.1	3.4	3.4
i-Pentane	2.7	3.6	3.2	3.3	3.1	8.7	7.8
n-Hexane	1.5	1.9	1.3	1.5	1.2	1.4	1.7
Ethene	8.4	6.1	7.9	7.0	7.1	11.2	9.6
Propene	2.6	1.3	2.9	3.0	1.6	4.1	3.9
Benzene	0.9	1.0	1.2	1.2	1.3	1.3	1.4
Toluene	7.5	9.2	5.2	4.2	4.1	3.4	3.0
Ethylbenzene	0.9	0.8	0.4	4.3*	0.4	0.6	0.6
m+p-Xylene	1.1	0.7	0.5	No Data	0.4	2.1	1.9
o-Xylene	0.4	0.2	0.2	No Data	0.2	0.8	0.7
Trimethylbenzenes	No Data	No Data	No Data	No Data	No Data	1.6	1.1
Ethyltoluenes	No Data	No Data	No Data	No Data	No Data	0.6	0.4
Propylbenzene	No Data	No Data	No Data	No Data	No Data	0.1	0.1

*In Bon et al. (2011), they reported the sum of C8 aromatics, which is the sum of ethylbenzene and xylenes

Table S11. Statistical analysis of the data used in Fig. 2 to determine if any point is influencing the slope, using the T-test, Cook's Distance test, and Difference in Fits test. For the T-test, the point is influential if the t value is < 0.05 while for the Cook's Distance and Difference in Fits test, the point is influential if the value is > 1.

Campaign	T-test	Cook's Distance	Difference in Fits
NE US Ship	0.63	0.06	-0.29
NE US Aircraft	0.12	0.27	0.73
Mexico City	0.39	0.06	0.33
Los Angeles	0.32	0.08	0.38
Changdao Island, China	0.41	0.09	-0.38
Beijing	0.42	0.06	-0.32
London	0.31	0.13	-0.48
NYC	0.90	0.00	-0.05
Seoul	0.99	0.00	0.01

505 **Table S12**. Rate constants used throughout this study.

Compound	Rate Constant (cm^3 $molec.^{-1}$ s^{-1})	References
Alkanes		
Ethane	$6.9\times10^{-12}\times\exp(-1000/T)$	Atkinson et al. (2006)
Propane	$7.6\times10^{-12}\times\exp(-585/T)$	Atkinson et al. (2006)
n-Butane	$9.8\times10^{-12}\times\exp(-425/T)$	Atkinson et al. (2006)
i-Butane	$1.17\times10^{-17}\times T^2\times\exp(213/T)$	Atkinson and Arey (2003)
n-Pentane	$2.52\times10^{-17}\times T^2\times\exp(158/T)$	Atkinson and Arey (2003)
i-Pentane	3.6×10^{-12}	Atkinson and Arey (2003)
n-Hexane	$2.54\times10^{-14}\times T\times\exp(-112/T)$	Atkinson and Arey (2003)
Alkenes		
Ethene	$7.84\times10^{-12,a}$	Atkinson et al. (2006)
Propene	$2.86\times10^{-11,a}$	Atkinson et al. (2006)
Aromatics		
Benzene	$2.3\times10^{-12}\times\exp(-190/T)$	Atkinson et al. (2006)
Toluene	$1.8\times10^{-12}\times\exp(340/T)$	Atkinson et al. (2006)
Ethylbenzene	7×10^{-12}	Atkinson and Arey (2003)
m+p-xylene	$1.87\times10^{-11,b}$	Atkinson and Arey (2003)
o-xylene	1.36×10^{-11}	Atkinson and Arey (2003)
Trimethylbenzenes	$2.73\times10^{-12}\times\exp(730/T)$	Bohn and Zetzsch (2012)
Ethyltoluenes	1.2×10^{-11}	Atkinson and Arey (2003)
Propylbenzene	5.8×10^{-12}	Atkinson and Arey (2003)
S/IVOCs		
IVOCs C* = 4 - 6	2×10^{-11}	Jathar et al. (2014) McDonald et al. (2018)
IVOCs C* = 3	3×10^{-11}	
SVOCs & “aging”	4×10^{-11}	Tsimpidi et al. (2010)
NO_x/NO_y		
OH + NO_2	$1.23\times10^{-11,a}$	Mollner et al. (2010)

[a]Showing the rate constant at 298 K, 1013 hPa. However, for this study, we used the temperature and pressure dependent formulation listed in each respective reference.
[b]This is the average of m-xylene and p-xylene rate constants.

509 **Table 13.** Parameters for VOC, IVOC, and SVOC aerosol yields. The yields are taken from Ma
510 et al. (2017).

Compound	Stoichiometric SOA yield High-NOx, 298 K (μg m^{-3})				
	0.1	1	10	100	1000
Benzene Toluene Ethyltoluene Propylbenzenes	N/A	0.276	0.002	0.431	0.202
Xylenes Trimethylbenzenes	N/A	0.310	0.000	0.420	0.209
IVOC C* = 6	0.007	0.090	0.206	0.350	0.00
IVOC C* = 5	0.0498	0.0814	0.456	0.278	0.00
IVOC C* = 4	0.053	0.103	0.464	0.266	0.00
IVOC C* = 3	0.064	0.0914	0.562	0.209	0.00
HOA C* = 2	N/A	N/A	0.28	N/A	N/A
HOA C* = 1	N/A	0.18	N/A	N/A	N/A
HOA C* = 0	0.12	N/A	N/A	N/A	N/A
COA C* = 2	N/A	N/A	0.1881	N/A	N/A
COA C* = 1	N/A	0.1188	N/A	N/A	N/A
COA C* = 0	0.0594	N/A	N/A	N/A	N/A

511

Table S14. Table of GBD parameters, which is the mean of the draw values (see associated file) from the IHME website: http://ghdx.healthdata.org/record/global-burden-disease-study-2010-gbd-2010-ambient-air-pollution-risk-model-1990-2010.

Parameter	IHD	Stroke	COPD	LC	ALRI
α	1.4273	1.2641	15.224	114.74	2.2023
β	0.04764	0.00722	0.00095	0.000141	0.000284
ρ	0.376	1.314	0.684	0.741	1.183
$PM_{2.5,Threshold}$	7.462	7.387	7.374	7.380	7.283

Table S15. Table of GEMM parameters. The GEMM parameters are from Burnett et al. (2018), with the Chinese male cohort.

Cause of Death	Age Range (years)	θ	Standard Error θ	α	μ	π
NCD + LRI	>25	0.1430	0.01807	1.6	15.5	36.8
	27.5	0.1585	0.01477	1.6	15.5	36.8
	32.5	0.1577	0.01470	1.6	15.5	36.8
	37.5	0.1570	0.01463	1.6	15.5	36.8
	42.5	0.1558	0.01450	1.6	15.5	36.8
	47.5	0.1532	0.01425	1.6	15.5	36.8
	52.5	0.1499	0.01394	1.6	15.5	36.8
	57.5	0.1462	0.01361	1.6	15.5	36.8
	62.5	0.1421	0.01325	1.6	15.5	36.8
	67.5	0.1374	0.01284	1.6	15.5	36.8
	72.5	0.1319	0.01234	1.6	15.5	36.8
	77.5	0.1253	0.01174	1.6	15.5	36.8
	85	0.1141	0.01071	1.6	15.5	36.8
IHD	>25	0.2969	0.01787	1.9	12	40.2
	27.5	0.5070	0.02458	1.9	12	40.2
	32.5	0.4762	0.02309	1.9	12	40.2
	37.5	0.4455	0.02160	1.9	12	40.2
	42.5	0.4148	0.02011	1.9	12	40.2
	47.5	0.3841	0.01862	1.9	12	40.2
	52.5	0.3533	0.01713	1.9	12	40.2
	57.5	0.3226	0.01564	1.9	12	40.2
	62.5	0.2919	0.01415	1.9	12	40.2

520 **Table 15 cont.**

Cause of Death	Age Range (years)	θ	Standard Error θ	α	μ	π
IHD	67.5	0.2612	0.01266	1.9	12	40.2
	72.5	0.2304	0.01117	1.9	12	40.2
	77.5	0.1997	0.00968	1.9	12	40.2
	85	0.1536	0.00745	1.9	12	40.2
Stroke	>25	0.2720	0.07697	6.2	16.7	23.7
	27.5	0.4513	0.11919	6.2	16.7	23.7
	32.5	0.4240	0.11197	6.2	16.7	23.7
	37.5	0.3966	0.10475	6.2	16.7	23.7
	42.5	0.3693	0.09752	6.2	16.7	23.7
	47.5	0.3419	0.09030	6.2	16.7	23.7
	52.5	0.3146	0.08307	6.2	16.7	23.7
	57.5	0.2872	0.07585	6.2	16.7	23.7
	62.5	0.2598	0.06863	6.2	16.7	23.7
	67.5	0.2325	0.06190	6.2	16.7	23.7
	72.5	0.2051	0.05418	6.2	16.7	23.7
	77.5	0.1778	0.04695	6.2	16.7	23.7
	85	0.1368	0.03611	6.2	16.7	23.7
COPD	>25	0.2510	0.06762	6.5	2.5	3.2
Lung Cancer	>25	0.2942	0.06147	6.2	9.3	29.8
LRI	>25	0.4468	0.11735	6.4	5.7	8.4

521

Table S16. Calculated premature mortality from PM with all aerosol (base mortality) and removing ASOA, using the IER method.

Location[a]	Base Mortality	Mortality reduced due to removing ASOA	Percent mortality reduced due to removing ASOA
North America	43,408	18,479	43%
Central America	11,808	3,395	29%
South America	31,214	10,100	32%
Africa	258,294	14,869	6%
Western Europe	305,754	31,880	10%
Eastern Europe	195,749	16,003	8%
South Asia	938,967	75,085	8%
Southeastern Asia	135,433	31,886	24%
East Asia	1,315,720	122,190	9%
Oceania	95	27	28%
Rest of the World	72,385	13,337	18%
Total	3,308,957	337,224	10%

[a]Locations defined by:
http://themasites.pbl.nl/tridion/en/themasites/_disabled_image/background/regions/index-2.html

Table S17. Calculated premature mortality from PM with all aerosol (base mortality) and removing ASOA, using the GEMM method.

Location[a]	Base Mortality	Mortality reduced due to removing ASOA	Percent mortality reduced due to removing ASOA
North America	178,793	24,892	14%
Central America	58,516	7,298	12%
South America	145,395	22,372	15%
Africa	765,946	34,528	5%
Western Europe	768,991	50,427	7%
Eastern Europe	465,341	25,552	5%
South Asia	2,285,903	166,228	7%
Southeastern Asia	347,191	50,802	15%
East Asia	2,487,349	220,264	9%
Oceania	3,375	428	13%
Rest of the World	269,769	35,051	13%
Total	7,776,570	638,219	8%

[a]Locations defined by:
http://themasites.pbl.nl/tridion/en/themasites/_disabled_image/background/regions/index-2.html

Table S18. List of total final consumption, in millions of tonnes of oil equivalent, of oil products and oil, for each organization. Total final consumption includes imports, and does not include exports (IEA, 2019).

Organization	Industry	Transportation	Non-Energy
World	307	2533	645
OECD	89	1147	326
Africa	18.4	115.4	7.9
Non-OECD	28.3	135	20
Middle East	33.5	126.3	47.5
Non-OECD Europe and Eurasia	35	101	53

Supplemental figures for this study

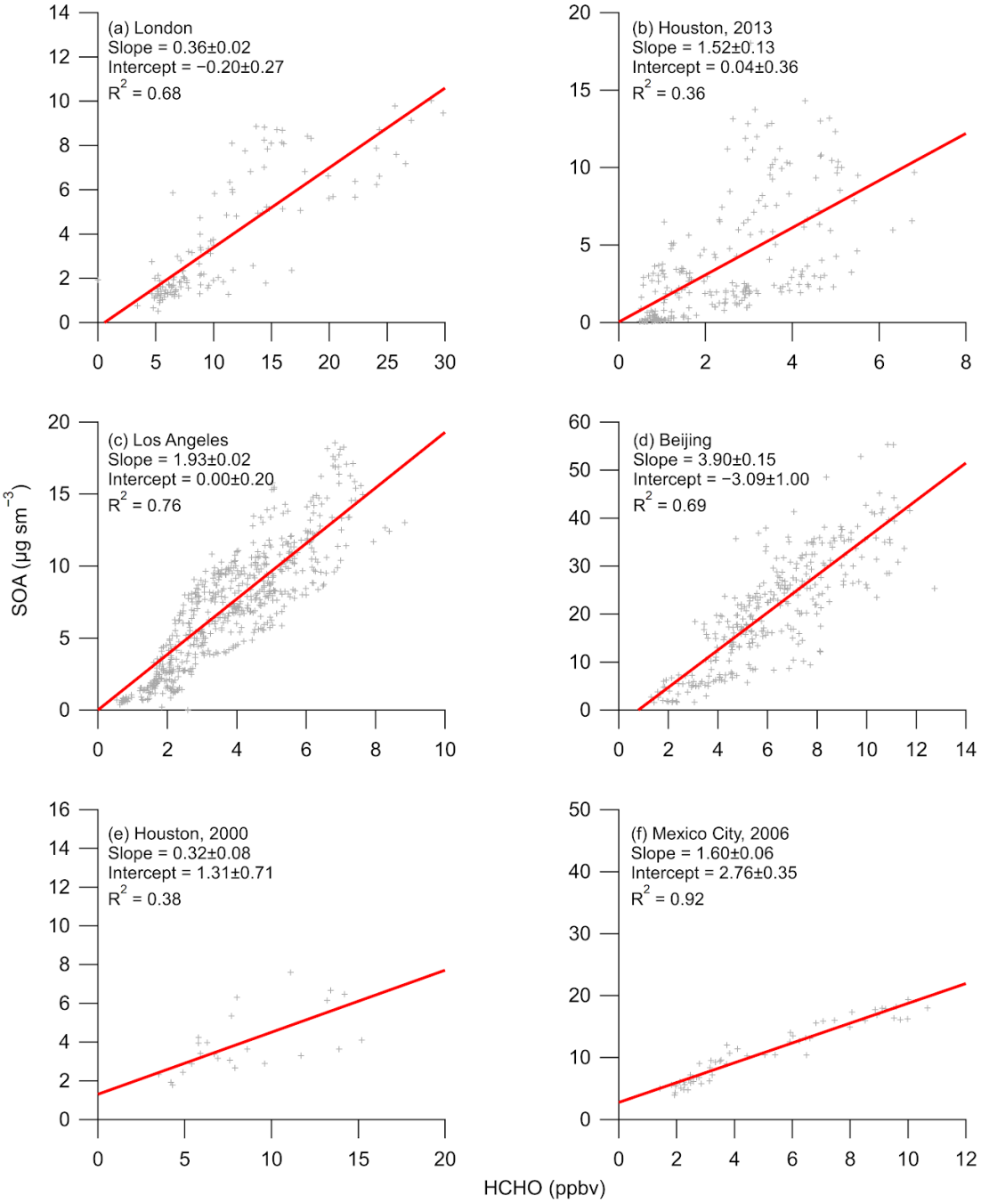

Figure S1. Regression plot of SOA versus HCHO from different campaigns around the world that have not been previously published. Note, for (c), HCHO is 1.24×Hantzsch HCHO, to account for the differences between the two HCHO measurements during CalNex. Note, for (a), SOA is 0.5×OA, estimated from Young et al. (2015), and for (f), SOA is 0.8×OA, estimated from DeCarlo et al. (2010).

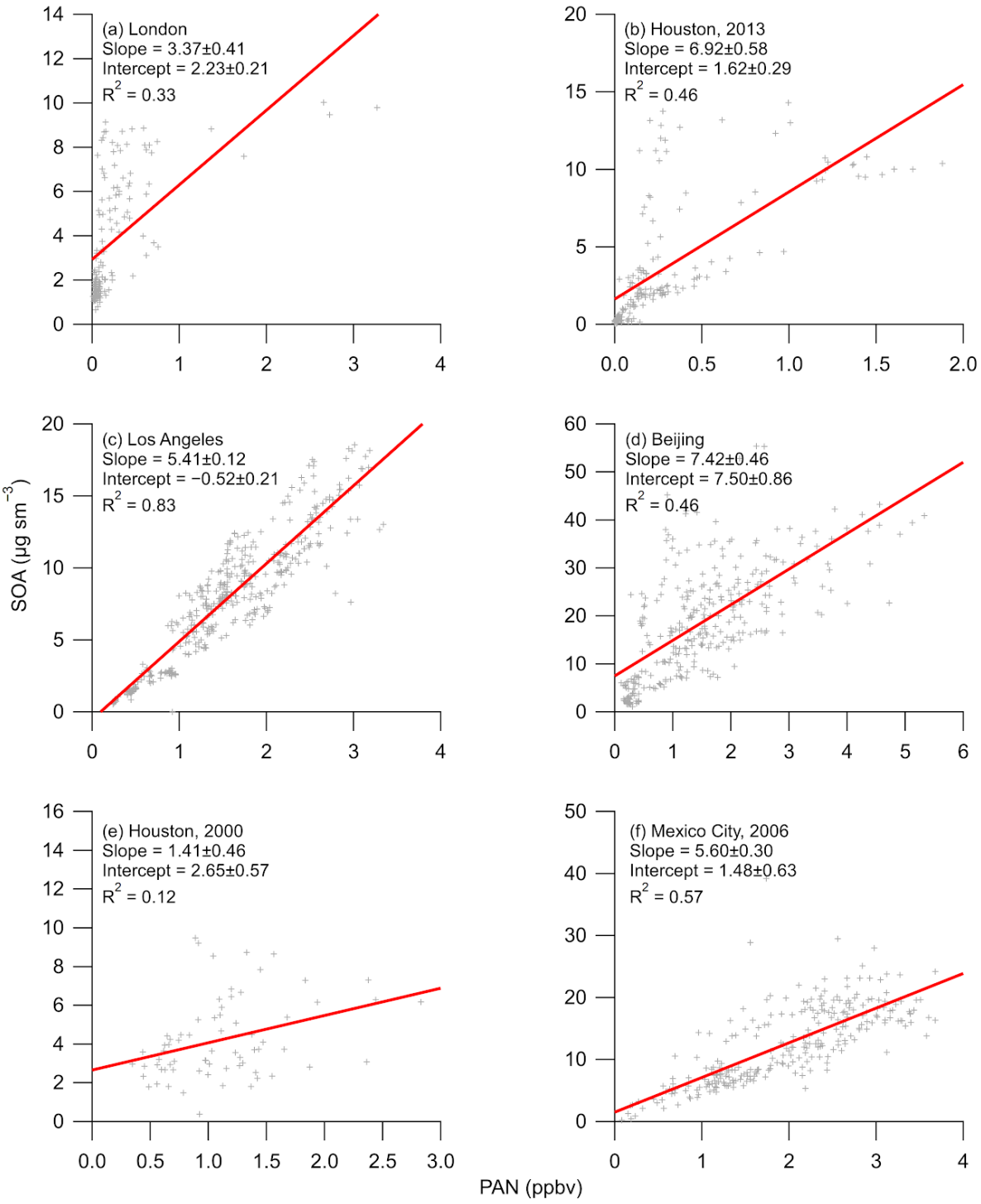

542

543 **Figure S2**. Regression plot of SOA versus PAN from different campaigns around the world that
544 have not been previously published. Note, for (a), SOA is 0.5×OA, estimated from Young et al.
545 (2015), and for (f), SOA is 0.8×OA, estimated from DeCarlo et al. (2010).

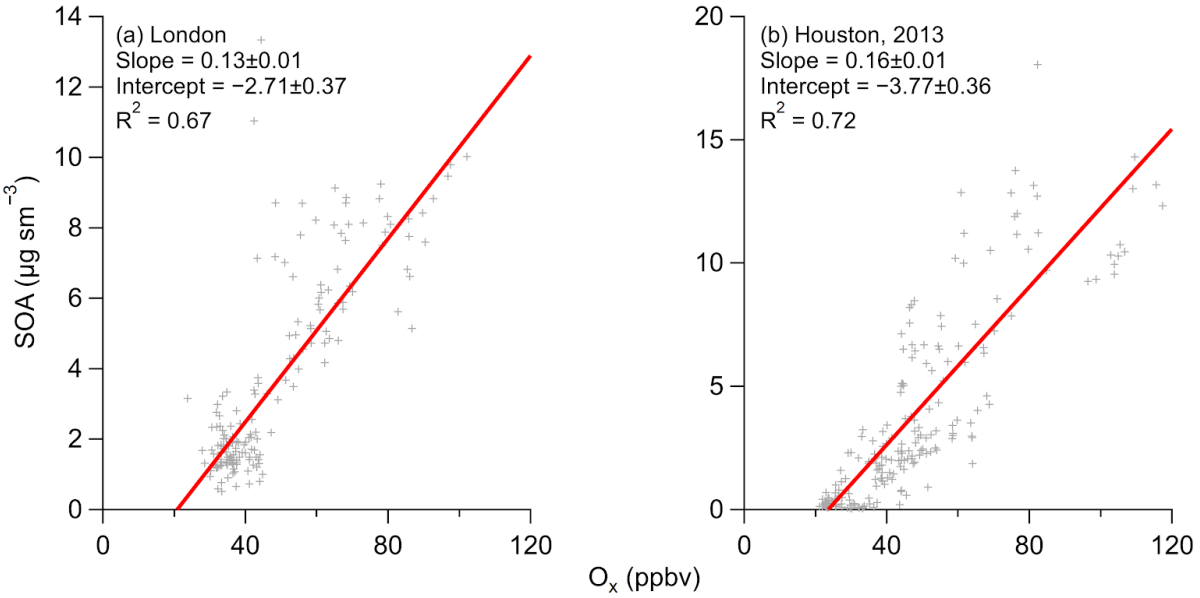

Figure S3. Regression plot of SOA versus Ox from different campaigns around the world that have not been previously published. Note, for (a), SOA is 0.5×OA, estimated from Young et al. (2015).

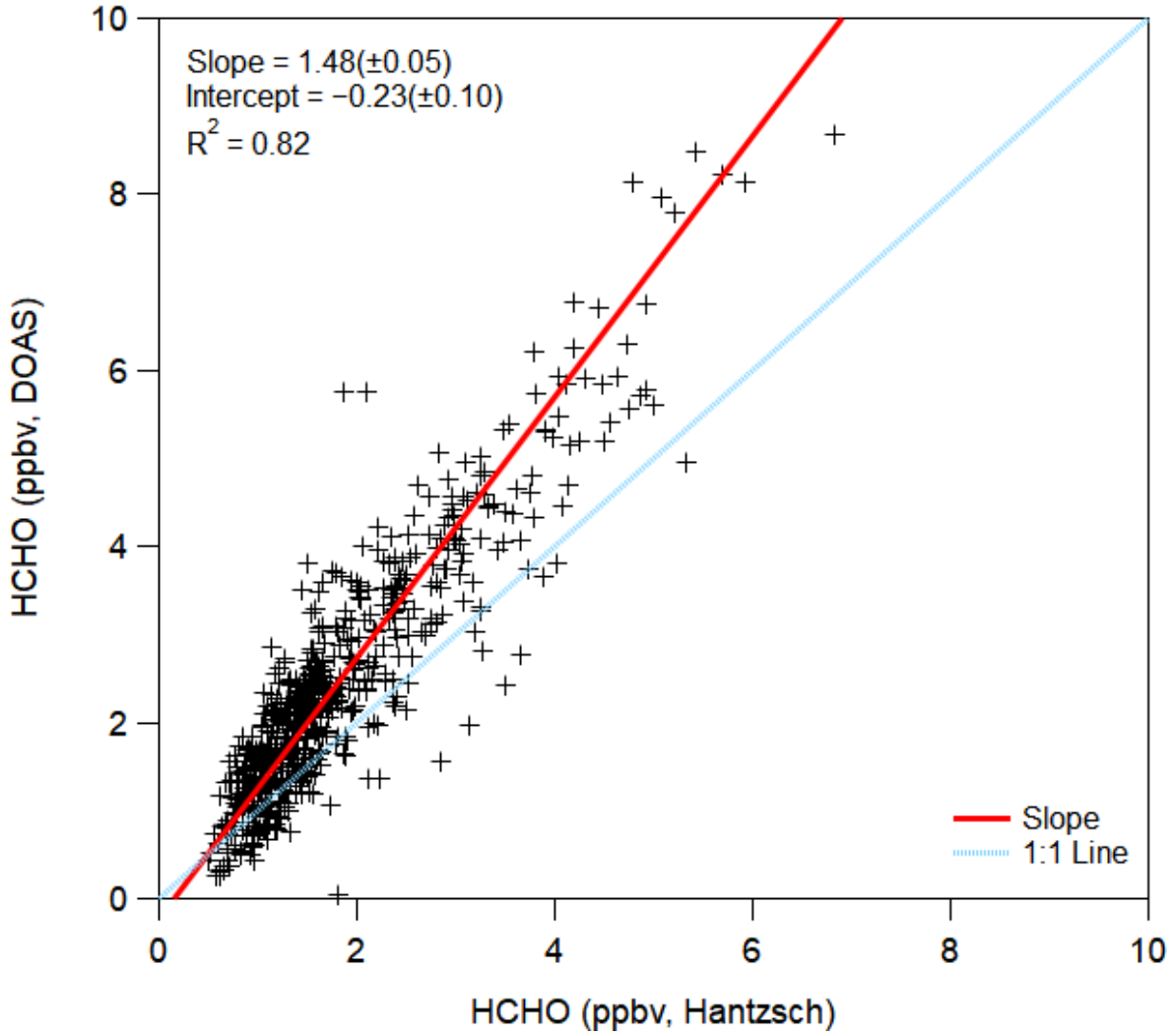

Figure S4. Comparison of HCHO measured by the DOAS (Stutz and Platt, 1996, 1997) and Hantzsch reaction (Cárdenas et al., 2000) methods during the CalNex 2010 study in Pasadena, CA, ground site (Ryerson et al., 2013).

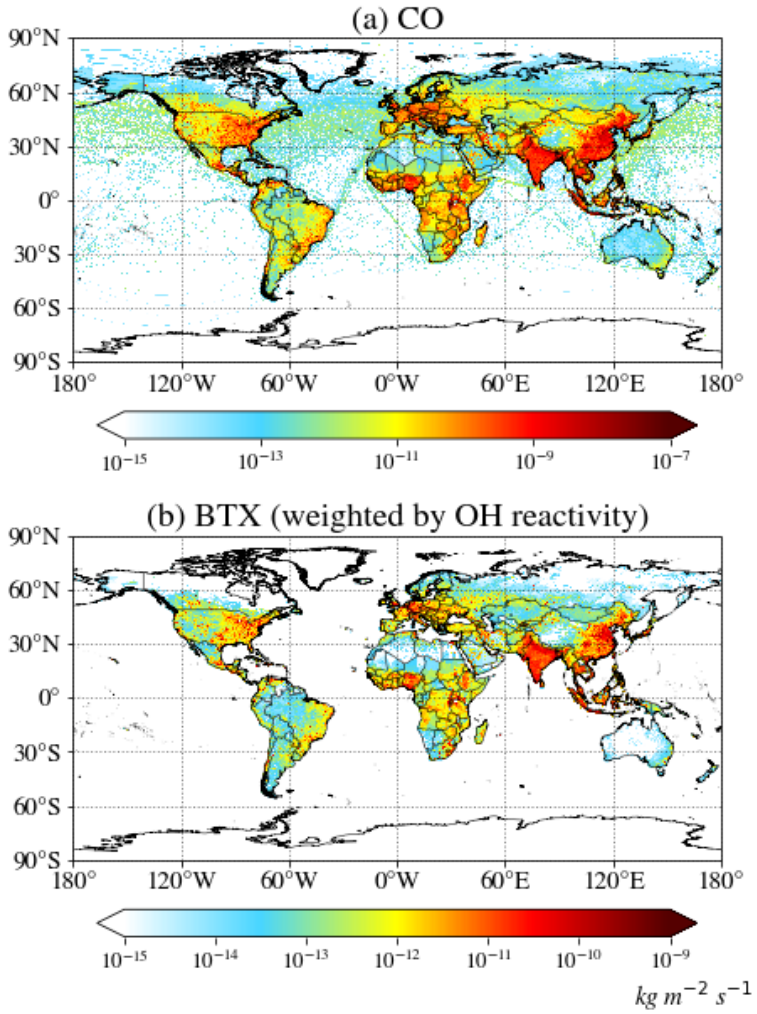

555

556 **Figure S5.** (a) Annually average CO emissions from HTaP. (b) Annually average benzene,
557 toluene, and xylenes (BTX) emissions, weighted by their OH reaction rate

558 ($E_{weight} = N \frac{\sum_i E_i k_{OH,i}}{\sum_i k_{OH,i}}$, $i = B, T, X$; N=3).

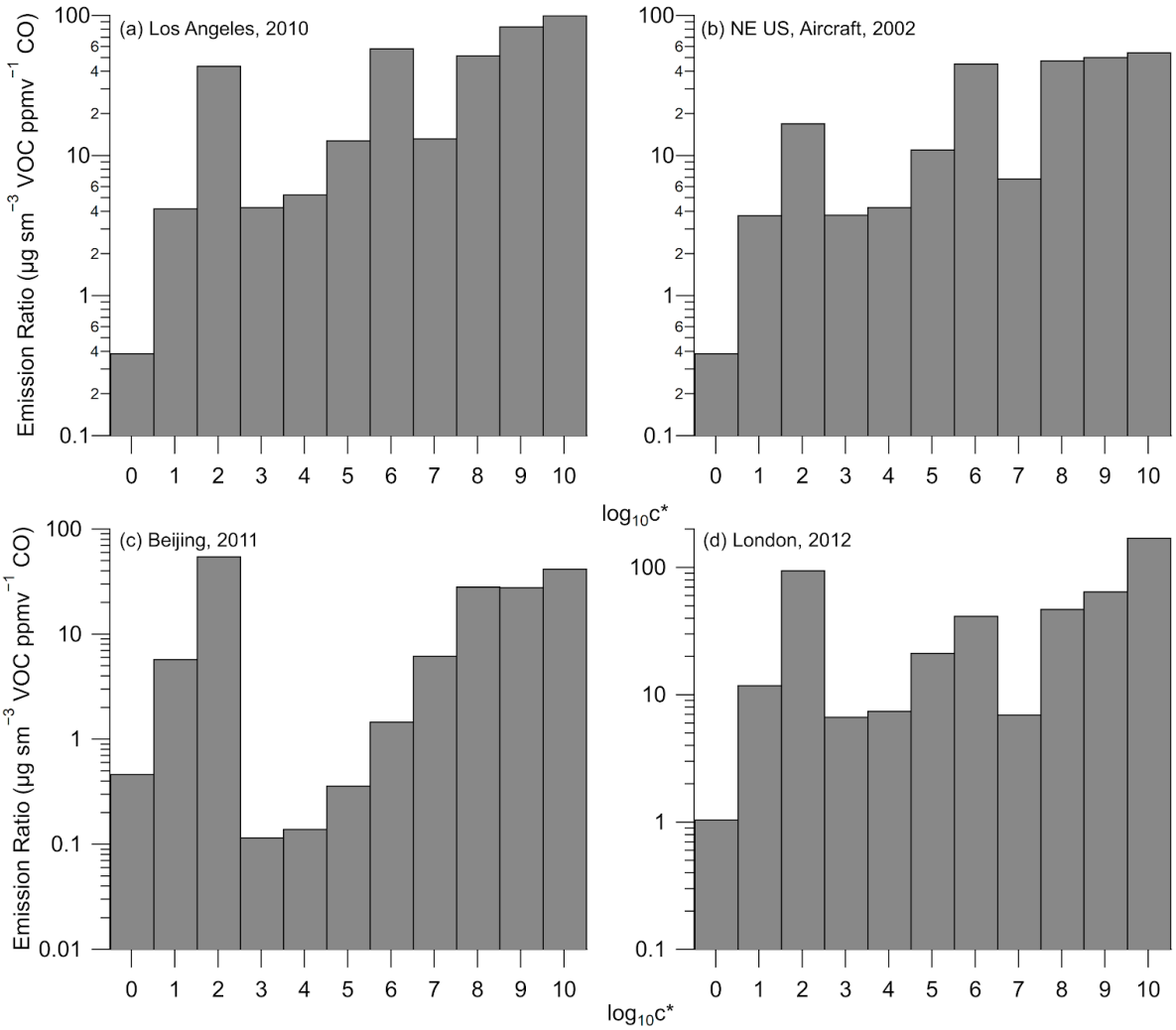

559

560 **Figure S6.** Emission ratio versus saturation concentration ($\log_{10}$(c*)) for (a) Los Angeles, (b) NE
561 US, aircraft, (c) Beijing, and (d) London. The emission ratios for VOCs ($\log_{10}$(c*) ≥ 7) were
562 taken from de Gouw et al. (2017) and Ma et al. (2017) for Los Angeles, Warneke et al. (2007) for
563 NE US, aircraft, and Wang et al. (2014) for Beijing while the VOC emission ratio for London is
564 from Table S6 to Table S8. For VOCs between $\log_{10}$(c*) of 3 and 6 (IVOCs), the volatility
565 distribution from McDonald et al. (2018), along with the ratio of IVOC to BTEX from Figure
566 SI-6 and the emission ratio of BTEX (Table S6), were used to determine the emission ratio
567 versus saturation concentration. Finally, for VOCs between $\log_{10}$(c*) 0 and 2 (SVOCs), the
568 volatility distributions from Robinson et al. (2007) for non-fossil fuel POA and from Worton et
569 al. (2014) for fossil fuel POA were used to convert the normalized POA mass concentration
570 (Table S9) to VOC emission ratios. Note, the emission ratio versus saturation concentration for
571 New York City, 2015, was similar to (b), as the emissions were similar (Fig. 5) and the BTEX for
572 New York City is the same as NE US (Table S5).

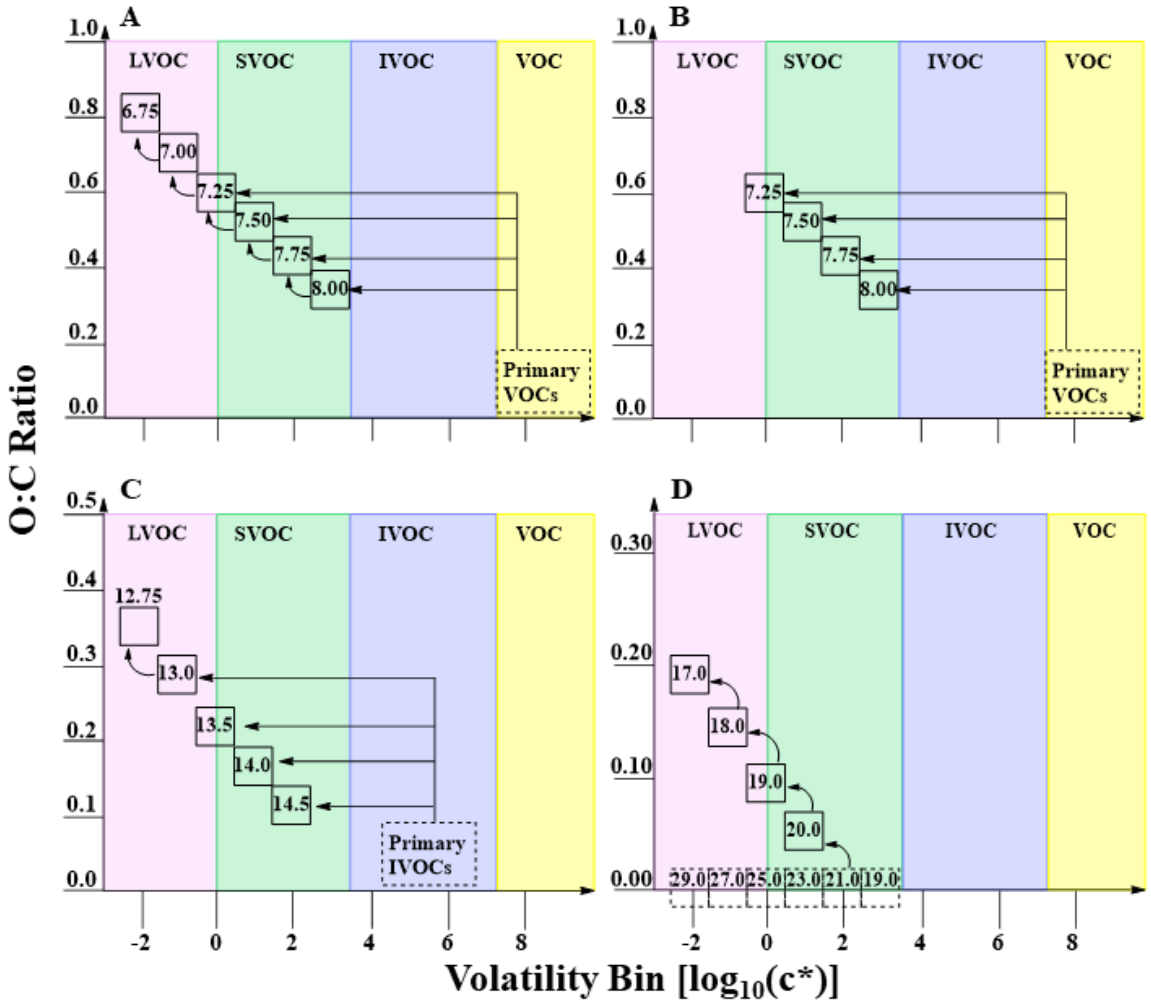

573

574 **Figure S7**. 2-D VBS space defined by oxygen to carbon (O:C) ratio and saturation concentration
575 [$\log_{10}$(c*)] for different oxidation mechanisms and primary sources of OA precursors. Dashed
576 boxes represent primary emissions, while the full boxes represent the secondary oxidation
577 products. (A) and (B) represent different parameterizations for treating traditional anthropogenic
578 and biogenic sources of SOA. Both parameterizations depict the oxidation of an 8-carbon
579 precursor VOC. (A) represents the TSI, or aging, parameterization; (B) represents the MA, or
580 wall-loss corrected, parameterization. (C) Represents the initial oxidation and aging pathway of
581 P-IVOCs following the ZHAO parameterization. It should be noted that the carbon number
582 corresponds to first generation aging and subsequent oxidation results in a 0.25 reduction in
583 carbon number. (D) Represents the decadal aging of SVOCs by hydroxyl radicals. In (D), the full
584 aging pathway of only the C21 species is depicted as an example, though all primary species are
585 allowed to age until the $\log_{10}$(c*) = -2 bin. All emitted P-SVOC species undergo the same
586 decadal aging scheme which begins from the saturation concentration bin of the emitted species.

587

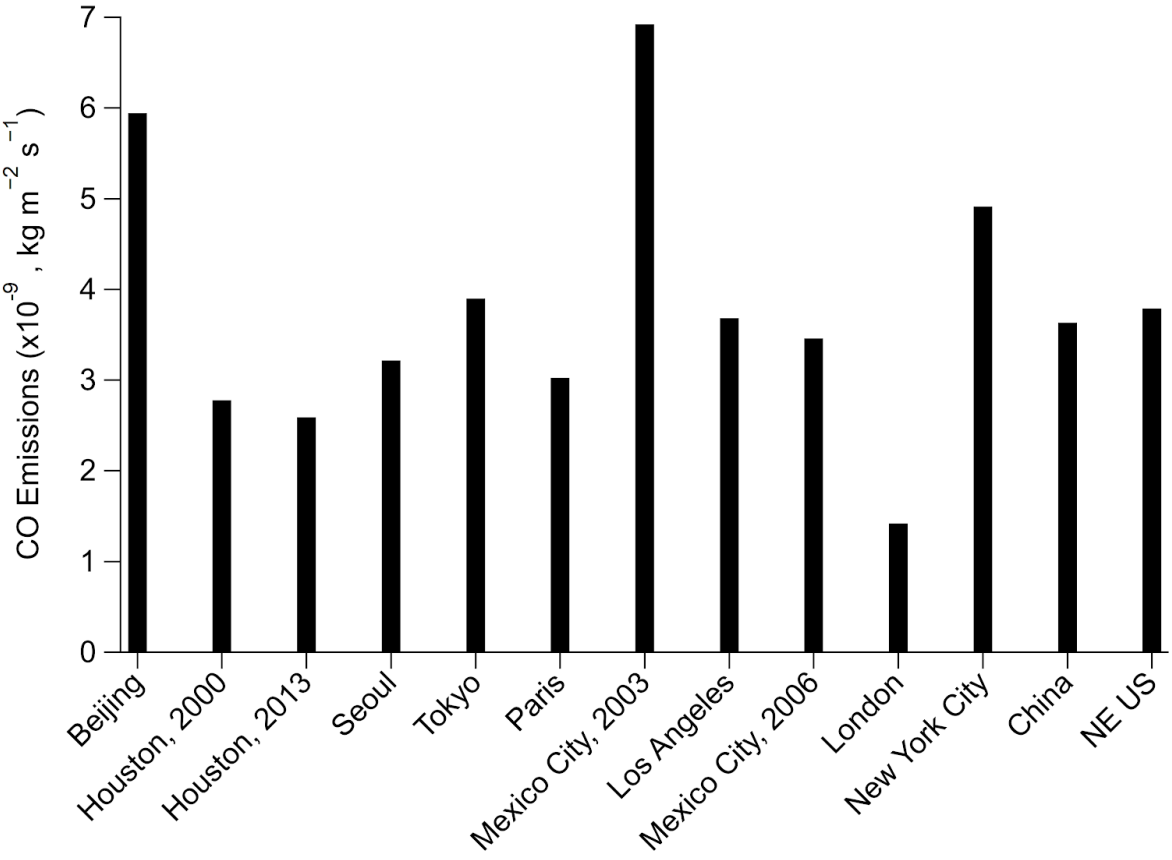

588 **Figure S8**. CO emissions for the cities investigated here from HTAP (Janssens-Maenhout et al.,
589 2015).

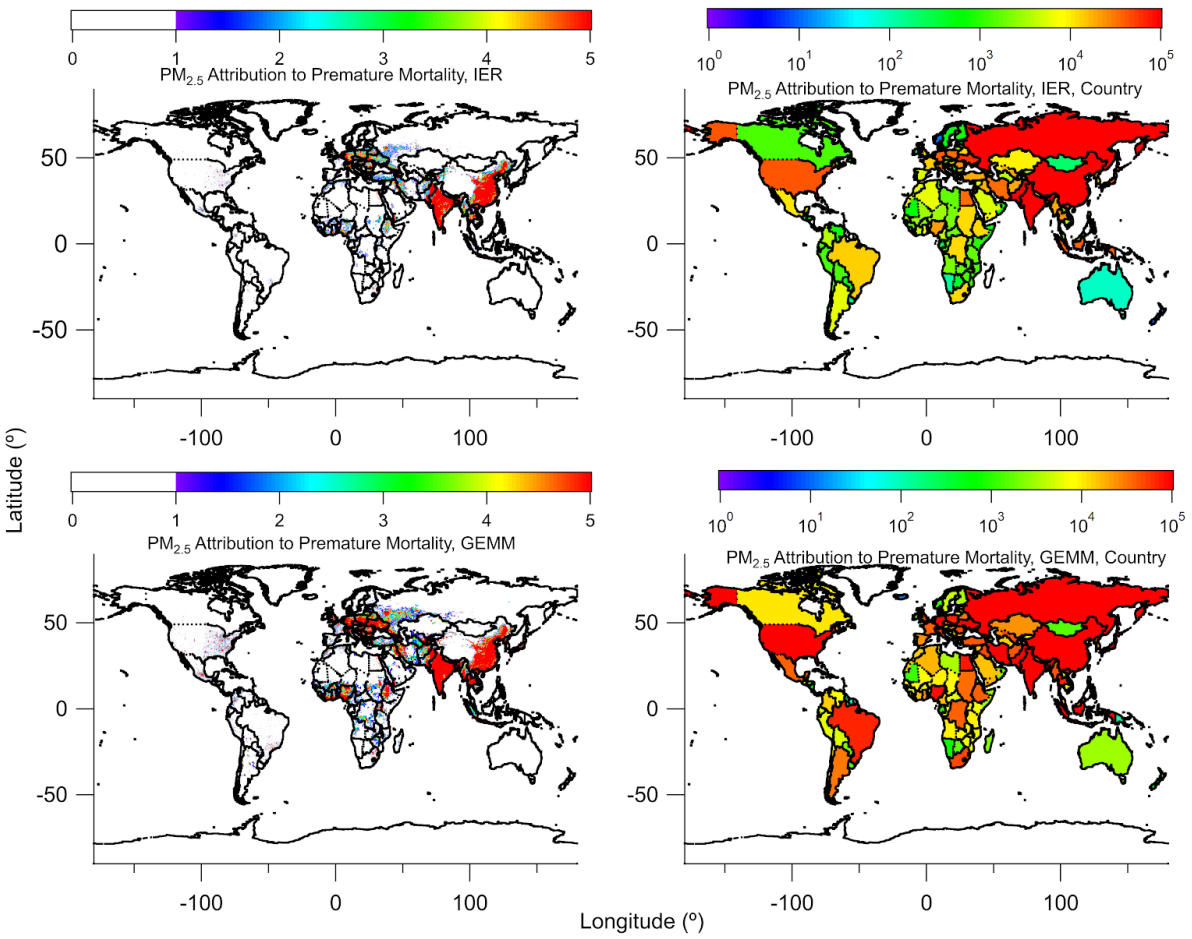

590

591 **Figure S9**. (top) Total deaths associated to $PM_{2.5}$ (left) per 10×10 km^2 area and (right) summed
592 up for each country, using the Integrated Exposure-Response (IER) method (Burnett et al.,
593 2014). These values are derived from satellite. (bottom) Same as above, but using the Global
594 Exposure Mortality Model (GEMM) (Burnett et al., 2018) for $PM_{2.5}$ per 10×10 km^2 area (left)
595 and summed up for each country (right). Premature mortality was determined with $PM_{2.5}$ derived
596 by the methods described in van Donkelaar (2015), which includes satellite and ground-based
597 observations of aerosol.

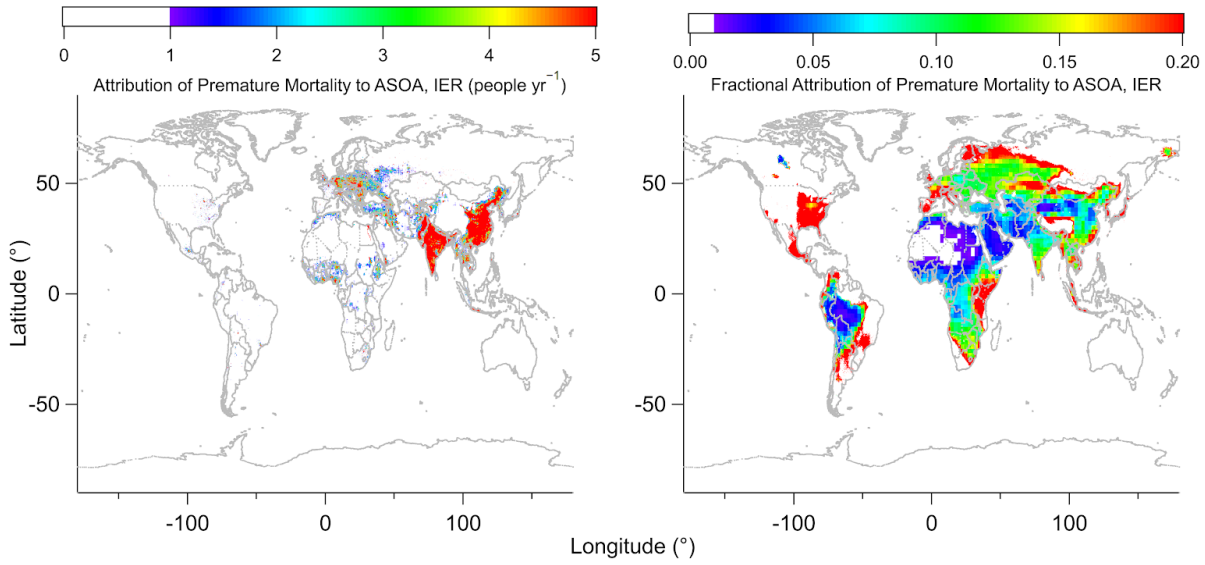

598

599 **Figure S10**. Same as Fig. 8, where top are the results per 10×10 km^2 area for the attribution of
600 premature mortality to ASOA (people yr^{-1}, left) and fractional attribution of premature mortality
601 to ASOA for one year (right) by the IER method. See Fig. 8 for per country comparison.

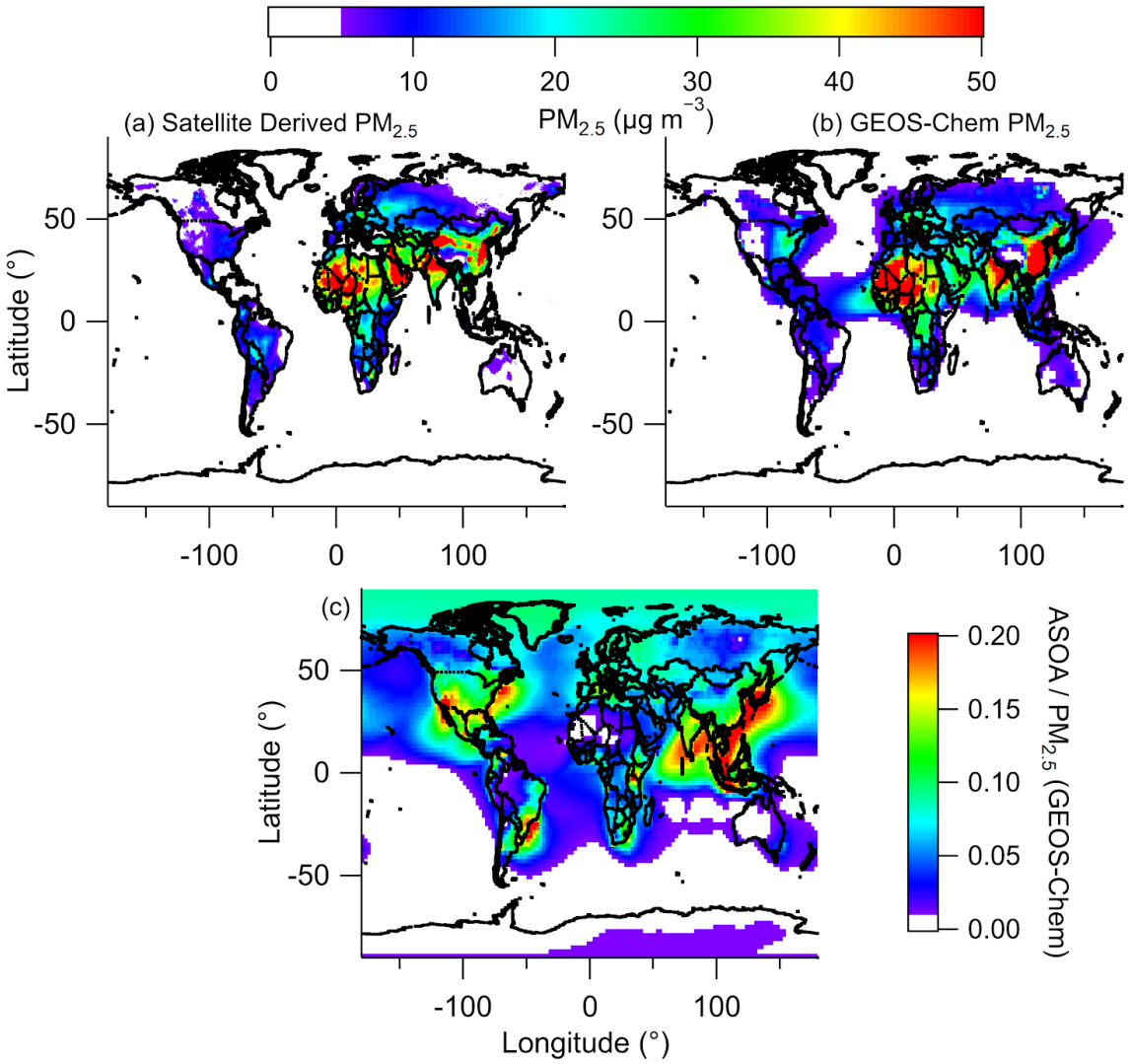

602

603 **Figure S11**. Comparison of satellite retrieved $PM_{2.5}$ (upper left) versus modeled $PM_{2.5}$ (upper
604 right). (Bottom) Fractional contribution of ASOA to total modeled $PM_{2.5}$.

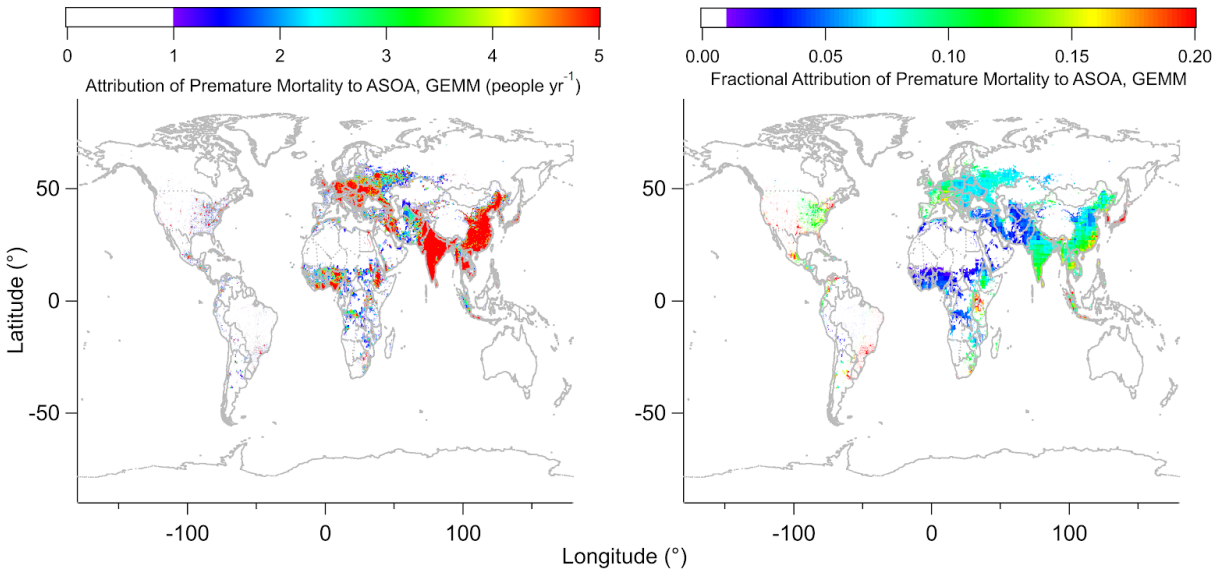

605

606 **Figure S12**. Same as Fig. S10, but using the GEMM from Burnett et al. (2018). (top). (Left)
607 Attribution of premature mortality to ASOA per 10×10 km^2 area (people yr^{-1}) and (Right)
608 fractional attribution of preamture mortality to ASOA per 10×10^2 km for one year.

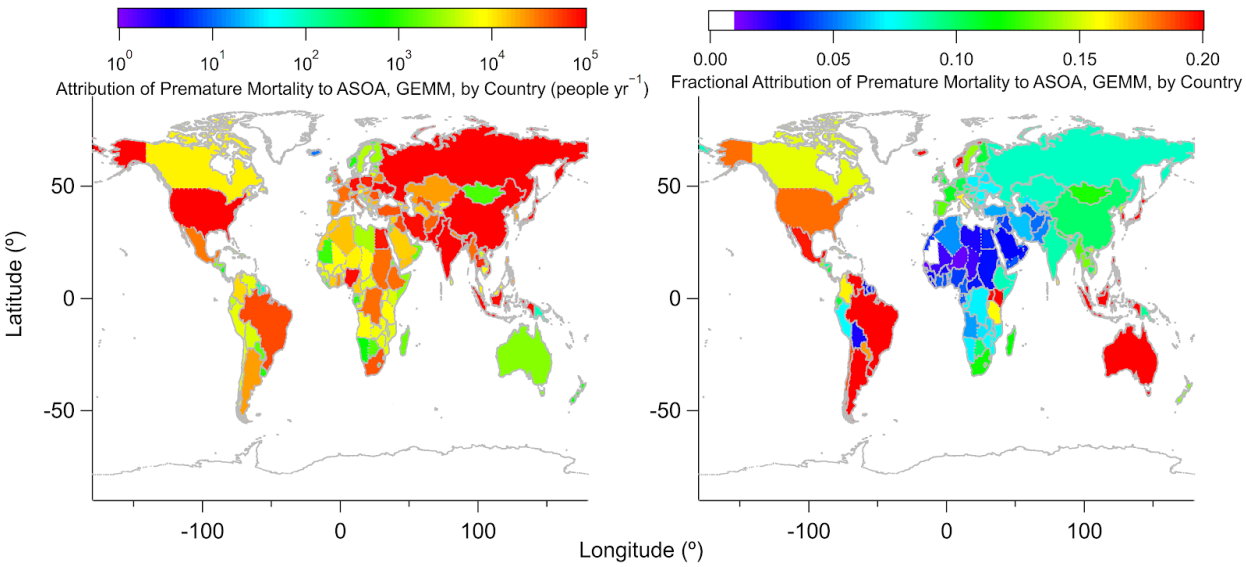

609

610 **Figure S13**. Same as Fig. S12 but summed up for each country for the (left) attribution of
611 premature mortality to ASOA (people yr^{-1}) and (right) the fractional attribution of premature
612 mortality to ASOA for one year.

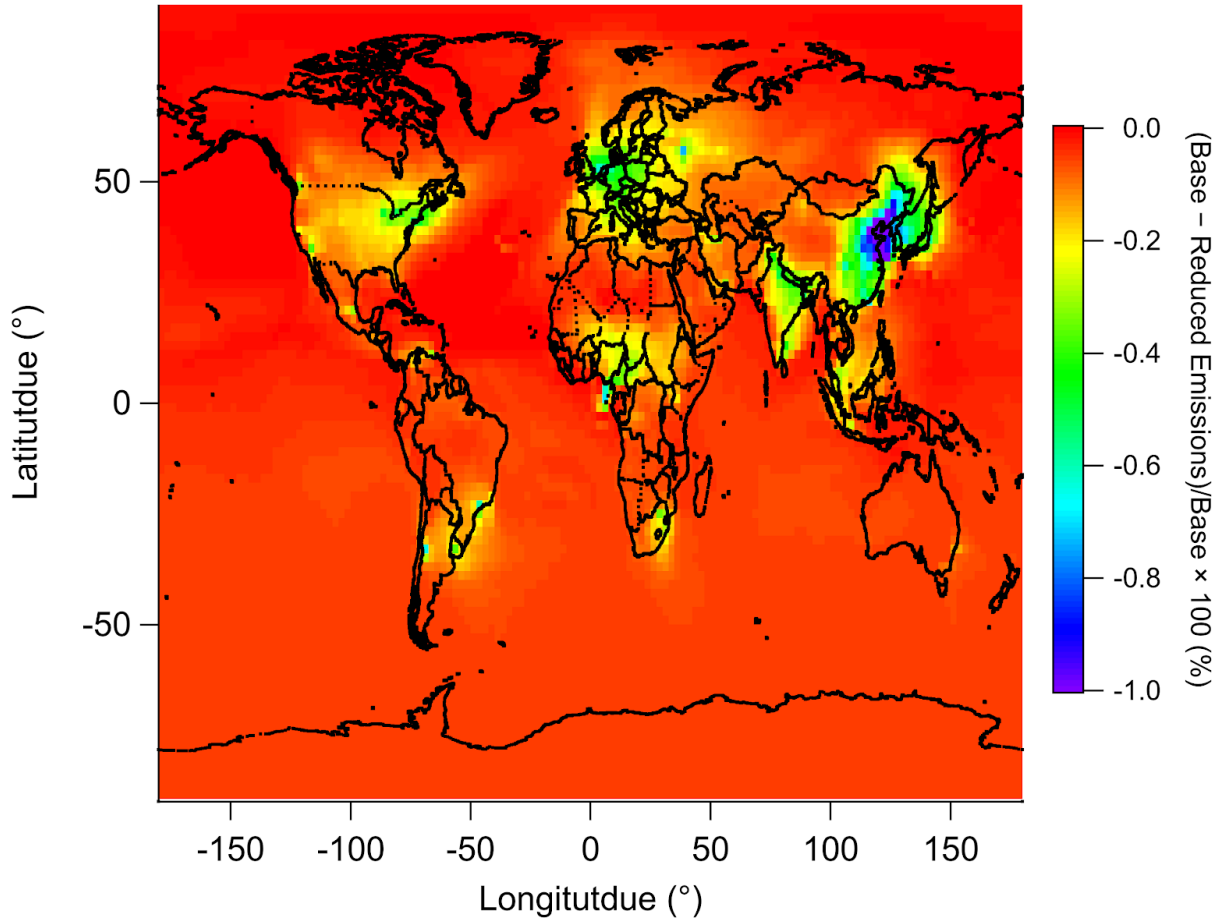

Figure S14. Comparison for surface level ozone upon reducing SOA precursors by 20%.

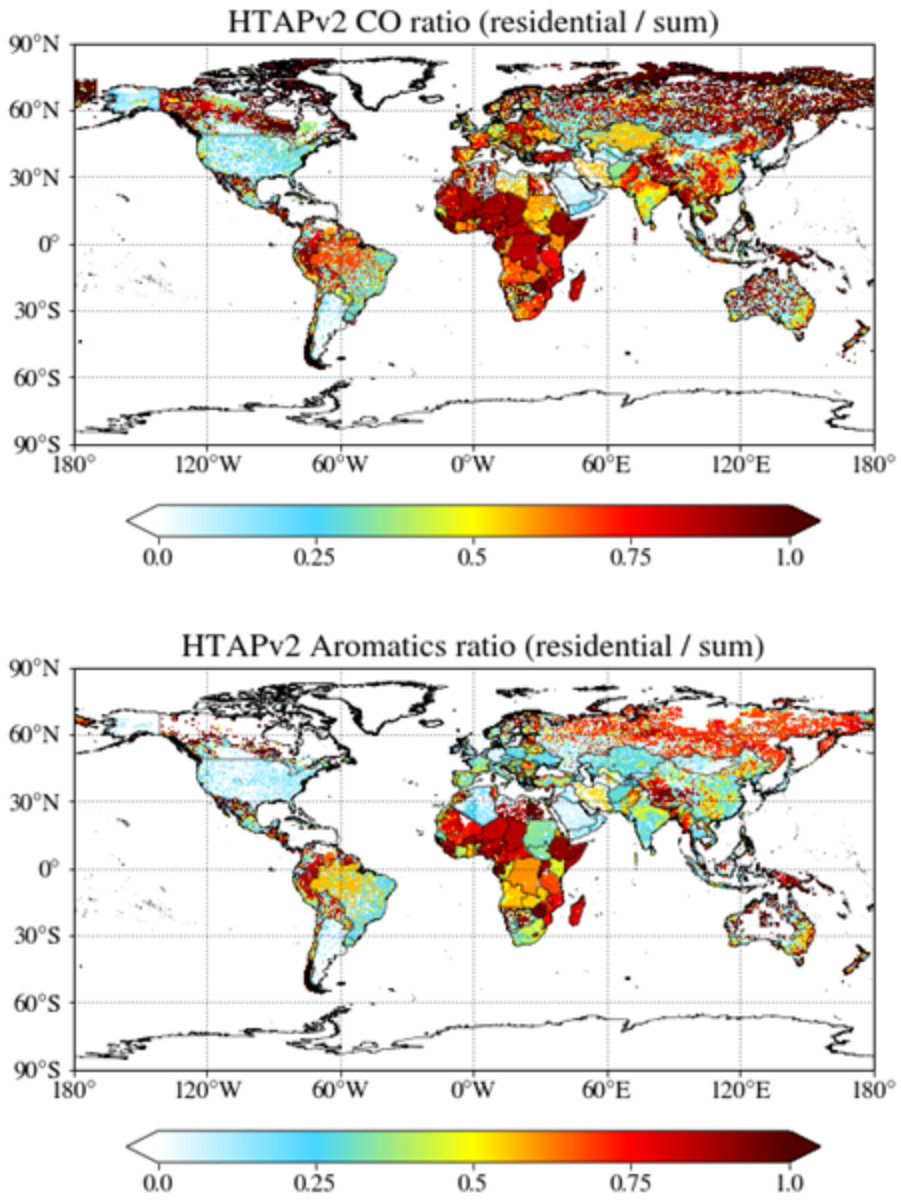

Figure S15. (top) Fractional contribution of CO emissions from residential sources to total emission sources from HTaP. (bottom) Fractional contribution of BTEX emissions from residential sources to total emission sources from HTAP. Residential sources include small-scale combustion, such as heating and cooking, which may include solid-fuel emissions.

References

Apel, E. C., Emmons, L. K., Karl, T., Flocke, F., Hills, a. J., Madronich, S., Lee-Taylor, J., Fried, A., Weibring, P., Walega, J., Richter, D., Tie, X., Mauldin, L., Campos, T., Weinheimer, A., Knapp, D., Sive, B., Kleinman, L., Springston, S., Zaveri, R., Ortega, J., Voss, P., Blake, D., Baker, A., Warneke, C., Welsh-Bon, D., de Gouw, J., Zheng, J., Zhang, R., Rudolph, J., Junkermann, W. and Riemer, D. D.: Chemical evolution of volatile organic compounds in the outflow of the Mexico City Metropolitan area, Atmos. Chem. Phys., 10(5), 2353–2375, 2010.

Atkinson, R. and Arey, J.: Atmospheric Degradation of Volatile Organic Compounds, Chem. Rev., 103, 4605–4638, 2003.

Atkinson, R., Baulch, D. L., Cox, R. A., Crowley, J. N., Hampson, R. F., Hynes, R. G., Jenkin, M. E., Rossi, M. J., Troe, J. and IUPAC Subcommittee: Evaluated kinetic and photochemical data for atmospheric chemistry: Volume II - gas phase reactions of organic species, Atmos. Chem. Phys., 6(11), 3625–4055, 2006.

Bahreini, R., Ervens, B., Middlebrook, A. M., Warneke, C., de Gouw, J. A., DeCarlo, P. F., Jimenez, J. L., Brock, C. A., Neuman, J. A., Ryerson, T. B., Stark, H., Atlas, E., Brioude, J., Fried, A., Holloway, J. S., Peischl, J., Richter, D., Walega, J., Weibring, P., Wollny, A. G. and Fehsenfeld, F. C.: Organic aerosol formation in urban and industrial plumes near Houston and Dallas, Texas, J. Geophys. Res., 114, 1185, 2009.

Baker, A. K., Beyersdorf, A. J., Doezema, L. A., Katzenstein, A., Meinardi, S., Simpson, I. J., Blake, D. R. and Sherwood Rowland, F.: Measurements of nonmethane hydrocarbons in 28 United States cities, Atmos. Environ., 42(1), 170–182, 2008.

Bey, I., Jacob, D. J., Yantosca, R. M., Logan, J. A., Field, B. D., Fiore, A. M., Li, Q., Liu, H. Y., Mickley, L. J. and Schultz, M. G.: Global modeling of tropospheric chemistry with assimilated meteorology: Model description and evaluation, J. Geophys. Res. D: Atmos., 106(D19), 23073–23095, 2001.

Blake, N. J., Blake, D. R., Simpson, I. J., Meinardi, S., Swanson, A. L., Lopez, J. P., Katzenstein, A. S., Barletta, B., Shirai, T., Atlas, E., Sachse, G., Avery, M., Vay, S., Fuelberg, H. E., Kiley, C. M., Kita, K. and Rowland, F. S.: NMHCs and halocarbons in Asian continental outflow during the Transport and Chemical Evolution over the Pacific (TRACE-P) Field Campaign: Comparison with PEM-West B, Journal of Geophysical Research-Atmospheres, 108(D20), 8806, 2003.

Bohn, B. and Zetzsch, C.: Kinetics and mechanism of the reaction of OH with the trimethylbenzenes – experimental evidence for the formation of adduct isomers, Phys. Chem. Chem. Phys., 14(40), 13933, 2012.

Bon, D. M., Ulbrich, I. M., de Gouw, J. A., Warneke, C., Kuster, W. C., Alexander, M. L., Baker, A., Beyersdorf, A. J., Blake, D., Fall, R., Jimenez, J. L., Herndon, S. C., Huey, L. G., Knighton, W. B., Ortega, J., Springston, S. and Vargas, O.: Measurements of volatile organic compounds at a suburban ground site (T1) in Mexico City during the MILAGRO 2006 campaign: measurement

comparison, emission ratios, and source attribution, Atmos. Chem. Phys., 11(6), 2399–2421, 2011.

Burnett, R., Chen, H., Szyszkowicz, M., Fann, N., Hubbell, B., Pope, C. A., Apte, J. S., Brauer, M., Cohen, A., Weichenthal, S., Coggins, J., Di, Q., Brunekreef, B., Frostad, J., Lim, S. S., Kan, H., Walker, K. D., Thurston, G. D., Hayes, R. B., Lim, C. C., Turner, M. C., Jerrett, M., Krewski, D., Gapstur, S. M., Diver, W. R., Ostro, B., Goldberg, D., Crouse, D. L., Martin, R. V., Peters, P., Pinault, L., Tjepkema, M., van Donkelaar, A., Villeneuve, P. J., Miller, A. B., Yin, P., Zhou, M., Wang, L., Janssen, N. A. H., Marra, M., Atkinson, R. W., Tsang, H., Quoc Thach, T., Cannon, J. B., Allen, R. T., Hart, J. E., Laden, F., Cesaroni, G., Forastiere, F., Weinmayr, G., Jaensch, A., Nagel, G., Concin, H. and Spadaro, J. V.: Global estimates of mortality associated with long-term exposure to outdoor fine particulate matter, Proc. Natl. Acad. Sci. U. S. A., 115(38), 9592–9597, 2018.

Burnett, R. T., Pope, C. A., Ezzati, M., Olives, C., Lim, S. S., Mehta, S., Shin, H. H., Singh, G., Hubbell, B., Brauer, M., Anderson, H. R., Smith, K. R., Balmes, J. R., Bruce, N. G., Kan, H., Laden, F., Prüss-Ustün, A., Turner, M. C., Gapstur, S. M., Diver, W. R. and Cohen, A.: An integrated risk function for estimating the global burden of disease attributable to ambient fine particulate matter exposure, Environ. Health Perspect., 122(4), 397–403, 2014.

CARB: CEPAM: 2013 Almanac - Standard Emissions Tool, [online] Available from: https://www.arb.ca.gov/app/emsinv/fcemssumcat2013.php, 2013.

Cárdenas, L. M., Brassington, D. J., Allan, B. J., Coe, H., Alicke, B., Platt, U., Wilson, K. M., Plane, J. M. C. and Penkett, S. A.: Intercomparison of Formaldehyde Measurements in Clean and Polluted Atmospheres, J. Atmos. Chem., 37(1), 53–80, 2000.

Cazorla, M., Wolfe, G. M., Bailey, S. A., Swanson, A. K., Arkinson, H. L. and Hanisco, T. F.: A new airborne laser-induced fluorescence instrument for in situ detection of formaldehyde throughout the troposphere and lower stratosphere, Atmos. Meas. Tech., 8(2), 541–552, 2015.

CCPR: The California Consumer Products Regulation., 2015.

Davis, M. S.: 2005 Architectural Coatings Survey Final Report, CARB., 2007.

DeCarlo, P. F., Kimmel, J. R., Trimborn, A., Northway, M. J., Jayne, J. T., Aiken, A. C., Gonin, M., Fuhrer, K., Horvath, T., Docherty, K. S., Worsnop, D. R. and Jimenez, J. L.: Field-deployable, high-resolution, time-of-flight aerosol mass spectrometer, Anal. Chem., 78(24), 8281–8289, 2006.

DeCarlo, P. F., Ulbrich, I. M., Crounse, J., de Foy, B., Dunlea, E. J., Aiken, A. C., Knapp, D., Weinheimer, A. J., Campos, T., Wennberg, P. O. and Jimenez, J. L.: Investigation of the sources and processing of organic aerosol over the Central Mexican Plateau from aircraft measurements during MILAGRO, Atmos. Chem. Phys., 10(12), 5257–5280, 2010.

van Donkelaar, A., Martin, R. V., Brauer, M. and Boys, B. L.: Use of Satellite Observations for Long-Term Exposure Assessment of Global Concentrations of Fine Particulate Matter, Environ.

694 Health Perspect., 123(2), 135–143, 2015.

695 Drewnick, F., Hings, S. S., DeCarlo, P., Jayne, J. T., Gonin, M., Fuhrer, K., Weimer, S., Jimenez,
696 J. L., Demerjian, K. L., Borrmann, S. and Worsnop, D. R.: A New Time-of-Flight Aerosol Mass
697 Spectrometer (TOF-AMS)—Instrument Description and First Field Deployment, Aerosol Sci.
698 Technol., 39(7), 637–658, 2005.

699 Duncan Fairlie, T., Jacob, D. J. and Park, R. J.: The impact of transpacific transport of mineral
700 dust in the United States, Atmos. Environ., 41(6), 1251–1266, 2007.

701 Dunmore, R. E., Hopkins, J. R., Lidster, R. T., Lee, J. D., Evans, M. J., Rickard, A. R., Lewis, A.
702 C. and Hamilton, J. F.: Diesel-related hydrocarbons can dominate gas phase reactive carbon in
703 megacities, Atmos. Chem. Phys., 15, 9983–9996, 2015.

704 Dzepina, K., Volkamer, R. M., Madronich, S., Tulet, P., Ulbrich, I. M., Zhang, Q., Cappa, C. D.,
705 Ziemann, P. J. and Jimenez, J. L.: Evaluation of recently-proposed secondary organic aerosol
706 models for a case study in Mexico City, Atmos. Chem. Phys., 9(15), 5681–5709, 2009.

707 EMEP/EEA: EMEP/EEA Air Pollutant Emission Inventory Guidebook 2016, EEA,
708 Luxembourg., 2016.

709 EPA: SPECIATE v4.4, US Environmental Protection Agency., 2014.

710 Fisher, J. A., Jacob, D. J., Travis, K. R., Kim, P. S., Marais, E. A., Miller, C. C., Yu, K., Zhu, L.,
711 Yantosca, R. M., Sulprizio, M. P., Mao, J., Wennberg, P. O., Crounse, J. D., Teng, A. P., Nguyen,
712 T. B., Clair, J. M. S., Cohen, R. C., Romer, P., Nault, B. A., Wooldridge, P. J., Jimenez, J. L.,
713 Campuzano-Jost, P., Day, D. A., Hu, W., Shepson, P. B., Xiong, F., Blake, D. R., Goldstein, A.
714 H., Misztal, P. K., Hanisco, T. F., Wolfe, G. M., Ryerson, T. B., Wisthaler, A. and Mikoviny, T.:
715 Organic nitrate chemistry and its implications for nitrogen budgets in an isoprene- and
716 monoterpene-rich atmosphere: Constraints from aircraft ($SEAC^4RS$) and ground-based (SOAS)
717 observations in the Southeast US, Atmos. Chem. Phys., 16(9), doi:10.5194/acp-16-5969-2016,
718 2016.

719 Fried, A., Crawford, J., Olson, J., Walega, J., Potter, W., Wert, B., Jordan, C., Anderson, B.,
720 Shetter, R., Lefer, B., Blake, D., Blake, N., Meinardi, S., Heikes, B., O'Sullivan, D., Snow, J.,
721 Fuelberg, H., Kiley, C. M., Sandholm, S., Tan, D., Sachse, G., Singh, H., Faloona, I., Harward,
722 C. N. and Carmichael, G. R.: Airborne tunable diode laser measurements of formaldehyde during
723 TRACE-P: Distributions and box model comparisons, J. Geophys. Res. D: Atmos., 108(D20),
724 8798, 2003.

725 Gately, C. K., Hutyra, L. R. and Wing, I. S.: Cities, traffic, and CO_2: A multidecadal assessment
726 of trends, drivers, and scaling relationships, Proc. Natl. Acad. Sci. U. S. A., 112(16), 4999–5004,
727 2015.

728 Gentner, D. R., Isaacman, G., Worton, D. R., Chan, A. W. H., Dallmann, T. R., Davis, L., Liu, S.,
729 Day, D. A., Russell, L. M., Wilson, K. R., Weber, R., Guha, A., Harley, R. A. and Goldstein, A.
730 H.: Elucidating secondary organic aerosol from diesel and gasoline vehicles through detailed

731 characterization of organic carbon emissions, Proc. Natl. Acad. Sci. U. S. A., 109(45),
732 18318–18323, 2012.

733 Gentner, D. R., Worton, D. R., Isaacman, G., Davis, L. C., Dallmann, T. R., Wood, E. C.,
734 Herndon, S. C., Goldstein, A. H. and Harley, R. A.: Chemical Composition of Gas-Phase
735 Organic Carbon Emissions from Motor Vehicles and Implications for Ozone Production,
736 Environ. Sci. Technol., 47(20), 11837–11848, 2013.

737 Gerbig, C., Schmitgen, S., Kley, D., Volz-Thomas, A., Dewey, K. and Haaks, D.: An improved
738 fast-response vacuum-UV resonance fluorescence CO instrument, J. Geophys. Res. D: Atmos.,
739 104(D1), 1699–1704, 1999.

740 Gilman, J. B., Burkhart, J. F., Lerner, B. M., Williams, E. J., Kuster, W. C., Goldan, P. D.,
741 Murphy, P. C., Warneke, C., Fowler, C., Montzka, S. A., Miller, B. R., Miller, L., Oltmans, S. J.,
742 Ryerson, T. B., Cooper, O. R., Stohl, A. and de Gouw, J. A.: Ozone variability and halogen
743 oxidation within the Arctic and sub-Arctic springtime boundary layer, Atmos. Chem. Phys.,
744 10(21), 10223–10236, 2010.

745 de Gouw, J. A., Middlebrook, A. M., Warneke, C., Goldan, P. D., Kuster, W. C., Roberts, J. M.,
746 Fehsenfeld, F. C., Worsnop, D. R., Canagaratna, M. R., Pszenny, A. A. P., Keene, W. C.,
747 Marchewka, M., Bertman, S. B. and Bates, T. S.: Budget of organic carbon in a polluted
748 atmosphere: Results from the New England Air Quality Study in 2002, J. Geophys. Res. D:
749 Atmos., 110(16), 1–22, 2005.

750 de Gouw, J. A., Gilman, J. B., Kim, S.-W., Lerner, B. M., Isaacman-VanWertz, G., McDonald, B.
751 C., Warneke, C., Kuster, W. C., Lefer, B. L., Griffith, S. M., Dusanter, S., Stevens, P. S. and
752 Stutz, J.: Chemistry of Volatile Organic Compounds in the Los Angeles basin: Nighttime
753 Removal of Alkenes and Determination of Emission Ratios, J. Geophys. Res.: Atmos., 122(21),
754 11,843–11,861, 2017.

755 Griffith, S. M., Hansen, R. F., Dusanter, S., Michoud, V., Gilman, J. B., Kuster, W. C., Veres, P.
756 R., Graus, M., Gouw, J. A., Roberts, J., Young, C., Washenfelder, R., Brown, S. S., Thalman, R.,
757 Waxman, E., Volkamer, R., Tsai, C., Stutz, J., Flynn, J. H., Grossberg, N., Lefer, B., Alvarez, S.
758 L., Rappenglueck, B., Mielke, L. H., Osthoff, H. D. and Stevens, P. S.: Measurements of
759 hydroxyl and hydroperoxy radicals during CalNex-LA: Model comparisons and radical budgets,
760 J. Geophys. Res. D: Atmos., 121(8), 4211–4232, 2016.

761 Hassler, B., McDonald, B. C., Frost, G. J., Borbon, A., Carslaw, D. C., Civerolo, K., Granier, C.,
762 Monks, P. S., Monks, S., Parrish, D. D., Pollack, I. B., Rosenlof, K. H., Ryerson, T. B., von
763 Schneidemesser, E. and Trainer, M.: Analysis of long-term observations of NO_x and CO in
764 megacities and application to constraining emissions inventories, Geophys. Res. Lett., 43(18),
765 9920–9930, 2016.

766 Hayes, P. L., Ortega, A. M., Cubison, M. J., Froyd, K. D., Zhao, Y., Cliff, S. S., Hu, W. W.,
767 Toohey, D. W., Flynn, J. H., Lefer, B. L., Grossberg, N., Alvarez, S., Rappenglück, B., Taylor, J.
768 W., Allan, J. D., Holloway, J. S., Gilman, J. B., Kuster, W. C., de Gouw, J. A., Massoli, P.,

Zhang, X., Liu, J., Weber, R. J., Corrigan, A. L., Russell, L. M., Isaacman, G., Worton, D. R., Kreisberg, N. M., Goldstein, A. H., Thalman, R., Waxman, E. M., Volkamer, R., Lin, Y. H., Surratt, J. D., Kleindienst, T. E., Offenberg, J. H., Dusanter, S., Griffith, S., Stevens, P. S., Brioude, J., Angevine, W. M. and Jimenez, J. L.: Organic aerosol composition and sources in Pasadena, California, during the 2010 CalNex campaign, J. Geophys. Res. D: Atmos., 118(16), 9233–9257, 2013.

Hayes, P. L., Carlton, A. G., Baker, K. R., Ahmadov, R., Washenfelder, R. A., Alvarez, S., Rappenglück, B., Gilman, J. B., Kuster, W. C., de Gouw, J. A., Zotter, P., Prévôt, A. S. H., Szidat, S., Kleindienst, T. E., Ma, P. K. and Jimenez, J. L.: Modeling the formation and aging of secondary organic aerosols in Los Angeles during CalNex 2010, Atmos. Chem. Phys., 15(10), 5773–5801, 2015.

Hodzic, A. and Jimenez, J. L.: Modeling anthropogenically controlled secondary organic aerosols in a megacity: A simplified framework for global and climate models, Geosci. Model Dev., 4(4), 901–917, 2011.

Hodzic, A., Jimenez, J. L., Madronich, S., Canagaratna, M. R., DeCarlo, P. F., Kleinman, L. and Fast, J.: Modeling organic aerosols in a megacity: potential contribution of semi-volatile and intermediate volatility primary organic compounds to secondary organic aerosol formation, Atmos. Chem. Phys., 10(12), 5491–5514, 2010.

Huey L Tanner D Slusher D Dibb J Arimoto R Chen G Davis D Buhr M Nowak J Mauldin R Eisele F, K. E.: CIMS measurements of HNO3 and SO2 at the South Pole during ISCAT 2000, Atmos. Environ., 38(32), 5411–5421, 2004.

Hu, W., Hu, M., Hu, W., Jimenez, J. L., Yuan, B., Chen, W., Wang, M., Wu, Y., Chen, C., Wang, Z., Peng, J., Zeng, L. and Shao, M.: Chemical composition, sources, and aging process of submicron aerosols in Beijing: Contrast between summer and winter, J. Geophys. Res. D: Atmos., 121(4), 1955–1977, 2016.

IEA: World energy balances, IEA World Energy Statistics and Balances, doi:10.1787/data-00521-en, 2019.

Jaeglé, L., Quinn, P. K., Bates, T. S., Alexander, B. and Lin, J.-T.: Global distribution of sea salt aerosols: new constraints from in situ and remote sensing observations, Atmos. Chem. Phys., 11(7), 3137–3157, 2011.

Janssens-Maenhout, G., Crippa, M., Guizzardi, D., Dentener, F., Muntean, M., Pouliot, G., Keating, T., Zhang, Q., Kurokawa, J., Wankmüller, R., Denier van der Gon, H., Kuenen, J. J. P., Klimont, Z., Frost, G., Darras, S., Koffi, B. and Li, M.: HTAP_v2.2: a mosaic of regional and global emission grid maps for 2008 and 2010 to study hemispheric transport of air pollution, Atmos. Chem. Phys., 15(19), 11411–11432, 2015.

Jathar, S. H., Gordon, T. D., Hennigan, C. J., Pye, H. O. T., Pouliot, G., Adams, P. J., Donahue, N. M. and Robinson, A. L.: Unspeciated organic emissions from combustion sources and their

influence on the secondary organic aerosol budget in the United States, Proc. Natl. Acad. Sci. U. S. A., 111(29), 10473–10478, 2014.

Jayne, J. T., Leard, D. C., Zhang, X. F., Davidovits, P., Smith, K. A., Kolb, C. E. and Worsnop, D. R.: Development of an aerosol mass spectrometer for size and composition analysis of submicron particles, Aerosol Sci. Technol., 33(1-2), 49–70, 2000.

Kaiser, J., Jacob, D. J., Zhu, L., Travis, K. R., Fisher, J. A., González Abad, G., Zhang, L., Zhang, X., Fried, A., Crounse, J. D., St. Clair, J. M. and Wisthaler, A.: High-resolution inversion of OMI formaldehyde columns to quantify isoprene emission on ecosystem-relevant scales: application to the southeast US, Atmos. Chem. Phys., 18(8), 5483–5497, 2018.

Kim, S., Huey, L. G., Stickel, R. E., Tanner, D. J., Crawford, J. H., Olson, J. R., Chen, G., Brune, W. H., Ren, X., Lesher, R., Wooldridge, P. J., Bertram, T. H., Perring, A., Cohen, R. C., Lefer, B. L., Shetter, R. E., Avery, M., Diskin, G. and Sokolik, I.: Measurement of HO_2NO_2 in the free troposphere during the Intercontinental Chemical Transport Experiment–North America 2004, J. Geophys. Res. D: Atmos., 112, D12S01, 2007.

Kleinman, L. I., Daum, P. H., Lee, Y.-N., Senum, G. I., Springston, S. R., Wang, J., Berkowitz, C., Hubbe, J., Zaveri, R. A., Brechtel, F. J., Jayne, J., Onasch, T. B. and Worsnop, D.: Aircraft observations of aerosol composition and ageing in New England and Mid-Atlantic States during the summer 2002 New England Air Quality Study field campaign, J. Geophys. Res. D: Atmos., 112(D9), D09310, 2007.

Koo, B., Knipping, E. and Yarwood, G.: 1.5-Dimensional volatility basis set approach for modeling organic aerosol in CAMx and CMAQ, Atmos. Environ., 95, 158–164, 2014.

Kuwata, M., Zorn, S. R. and Martin, S. T.: Using Elemental Ratios to Predict the Density of Organic Material Composed of Carbon, Hydrogen, and Oxygen, Environ. Sci. Technol., 46(2), 787–794, 2012.

Langford, B., Nemitz, E., House, E., Phillips, G. J., Famulari, D., Davison, B., Hopkins, J. R., Lewis, A. C. and Hewitt, C. N.: Fluxes and concentrations of volatile organic compounds above central London, UK, Atmos. Chem. Phys., 10(2), 627–645, 2010.

Li, M., Zhang, Q., Streets, D. G., He, K. B., Cheng, Y. F., Emmons, L. K., Huo, H., Kang, S. C., Lu, Z., Shao, M., Su, H., Yu, X. and Zhang, Y.: Mapping Asian anthropogenic emissions of non-methane volatile organic compounds to multiple chemical mechanisms, Atmos. Chem. Phys., 14(11), 5617–5638, 2014.

Li, M., Liu, H., Geng, G., Hong, C., Liu, F., Song, Y., Tong, D., Zheng, B., Cui, H., Man, H., Zhang, Q. and He, K.: Anthropogenic emission inventories in China: a review, Natl Sci Rev, 4(6), 834–866, 2017.

Li, M., Zhang, Q., Zheng, B., Tong, D., Lei, Y., Liu, F., Chaopeng, H., Kang, S., Yan, L., Zhang, Y., Bo, Y., Su, H., Cheng, Y. and He, K.: Persistent growth of anthropogenic non-methane volatile organic compound (NMVOC) emissions in China during 1990-2017: drivers, speciation

and ozone formation potential, Atmos. Chem. Phys., 19, 8897–8913, 2019.

Liu, F., Zhang, Q., Tong, D., Zheng, B., Li, M., Huo, H. and He, K. B.: High-resolution inventory of technologies, activities, and emissions of coal-fired power plants in China from 1990 to 2010, Atmos. Chem. Phys., 15(23), 13299–13317, 2015.

Lu, Q., Zhao, Y. and Robinson, A. L.: Comprehensive organic emission profiles for gasoline, diesel, and gas-turbine engines including intermediate and semi-volatile organic compound emissions, Atmos. Chem. Phys., 18, 17637–17654, 2018.

Ma, P. K., Zhao, Y., Robinson, A. L., Worton, D. R., Goldstein, A. H., Ortega, A. M., Jimenez, J. L., Zotter, P., Prévôt, A. S. H., Szidat, S. and Hayes, P. L.: Evaluating the impact of new observational constraints on P-S/IVOC emissions, multi-generation oxidation, and chamber wall losses on SOA modeling for Los Angeles, CA, Atmos. Chem. Phys., 17(15), 9237–9259, 2017.

Marais, E. A., Jacob, D. J., Jimenez, J. L., Campuzano-Jost, P., Day, D. A., Hu, W., Krechmer, J., Zhu, L., Kim, P. S., Miller, C. C., Fisher, J. A., Travis, K., Yu, K., Hanisco, T. F., Wolfe, G. M., Arkinson, H. L., Pye, H. O. T., Froyd, K. D., Liao, J. and McNeill, V. F.: Aqueous-phase mechanism for secondary organic aerosol formation from isoprene: application to the southeast United States and co-benefit of SO_2 emission controls, Atmos. Chem. Phys., 16(3), 1603–1618, 2016.

Matheson, R. R.: 20th- to 21st-Century Technological Challenges in Soft Coatings, Science, 297(5583), 976–979, 2002.

McDonald, B. C., Gentner, D. R., Goldstein, A. H. and Harley, R. A.: Long-Term Trends in Motor Vehicle Emissions in U.S. Urban Areas, Environ. Sci. Technol., 47(17), 10022–10031, 2013.

McDonald, B. C., Goldstein, A. H. and Harley, R. A.: Long-Term Trends in California Mobile Source Emissions and Ambient Concentrations of Black Carbon and Organic Aerosol, Environ. Sci. Technol., 49(8), 5178–5188, 2015.

McDonald, B. C., de Gouw, J. A., Gilman, J. B., Jathar, S. H., Akherati, A., Cappa, C. D., Jimenez, J. L., Lee-Taylor, J., Hayes, P. L., McKeen, S. A., Cui, Y. Y., Kim, S.-W., Gentner, D. R., Isaacman-VanWertz, G., Goldstein, A. H., Harley, R. A., Frost, G. J., Roberts, J. M., Ryerson, T. B. and Trainer, M.: Volatile chemical products emerging as largest petrochemical source of urban organic emissions, Science, 359(6377), 760–764, 2018.

Mollner, A. K., Valluvadasan, S., Feng, L., Sprague, M. K., Okumura, M., Milligan, D. B., Bloss, W. J., Sander, S. P., Martien, P. T., Harley, R. A., McCoy, A. B. and Carter, W. P. L.: Rate of Gas Phase Association of Hydroxyl Radical and Nitrogen Dioxide, Science, 330(6004), 646–649, 2010.

MOVES: MOVES2014a User Guide., 2015.

Nault, B. A., Campuzano-Jost, P., Day, D. A., Schroder, J. C., Anderson, B., Beyersdorf, A. J.,

Blake, D. R., Brune, W. H., Choi, Y., Corr, C. A., de Gouw, J. A., Dibb, J., DiGangi, J. P., Diskin, G. S., Fried, A., Huey, L. G., Kim, M. J., Knote, C. J., Lamb, K. D., Lee, T., Park, T., Pusede, S. E., Scheuer, E., Thornhill, K. L., Woo, J.-H. and Jimenez, J. L.: Secondary Organic Aerosol Production from Local Emissions Dominates the Organic Aerosol Budget over Seoul, South Korea, during KORUS-AQ, Atmos. Chem. Phys., 18, 17769–17800, 2018.

NEI: National Emissions Inventory (NEI) 2011, version 1, Research Triangle Park., 2015.

Pai, S. J., Heald, C. L., Pierce, J. R., Farina, S. C., Marais, E. A., Jimenez, J. L., Campuzano-Jost, P., Nault, B. A., Middlebrook, A. M., Coe, H., Shilling, J. E., Bahreini, R., Dingle, J. H. and Vu, K.: An evaluation of global organic aerosol schemes using airborne observations, Atmos. Chem. Phys., 20(5), 2637–2665, 2020.

Pankow, J. F. and Asher, W. E.: SIMPOL.1: a simple group contribution method for predicting vapor pressures and enthalpies of vaporization of multifunctional organic compounds, Atmos. Chem. Phys., 8(10), 2773–2796, 2008.

Park, R. J., Jacob, D. J., Palmer, P. I., Clarke, A. D., Weber, R. J., Zondlo, M. A., Eisele, F. L., Bandy, A. R., Thornton, D. C., Sachse, G. W. and Bond, T. C.: Export efficiency of black carbon aerosol in continental outflow: Global implications, J. Geophys. Res. D: Atmos., 110(D11), D11205, 2005.

Park, R. J., Jacob, D. J., Kumar, N. and Yantosca, R. M.: Regional visibility statistics in the United States: Natural and transboundary pollution influences, and implications for the Regional Haze Rule, Atmos. Environ., 40(28), 5405–5423, 2006.

Peng, Z. and Jimenez, J. L.: KinSim: A Research-Grade, User-Friendly, Visual Kinetics Simulator for Chemical-Kinetics and Environmental-Chemistry Teaching, J. Chem. Educ., 96(4), 806–811, 2019.

Pierson, W. R., Schorran, D. E., Fujita, E. M., Sagebiel, J. C., Lawson, D. R. and Tanner, R. L.: Assessment of Nontailpipe Hydrocarbon Emissions from Motor Vehicles, J. Air Waste Manage. Assoc., 49(5), 498–519, 1999.

Pollack, I. B., Lerner, B. M. and Ryerson, T. B.: Evaluation of ultraviolet light-emitting diodes for detection of atmospheric NO_2 by photolysis - chemiluminescence, J. Atmos. Chem., 65(2-3), 111–125, 2010.

Pye, H. O. T. and Seinfeld, J. H.: A global perspective on aerosol from low-volatility organic compounds, Atmos. Chem. Phys., 10, 4377–4401, 2010.

Roberts, J. M., Stroud, C. A., Jobson, B. T., Trainer, M., Hereid, D., Williams, E., Fehsenfeld, F., Brune, W., Martinez, M. and Harder, H.: Application of a sequential reaction model to PANs and aldehyde measurements in two urban areas, Geophys. Res. Lett., 28(24), 4583–4586, 2001.

Roberts, J. M., Flocke, F., Stroud, C. A., Hereid, D., Williams, E., Fehsenfeld, F., Brune, W., Martinez, M. and Harder, H.: Ground-based measurements of peroxycarboxylic nitric anhydrides

(PANs) during the 1999 Southern Oxidants Study Nashville Intensive, J. Geophys. Res. D: Atmos., 107(D21), 4554, 2002.

Robinson, A. L., Donahue, N. M., Shrivastava, M. K., Weitkamp, E. A., Sage, A. M., Grieshop, A. P., Lane, T. E., Pierce, J. R. and Pandis, S. N.: Rethinking Organic Aerosols: Semivolatile Emissions and Photochemical Aging, Science, 315(5816), 1259–1262, 2007.

Rubin, J. I., Kean, A. J., Harley, R. A., Millet, D. B. and Goldstein, A. H.: Temperature dependence of volatile organic compound evaporative emissions from motor vehicles, J. Geophys. Res. D: Atmos., 111(D3), D03305, 2006.

Rumble, J. R., Ed.: CRC Handbook of Chemistry and Physics, 100th Edition, 2019 - 2020, Taylor & Francis Group., 2019.

Ryerson, T. B., Huey, L. G., Knapp, K., Neuman, J. A., Parrish, D. D., Sueper, D. T. and Fehsenfeld, F. C.: Design and initial characterization of an inlet for gas-phase NO_y measurements from aircraft, J. Geophys. Res. D: Atmos., 104(D5), 5483–5492, 1999.

Ryerson, T. B., Andrews, A. E., Angevine, W. M., Bates, T. S., Brock, C. A., Cairns, B., Cohen, R. C., Cooper, O. R., de Gouw, J. A., Fehsenfeld, F. C., Ferrare, R. A., Fischer, M. L., Flagan, R. C., Goldstein, A. H., Hair, J. W., Hardesty, R. M., Hostetler, C. A., Jimenez, J. L., Langford, A. O., McCauley, E., McKeen, S. A., Molina, L. T., Nenes, A., Oltmans, S. J., Parrish, D. D., Pederson, J. R., Pierce, R. B., Prather, K., Quinn, P. K., Seinfeld, J. H., Senff, C. J., Sorooshian, A., Stutz, J., Surratt, J. D., Trainer, M., Volkamer, R., Williams, E. J. and Wofsy, S. C.: The 2010 California Research at the Nexus of Air Quality and Climate Change (CalNex) field study, J. Geophys. Res. D: Atmos., 118(11), 5830–5866, 2013.

Sachse, G. W., Hill, G. F., Wade, L. O. and Perry, M. G.: Fast-Response, High-Precision Carbon Monoxide Sensor using a Tunable Diode Laser Absorption Technique, J. Geophys. Res.: Atmos., 92(D2), 2071–2081, 1987.

Schroder, J. C., Campuzano-Jost, P., Day, D. A., Shah, V., Larson, K., Sommers, J. M., Sullivan, A. P., Campos, T., Reeves, J. M., Hills, A., Hornbrook, R. S., Blake, N. J., Scheuer, E., Guo, H., Fibiger, D. L., McDuffie, E. E., Hayes, P. L., Weber, R. J., Dibb, J. E., Apel, E. C., Jaeglé, L., Brown, S. S., Thronton, J. A. and Jimenez, J. L.: Sources and Secondary Production of Organic Aerosols in the Northeastern US during WINTER, J. Geophys. Res. D: Atmos., doi:10.1029/2018JD028475, 2018.

Seinfeld, J. H. and Pandis, S. N.: Atmospheric Chemistry and Physics: From Air Pollution to Climate Change, Second., John Wiley & Sons, Inc., Hoboken, NJ USA., 2006.

Simon, H., Beck, L., Bhave, P. V., Divita, F., Hsu, Y., Luecken, D., Mobley, J. D., Pouliot, G. A., Reff, A., Sarwar, G. and Strum, M.: The development and uses of EPA's SPECIATE database, Atmos. Pollut. Res., 1(4), 196–206, 2010.

Slusher, D. L., Huey, L. G., Tanner, D. J., Flocke, F. M. and Roberts, J. M.: A thermal dissociation-chemical ionization mass spectrometry (TD-CIMS) technique for the simultaneous

measurement of peroxyacyl nitrates and dinitrogen pentoxide, J. Geophys. Res.: Atmos., 109(D19), D19315–D19315, 2004.

Stutz, J. and Platt, U.: Numerical analysis and estimation of the statistical error of differential optical absorption spectroscopy measurements with least-squares methods, Appl. Opt., 35(30), 6041, 1996.

Stutz, J. and Platt, U.: Improving long-path differential optical absorption spectroscopy with a quartz-fiber mode mixer, Appl. Opt., 36(6), 1105, 1997.

The International GEOS-Chem User Community: geoschem/geos-chem: GEOS-Chem 12.0.0 release, , doi:10.5281/ZENODO.1343547, 2018.

Travis, K. R., Jacob, D. J., Fisher, J. A., Kim, P. S., Marais, E. A., Zhu, L., Yu, K., Miller, C. C., Yantosca, R. M., Sulprizio, M. P., Thompson, A. M., Wennberg, P. O., Crounse, J. D., St. Clair, J. M., Cohen, R. C., Laughner, J. L., Dibb, J. E., Hall, S. R., Ullmann, K., Wolfe, G. M., Pollack, I. B., Peischl, J., Neuman, J. A. and Zhou, X.: Why do models overestimate surface ozone in the Southeast United States?, Atmos. Chem. Phys., 16(21), 13561–13577, 2016.

Tsimpidi, A. P., Karydis, V. A., Zavala, M., Lei, W., Molina, L., Ulbrich, I. M., Jimenez, J. L. and Pandis, S. N.: Evaluation of the volatility basis-set approach for the simulation of organic aerosol formation in the Mexico City metropolitan area, Atmos. Chem. Phys., 10(2), 525–546, 2010.

Vaden, T. D., Imre, D., Beránek, J., Shrivastava, M. and Zelenyuk, A.: Evaporation kinetics and phase of laboratory and ambient secondary organic aerosol, Proc. Natl. Acad. Sci. U. S. A., 108(6), 2190–2195, 2011.

Vaughan, A. R., Lee, J. D., Shaw, M. D., Misztal, P. K., Metzger, S., Vieno, M., Davison, B., Karl, T. G., Carpenter, L. J., Lewis, A. C., Purvis, R. M., Goldstein, A. H. and Hewitt, C. N.: VOC emission rates over London and South East England obtained by airborne eddy covariance, Faraday Discuss., 200(0), 599–620, 2017.

Wang, M., Shao, M., Chen, W., Yuan, B., Lu, S., Zhang, Q., Zeng, L. and Wang, Q.: A temporally and spatially resolved validation of emission inventories by measurements of ambient volatile organic compounds in Beijing, China, Atmos. Chem. Phys., 14(12), 5871–5891, 2014.

Warneke, C., McKeen, S. A., de Gouw, J. A., Goldan, P. D., Kuster, W. C., Holloway, J. S., Williams, E. J., Lerner, B. M., Parrish, D. D., Trainer, M., Fehsenfeld, F. C., Kato, S., Atlas, E. L., Baker, A. and Blake, D. R.: Determination of urban volatile organic compound emission ratios and comparison with an emissions database, J. Geophys. Res. D: Atmos., 112(D10), doi:10.1029/2006JD007930, 2007.

Warneke, C., Veres, P., Holloway, J. S., Stutz, J., Tsai, C., Alvarez, S., Rappenglueck, B., Fehsenfeld, F. C., Graus, M., Gilman, J. B. and de Gouw, J. A.: Airborne formaldehyde measurements using PTR-MS: calibration, humidity dependence, inter-comparison and initial results, Atmos. Meas. Tech., 4(10), 2345–2358, 2011.

Warneke, C., de Gouw, J. A., Holloway, J. S., Peischl, J., Ryerson, T. B., Atlas, E., Blake, D., Trainer, M. and Parrish, D. D.: Multiyear trends in volatile organic compounds in Los Angeles, California: Five decades of decreasing emissions, J. Geophys. Res. D: Atmos., 117(D21), D00V17, 2012.

Weibring, P., Richter, D., Walega, J. G., Rippe, L. and Fried, A.: Difference frequency generation spectrometer for simultaneous multispecies detection, Opt. Express, 18(26), 27670, 2010.

Weinheimer, A. J., Walega, J. G., Ridley, B. A., Gary, B. L., Blake, D. R., Blake, N. J., Rowland, F. S., Sachse, G. W., Anderson, B. E. and Collins, J. E.: Meridional distributions of NO_x , NO_y , and other species in the lower stratosphere and upper troposphere during AASE II, Geophys. Res. Lett., 21(23), 2583–2586, 1994.

Whalley, L. K., Stone, D., Bandy, B., Dunmore, R., Hamilton, J. F., Hopkins, J., Lee, J. D., Lewis, A. C. and Heard, D. E.: Atmospheric OH reactivity in central London: observations, model predictions and estimates of in situ ozone production, Atmos. Chem. Phys., 16(4), 2109–2122, 2016.

Williams, E. J., Roberts, J. M., Baumann, K., Bertman, S. B., Buhr, S., Norton, R. B. and Fehsenfeld, F. C.: Variations in NO_y composition at Idaho Hill, Colorado, J. Geophys. Res. D: Atmos., 102(D5), 6297–6314, 1997.

Williams, J., Roberts, J. M., Bertman, S. B., Stroud, C. A., Fehsenfeld, F. C., Baumann, K., Buhr, M. P., Knapp, K., Murphy, P. C., Nowick, M. and Williams, E. J.: A method for the airborne measurement of PAN, PPN, and MPAN, J. Geophys. Res. D: Atmos., 105(D23), 28943–28960, 2000.

Worton, D. R., Isaacman, G., Gentner, D. R., Dallmann, T. R., Chan, A. W. H., Ruehl, C., Kirchstetter, T. W., Wilson, K. R., Harley, R. A. and Goldstein, A. H.: Lubricating Oil Dominates Primary Organic Aerosol Emissions from Motor Vehicles, Environ. Sci. Technol., 48(7), 3698–3706, 2014.

Young, D. E., Allan, J. D., Williams, P. I., Green, D. C., Flynn, M. J., Harrison, R. M., Yin, J., Gallagher, M. W. and Coe, H.: Investigating the annual behaviour of submicron secondary inorganic and organic aerosols in London, Atmos. Chem. Phys., 15, 6351–6366, 2015.

Yuan, B., Hu, W. W., Shao, M., Wang, M., Chen, W. T., Lu, S. H., Zeng, L. M. and Hu, M.: VOC emissions, evolutions and contributions to SOA formation at a receptor site in eastern China, Atmos. Chem. Phys., 13(17), 8815–8832, 2013.

Zhang, Q., Alfarra, M. R., Worsnop, D. R., James, D., Coe, H., Canagaratna, M. R. and Jimenez, J. L.: Deconvolution and Quantification of Hydrocarbon-like and Oxygenated Organic Aerosols Based on Aerosol Mass Spectrometry Deconvolution and Quantification of Hydrocarbon-like and Oxygenated Organic Aerosols Based on Aerosol Mass Spectrometry, Environ. Sci. Technol., 39(13), 4938–4952, 2005.

Zhang, Q., Streets, D. G., Carmichael, G. R., He, K. B., Huo, H., Kannari, A., Klimont, Z., Park,

I. S., Reddy, S., Fu, J. S., Chen, D., Duan, L., Lei, Y., Wang, L. T. and Yao, Z. L.: Asian emissions in 2006 for the NASA INTEX-B mission, Atmos. Chem. Phys., 9(14), 5131–5153, 2009.

Zhao, Y., Hennigan, C. J., May, A. A., Daniel, S., Gouw, J. A. D., Gilman, J. B., Kuster, W. C. and Robinson, A. L.: Intermediate-Volatility Organic Compounds: A Large Source of Secondary Organic Aerosol, Environ. Sci. Technol, 48(23), 13743–13750, 2014.

Zhao, Y., Saleh, R., Saliba, G., Presto, A. A., Gordon, T. D., Drozd, G. T., Goldstein, A. H., Donahue, N. M. and Robinson, A. L.: Reducing secondary organic aerosol formation from gasoline vehicle exhaust, Proc. Natl. Acad. Sci. U. S. A., 114(27), 6984–6989, 2017.

Zheng, B., Huo, H., Zhang, Q., Yao, Z. L., Wang, X. T., Yang, X. F., Liu, H. and He, K. B.: High-resolution mapping of vehicle emissions in China in 2008, Atmos. Chem. Phys., 14(18), 9787–9805, 2014.

Zheng, B., Tong, D., Li, M., Liu, F., Hong, C., Geng, G., Li, H., Li, X., Peng, L., Qi, J., Yan, L., Zhang, Y., Zhao, H., Zheng, Y., He, K. and Zhang, Q.: Trends in China's anthropogenic emissions since 2010 as the consequence of clean air actions, Atmos. Chem. Phys., 18(19), 14095–14111, 2018.